Mechanism of Molybdenum Mediated Carbon Monoxide Deoxygenation and Coupling: Mono- and Dicarbyne Complexes Precede C–O Bond Cleavage and C–C Bond Formation

Joshua A. Buss and Theodor Agapie*

Division of Chemistry and Chemical Engineering, California Institute of Technology, 1200 East California Boulevard, MC 127-72, Pasadena, California 91125, United States

Supporting Information

Contents

Experimental Details

General Considerations

Unless otherwise specified, all operations were carried out in an MBraun drybox under a nitrogen atmosphere or using standard Schlenk and vacuum line techniques. Pre-reduced Teflon-coated stir bars (prepared via stirring a $Na[C_{10}H_8]$ solution overnight followed by rinsing three times with THF) were utilized in any stirred reaction in which KC_8, $K[C_{10}H_8]$, $Na[C_{10}H_8]$, **3**, **4**, **13**, or **14** were employed as reagents or formed in the course of the reaction. Solvents for air- and moisture-sensitive reactions were dried over sodium benzophenone ketyl, calcium hydride, or by the method of Grubbs.[1] Deuterated solvents were purchased from Cambridge Isotope Laboratories and vacuum transferred from sodium benzophenone ketyl. Solvents, once dried and degassed, were vacuum transferred directly prior to use or stored under inert atmosphere over activated 4 Å molecular sieves. Molybdenum complexes **1-5**, **7**, **8**,[2,3] potassium graphite (KC_8),[4] and sodium trimethylsiloxide ($NaOSiMe_3$)[5] were prepared and purified according to literature procedures. Unless indicated otherwise, all other chemicals were utilized as received. Graphite (325 mesh), $(Me_3Si)_2O$ (dried over sodium benzophenone ketyl and distilled prior to use), and trimethylsilyl chloride (dried over CaH_2 and distilled prior to use) were purchased from Alfa Aesar. Naphthalene (sublimed at 40 °C), potassium metal (washed with hexanes), sodium metal (washed with hexanes), and CO gas were purchased from Sigma Aldrich. Triisopropylsilyl chloride (dried over CaH_2 and distilled prior to use) was purchased from Oakwood Chemicals. ^{13}CO gas was purchased from Monsanto Research; butane and NH_3 gas were purchased from Matheson. Trimethylsilylchloride-d_9 was purchased from CDN Isotopes and vacuum transferred immediately prior to use. ^1H, $^{13}C\{^1H\}$, and $^{31}P\{^1H\}$ NMR spectra were recorded on Varian 400 MHz or Varian INOVA-500 spectrometers with shifts reported in parts per million (ppm). ^1H and $^{13}C\{^1H\}$ NMR spectra are referenced to residual solvent peaks.[6] $^{31}P\{^1H\}$ chemical shifts are referenced to an external 85% H_3PO_4 (0 ppm) standard. Multiplicities are abbreviated as follows: s = singlet, d = doublet, t = triplet, q = quartet, dd = doublet of doublets, dt = doublet of triplets, td = triplet of doublets, qq = quartet of quartets, vt = virtual triplet, d vt = doublet of virtual triplets, m = multiplet, br = broad, and v br = very broad (multiplicity assignments are omitted for "v br" assignments due to poor resolution). Fourier transform infrared ATR spectra were collected from thin films or powders on a Thermo Scientific Nicolet iS5 Spectrometer with a diamond ATR crystal (utilized iD5 ATR insert).

*In Situ Preparation of **9-^{13}C***

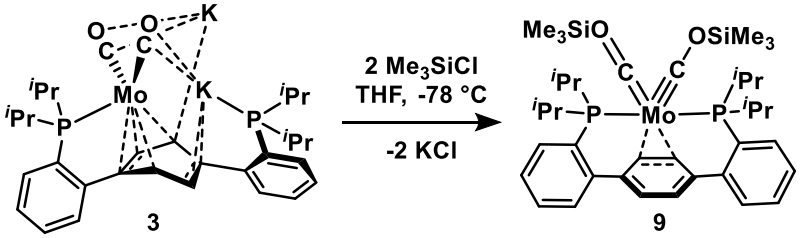

Due to thermal instability, **9-^{13}C** must be prepared *in situ*. In a typical procedure, a J. Young NMR tube was charged with solid **3-^{13}C** (25 mg, 0.027 mmol). The tube was evacuated, and THF-d_8 (*ca.* 300 μL) was admitted via vacuum transfer at -196 °C. The contents of the J. Young tube were warmed to room temperature and mixed thoroughly, providing a deep red solution. This solution was immersed in liquid nitrogen and THF-d_8 (*ca.* 100 μL) was again added to the reaction via vacuum transfer. Me_3SiCl (33.4 mL at 3.1 cm Hg, 0.57 mmol) was then condensed into the reaction from a calibrated gas volume. The tube was sealed and carefully thawed to -78 °C, avoiding mixing of the layers as much as possible (the bottom of the tube must be kept coldest to prevent bumping). Upon thawing, the tube was shaken vigorously to mix and immediately refrozen. Samples prepared this way show 80-90% conversion to the desired product, but minor oxidation to **2-^{13}C** typically occurs, as does some formation of bis(siloxy)acetylene **10-^{13}C**. Solutions of **9-^{13}C** were used for spectroscopic studies without further manipulation. At low temperatures, these

samples are stable for hours, but show slow conversion to **10**-^{13}**C**. Upon warming, **9**-^{13}**C** converts to a mixture of **2**-^{13}**C**, **8**-^{13}**C**, and **11**-^{13}**C** as observed by multinuclear NMR.

^{1}H NMR (500 MHz, THF-d_8, -80 °C) δ: 7.96 (br s, 2H, aryl-*H*), 7.67 (br s, 2H, aryl-*H*), 7.55 (br s, 2H, aryl-*H*), 7.50 (br s, 2H, aryl-*H*), 7.08 (br s, 2H, central arene-*H*), 6.24 (br s, 2H, central arene-*H*), 2.97 (br m, 2H, C*H*(CH$_3$)$_2$), 2.23 (br m, 2H, C*H*(CH$_3$)$_2$), 1.51 (br m, 6H, CH(C*H*$_3$)$_2$), 1.27-1.33 (br m, 12H, CH(C*H*$_3$)$_2$), 0.57 (br m, 6H, CH(C*H*$_3$)$_2$), 0.18 (br s, 9H, COSi(C*H*$_3$)$_3$), -0.43 (br s, 9H, COSi(C*H*$_3$)$_3$). ^{13}C{^{1}H} NMR (126 MHz, THF-d_8, -80 °C) δ: 284.27 (br s, Mo≡*C*OSi), 274.35 (br s, Mo≡*C*OSi), 149.59 (br s, aryl-*C*), 138.31 (br s, aryl-*C*), 133.27 (br s, aryl-*C*), 129.56 (br s, aryl-*C*), 128.84 (br s, aryl-*C*), 128.63 (v br, aryl-*C*), 127.40 (br s, aryl-*C*), 126.02 (v br, cental arene-*C*), 90.15 (v br, central arene-*C*), 36.19 (v br, *C*H(CH$_3$)$_2$), 29.86 (v br, *C*H(CH$_3$)$_2$), 18.67 (v br, CH(*C*H$_3$)$_2$), 18.53 (v br, CH(*C*H$_3$)$_2$), -0.31 (v br, COSi(*C*H$_3$)$_3$), -0.47 (v br, COSi(*C*H$_3$)$_3$). ^{31}P{^{1}H} NMR (202 MHz, THF-d_8, -80 °C) δ: 66.48 (br t, *J* = 17.32 Hz).

Cooling the sample further resolves the ^{2}J(P,C) of the carbyne carbons: ^{13}C{^{1}H} NMR (126 MHz, THF-d_8, -100 °C) δ: 284.10 (br t, *J* = 14.26 Hz, Mo≡*C*OSi), 273.84 (t, *J* = 23.05 Hz, Mo≡*C*OSi).

Though **9**-^{13}**C** began to react, the NMR spectra collected at -20 °C were consistent with two siloxycarbyne motifs in a fast exchange regime: ^{1}H NMR (500 MHz, THF-d_8, -20 °C) δ: 7.90 (br s, 2H, aryl-*H*), 7.61 (br s, 2H, aryl-*H*), 7.49 (br s, 2H, aryl-*H*), 7.45 (br s, 2H, aryl-*H*), 6.71 (br s, 4H, central arene-*H*), 2.59 (v br, 4H, C*H*(CH$_3$)$_2$), 1.30 (v br, 12H, CH(C*H*3)2), 1.04 (v br, 12H, CH(C*H*3)2), -0.09 (br s, 18H, COSi(C*H*$_3$)$_3$). ^{13}C{^{1}H} NMR (126 MHz, THF-d_8, -20 °C) δ: 280.79 (br s, Mo≡*C*OSi), 150.11 (br s, aryl-*C*), 138.67 (br s, aryl-*C*), 133.37 (br s, aryl-*C*), 130.74 (br s, aryl-*C*), 129.68 (br s, aryl-*C*), 129.08 (br s, aryl-*C*), 128,74 (v br, aryl-*C*), 127.54 (br s, aryl-*C*), 33.21 (v br, *C*H(CH$_3$)$_2$), 20.70 (br s, CH(*C*H$_3$)$_2$), 19.09 (br s, CH(*C*H$_3$)$_2$), 0.13 (br s, COSi(*C*H$_3$)$_3$). ^{31}P{^{1}H} NMR (202 MHz, THF-d_8, -20 °C) δ: 63.97 (t, *J* = 20.37 Hz).

9-^{13}**C**-***d*$_{18}$** was prepared analogously, substituting Me$_3$SiCl-d_9 for Me$_3$SiCl. These samples were prepared in proteo THF with a C$_6$D$_6$ spike to facilitate study by ^{2}H NMR spectroscopy. ^{2}H NMR (76 MHz, THF/C$_6$D$_6$, -80 °C) δ: -0.1 (v br, COSi(C*D*$_3$)$_3$), -0.6 (v br, COSi(C*D*$_3$)$_3$).

*Synthesis of **10***

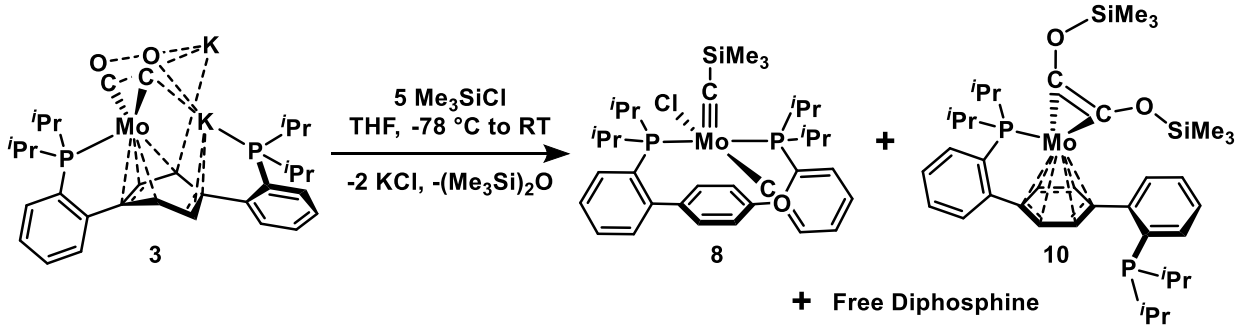

A Teflon stoppered Schlenk tube was charged with **3** (400 mg, 0.432 mmol), THF (20 mL), and a stir bar. The reaction vessel was placed in a dry ice/acetone bath and with a heavy dinitrogen counterflow, the stopper was replaced with a septum. With rapid stirring, Me$_3$SiCl (0.25 mL, 1.970 mmol) was added dropwise via syringe. The flask was stoppered once more and the reaction was left to slowly warm to room temperature over 16 hours, with stirring. At this time, volatiles were removed *in vacuo*, providing a red/brown residue comprised primarily of **8**, **10** (major), and free ligand. This residue was extracted with (Me$_3$Si)$_2$O (2 mL x 2) to separate the desired product from **8**. The (Me$_3$Si)$_2$O extract was dried under reduced pressure and subsequently extracted with MeCN. The deep red MeCN solution was filtered through a Celite plug and chilled to -35 °C. Upon standing for 12 hours, a burgundy microcrystalline precipitate

formed. These solids were collected via vacuum filtration as a 75:25 mixture of **10** and free diphosphine ligand (53 mg, *ca.* 0.077 mmol, 18%).

^{1}H NMR (400 MHz, C_6D_6, 23 °C) δ: 7.54 (s, 1H, aryl-*H*), 7.22 (v br, 3H, aryl-*H*), 6.96-7.08 (v br, 4H, aryl-*H*), 5.00 (v br, 4H, central arene-*H*), 2.37 (v br, 4H, C*H*$(CH_3)_2$), 1.14-1.19 (m, 12H, CH(C*H*$_3)_2$), 1.02-1.07 (m, 12H, CH(C*H*$_3)_2$), 0.22 (s, 18H, Si(C*H*$_3)_3$). ^{13}C{^{1}H} NMR (101 MHz, THF, 23 °C) δ: 208.06 (t, *J* = 9.82 Hz, *C*OSiMe_3), 150.79 (d, *J* = 27.38 Hz, aryl-*C*), 149.62 (d, *J* = 26.28 Hz, aryl-*C*), 141.48 (d, *J* = 5.63 Hz, aryl-*C*), 135.22 (d, *J* = 24.16 Hz, aryl-*C*), 132.79 (d, *J* = 2.81 Hz, aryl-*C*), 131.03 (d, *J* = 5.00 Hz, aryl-*C*), 130.59 (d, *J* = 5.09 Hz, aryl-*C*), 128.70 (br s, aryl-*C*), 128.65 (br s, aryl-*C*), 128.59 (s, aryl-*C*), 128.46 (v br, aryl-*C*), 128.35 (br s, aryl-*C*), 126.77 (s, aryl-*C*), 126.09 (v br, aryl-*C*), 77.39 (v br, central arene-*C*), 74.44 (v br, central arene-*C*), 25.52 (v br, *C*H$(CH_3)_2$), 24.93 (d, *J* = 16.46 Hz, *C*H$(CH_3)_2$), 20.48 (d, *J* = 20.12 Hz, CH(*C*H$_3)_2$), 20.18 (v br, CH(*C*H$_3)_2$), 19.90 (d, *J* = 11.45 Hz, CH(*C*H$_3)_2$), 19.40 (br s, CH(*C*H$_3)_2$), 0.78 (s, OSi(*C*H$_3)_3$). ^{31}P{^{1}H} NMR (162 MHz, THF, 23 °C) δ: 84.26 (br s, Mo-P), -4.70 (s).

Heating mixtures of **10** and free diphosphine to 70 °C provided ^{1}H and ^{13}C{^{1}H} NMR spectra in which the broad resonances in the room temperature spectrum are better resolved. A full ^{13}C{^{1}H} NMR spectrum could not be collected at this temperature as the sample began to decompose over the timescale of the experiment.

^{1}H NMR (400 MHz, C_6D_6, 70 °C) δ: 7.48 (br s, 1H, aryl-*H*), 7.27-7.30 (v br, 2H, aryl-*H*), 7.19-7.20 (v br, 1H, aryl-*H*), 7.00-7.06 (br m, 4H, aryl-*H*), 4.97 (v br, 4H, central arene-*H*), 2.39 (v br, 4H, C*H*$(CH_3)_2$), 1.15-1.20 (m, 12H, CH(C*H*$_3)_2$), 1.04-1.09 (m, 12H, CH(C*H*$_3)_2$), 0.21 (br s, 18H, Si(C*H*$_3)_3$). ^{13}C{^{1}H} NMR (101 MHz, THF, 70 °C) δ: 77.04 (v br, central arene-*C*), 75.56 (v br, central arene-*C*).

Single crystals of **10** were isolated while attempting to crystallize **9**. The low-temperature crystallization procedure is described below:

A small swivel frit was assembled with a 50 mL round-bottom flask charged with **3** (60 mg, 0.066 mmol) and a small a stir bar at one end and a 50 mL round-bottom flask charged with a stir bar at the other. The apparatus was sealed, and evacuated. THF was admitted to the flask containing **3** at -78 °C via vacuum transfer, resulting in a deep red solution. With a heavy argon counterflow, the Teflon pin in the side arm of the swivel frit was replaced with a rubber septum. The septum was pierced with a 12-gauge needle and an 8" section of Teflon cannula was carefully inserted. A Me_3SiCl (14.3 mg, 0.132 mmol) solution in THF (1 mL) was introduced to the stirring reaction mixture, via syringe, through the short cannula. The solution lightened slightly upon addition and the Teflon pin was replaced, sealed, and the reaction was left to stir for 20 minutes. Volatiles were removed *in vacuo*, maintaining a temperature between -40 and -78 °C.

The residue remaining in the flask was dissolved in hexanes, introduced via vacuum transfer at -78 °C. The top of the swivel frit (empty 50 mL flask) was pre-cooled with liquid nitrogen and the frit swiveled, utilizing a -78/-196 °C temperature gradient to draw the red hexanes solution through the frit. The filtrate was dried under reduced pressure, again maintaining a temperature between -40 and -78 °C, providing a red/orange powder.

Butane (20 mL) was condensed into a trap at -78 °C and freeze-pump-thawed three times to remove trace oxygen. It was then transferred from the trap (-78 °C) onto the powder (-196 °C), and stirring was initiated. Once the solids had dissolved, stirring was halted. The side-arm pin was once more replaced with a septum which was pierced with a 21-gauge needle. Solvent was evaporated at low temperature (-40 to -78 °C) with the aid of a slow argon flow, providing deep red single crystals of **10**.

10-^{13}C can be prepared analogously, starting from **3-^{13}C**. It is also observed spectroscopically in reactions employing **9-^{13}C**; the enhanced resonance is the acetylenic peak at 208.06 ppm. At room temperature,

$^{31}P/^{13}C$ scalar coupling is not resolved in the $^{31}P\{^{1}H\}$ nor the $^{13}C\{^{1}H\}$ NMR spectra; however, cooling samples containing **10-^{13}C** to -40 °C sharpened the resonances attributable to this species, resolving the ^{2}J(P,C):

$^{13}C\{^{1}H\}$ NMR (126 MHz, THF, -40 °C) δ: 206.74 (d, J = 19.57 Hz, *C*OSiMe$_3$). $^{31}P\{^{1}H\}$ NMR (202 MHz, THF, -40 °C) δ: 86.21 (t, J = 19.57 Hz, Mo-*P*), -5.56 (s).

*Synthesis of **11***

Due to conversion to **8**, **11** must be prepared and handled at low temperature. The following two methods were employed:

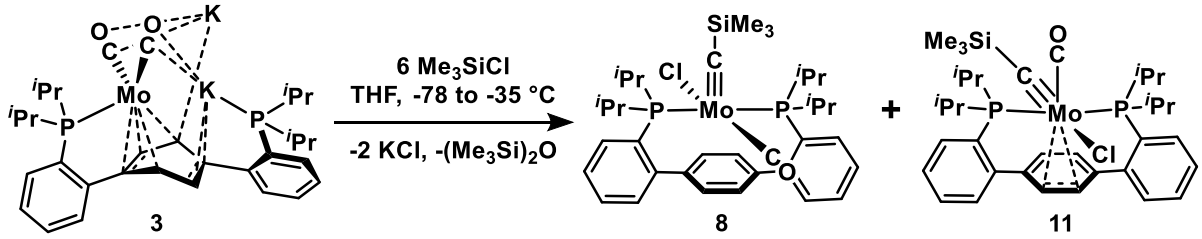

Method A (from **3**):
A 20 mL scintillation vial was charged with a deep red solution of **3** (80 mg, 0.088 mmol) in THF (2 mL) and a stir bar. The vial was capped and placed in a liquid nitrogen-cooled cold well. Once the solution had frozen, the vial was removed from the well. While thawing and stirring, Me_3SiCl (67 µL, 0.528 mmol) was added dropwise via Hamilton syringe. The vial was returned to the cold well, immediately upon completion of the addition and the contents re-frozen. The vial was allowed to thaw with stirring, and this process of low-temperature mixing was repeated three times, at which time the THF solution was frozen a final time. Pre-chilled pentane (10 mL) was layered onto the frozen THF solution and the vial was sealed and placed in a -35 °C freezer. After four days, X-ray quality crystals of a roughly 60:40 mixture of **11** and **8** had formed. ^{1}H NMR (500 MHz, THF-d_8, -80 °C) δ: 8.11 (br d, J = 4.89 Hz, 2H, aryl-*H*), 7.95 (v br, 2H, aryl-*H*), 7.72 (t, J = 7.34 Hz, 2H, aryl-*H*), 7.67 (d, J = 7.50 Hz, 2H, aryl-*H*), 7.64 (br s, 2H, aryl-H), 7.46 (s, 2H, central arene-*H*), 3.56 (v br, 2H, C*H*(CH$_3$)$_2$), 3.15 (v br, 2H, C*H*(CH$_3$)$_2$), 1.41 (m, 6H, CH(C*H*$_3$)$_2$), 1.25 (m, 12H, CH(C*H*$_3$)$_2$), -0.84 (s, 9H, Si(C*H*$_3$)$_3$). ^{31}P NMR (202 MHz, THF-d_8, -80 °C) δ: 41.88 (br s).

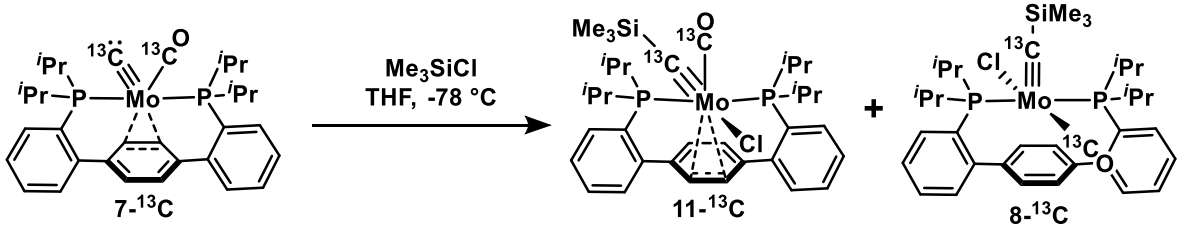

Method B (from **7-^{13}C**):
To a J. Young tube containing *in situ* prepared **7-^{13}C** (*ca.* 0.024 mmol) in THF (500 µL) at -78 °C, Me_3SiCl (14.5 µL, 0.114 mmol) was added via Hamilton syringe with a heavy counterflow of argon. The J. Young tube was sealed and shaken, providing a *ca.* 75:25 mixture of **11-^{13}C** and **8-^{13}C**. $^{13}C\{^{1}H\}$ NMR (126 MHz, THF-d_8, -80 °C) δ: 344.87 (br s, *C*SiMe$_3$), 241.82 (br s, *C*O). $^{31}P\{^{1}H\}$ NMR (202 MHz, THF-d_8, -80 °C) δ: 41.86 (s).

In Situ Preparation of **12-^{13}C**

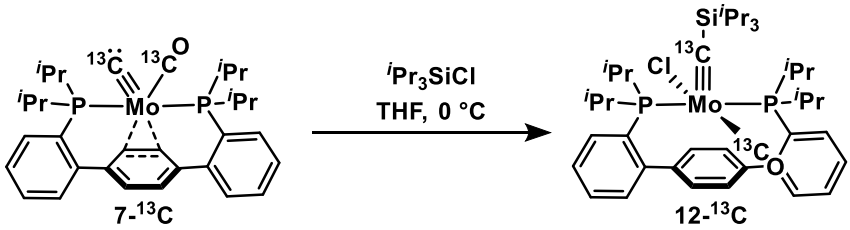

To a J. Young tube containing *in situ* prepared **7-^{13}C** (*ca.* 0.024 mmol) in THF (400 μL) at -78 °C, a THF solution (100 μL) of ^{i}Pr$_3$SiCl (4.6 mg, 0.024 mmol) was added via syringe with a heavy counterflow of argon. The tube was sealed and shaken thoroughly, ensuring the sample remained cold throughout. The J. Young tube was then transferred to an NMR spectrometer pre-cooled to -80 °C. The sample was warmed in the probe, in 10 °C increments. No conversion was observed up to 0 °C. At this temperature, new resonances attributable to **12-^{13}C** (*vide infra*) were observed by ^{13}C{^{1}H} and ^{31}P{^{1}H} NMR spectroscopy. Warming was continued and complete consumption of the starting material was observed by 10 °C.

^{13}C{^{1}H} NMR (126 MHz, THF, 0 °C) δ: 360.54 (br dt, *C*SiMe$_3$), 250.55 (br dt, *C*O). ^{31}P{^{1}H} NMR (202 MHz, THF, 0 °C) δ: 34.44 (s).

^{13}C{^{1}H} NMR (126 MHz, THF, 25 °C) δ: 360.96 (dt, *C*SiMe$_3$), 250.52 (dt, *C*O). ^{31}P{^{1}H} NMR (202 MHz, THF, 25 °C) δ: 33.95 (s).

In Situ Preparation of **13-^{13}C**

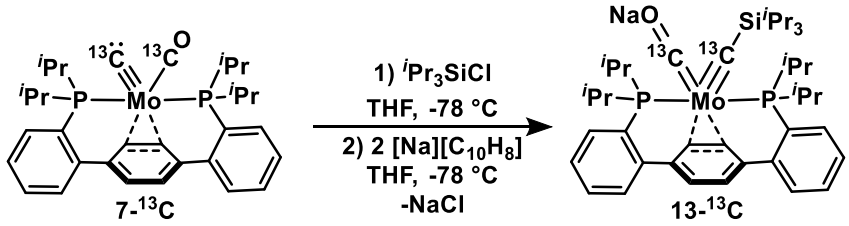

To a J. Young tube containing *in situ* prepared **7-^{13}C** (*ca.* 0.028 mmol) in THF (400 μL) at -78 °C, a THF solution (100 μL) of ^{i}Pr$_3$SiCl (10.8 mg, 0.056 mmol) was added via syringe with heavy counterflow of argon. The tube was sealed and the contents mixed, resulting in no noticeable color change. Again, under a heavy counterflow of argon, a deep green THF solution (200 μL) of [Na][C$_{10}$H$_8$] (0.056 mmol) was added via syringe. The tube was sealed and mixed, ensuring the sample remained cold throughout. The solution darkened to deep maroon. The J. Young tube was then transferred to an NMR spectrometer pre-cooled to -80 °C. Complete conversion of the starting material to **13-^{13}C** was observed by multinuclear NMR spectroscopy.

^{13}C{^{1}H} NMR (126 MHz, THF, -100 °C) δ: 326.15 (v br, *C*SiMe$_3$ or *C*ONa), 325.82 (v br, *C*SiMe$_3$ or *C*ONa). ^{31}P{^{1}H} NMR (202 MHz, THF, -100 °C) δ: 60.59 (br s).

^{13}C{^{1}H} NMR (126 MHz, THF, -60 °C) δ: 326.02 (br t, *J* = 19.24 Hz, *C*SiMe$_3$ or *C*ONa), 325.32 (br s, *C*SiMe$_3$ or *C*ONa). ^{31}P{^{1}H} NMR (202 MHz, THF, -60 °C) δ: 59.58 (br s).

In Situ Preparation of **14-^{13}C**

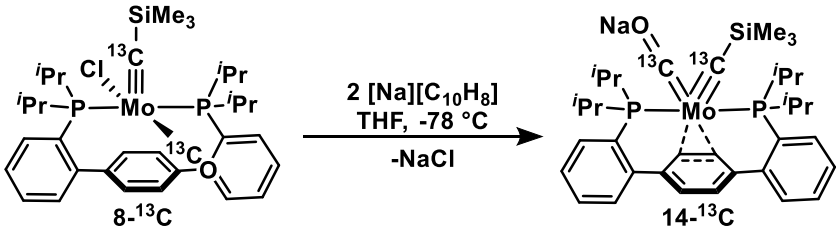

A J. Young tube was charged with homogenous red solution of **8-^{13}C** (18 mg, 0.025 mmol) in THF (400 µL). The tube was placed in a dry ice/acetone bath and the contents cooled to -78 °C; a deep green solution of [Na][$C_{10}H_8$] (0.059 mmol) in THF (200 µL) was added via syringe with a heavy argon counterflow. The J. Young tube was sealed and mixed thoroughly, changing color to reddish purple. It was transferred to an NMR spectrometer pre-cooled to -80 °C. Complete conversion of the starting material to **14-^{13}C** was observed by multinuclear NMR spectroscopy.

$^{13}C\{^1H\}$ NMR (126 MHz, THF, -100 °C) δ: 329.20 (br t, *J* = 21.09 Hz, *C*$SiMe_3$ or *C*ONa), 327.42 (br, *C*$SiMe_3$ or *C*ONa). $^{31}P\{^1H\}$ NMR (202 MHz, THF, -100 °C) δ: 57.81 (br s).

$^{13}C\{^1H\}$ NMR (126 MHz, THF, -80 °C) δ: 329.98 (br t, *J* = 19.16 Hz, *C*$SiMe_3$ and *C*ONa). $^{31}P\{^1H\}$ NMR (202 MHz, THF, -80 °C) δ: 58.49 (br s).

$^{13}C\{^1H\}$ NMR (126 MHz, THF, -60 °C) δ: 331.81 (br s, *C*$SiMe_3$ or *C*ONa), 330.50 (t, *J* = 20.39 Hz, *C*$SiMe_3$ or *C*ONa). $^{31}P\{^1H\}$ NMR (202 MHz, THF, -60 °C) δ: 59.05 (br s).

In Situ Preparation of **15-^{13}C**

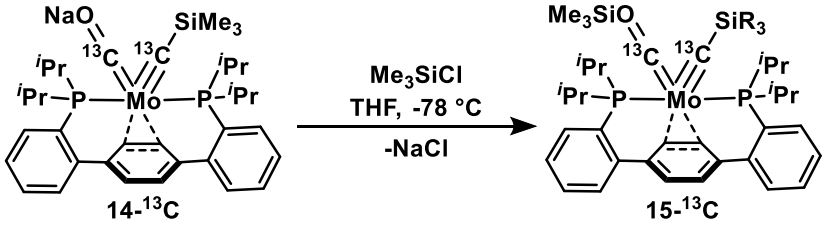

A solution of **14-^{13}C** was prepared in a J. Young NMR tube, as described above, from the reduction of **8-^{13}C** (20 mg, 0.028 mmol) with [Na][$C_{10}H_8$] (0.062 mmol) in THF (600 µL). This solution was frozen in liquid nitrogen and the headspace of the tube evacuated. Me_3SiCl (33.4 mL at 1.7 cm Hg, 0.031 mmol) was then admitted via condensation from a calibrated gas volume. The J. Young tube was sealed and the contents carefully thawed to -78 °C; the reaction was mixed thoroughly, ensuring the sample remained cold. The tube was transferred to an NMR spectrometer pre-cooled to -40 °C. Quantitative conversion to **15-^{13}C** was observed by multinuclear NMR.

$^{13}C\{^1H\}$ NMR (126 MHz, THF, -40 °C) δ: 379.45 (t, *J* = 19.92 Hz, *C*$SiMe_3$), 284.09 (t, *J* = 13.80 Hz, *C*O$SiMe_3$). $^{31}P\{^1H\}$ NMR (202 MHz, THF, -40 °C) δ: 57.41(dd, *J* = 19.92, 13.80 Hz).

$^{13}C\{^1H\}$ NMR (126 MHz, THF, 0 °C) δ: 379.52 (t, *J* = 18.97 Hz, *C*$SiMe_3$), 284.81 (t, *J* = 14.47 Hz, *C*O$SiMe_3$). $^{31}P\{^1H\}$ NMR (202 MHz, THF, 0 °C) δ: 57.95 (dd, *J* = 18.97, 14.47 Hz).

Electrophilic Quenching of 3-^{13}C with ^{i}Pr$_3$SiCl

A J. Young NMR tube was charged with **3-^{13}C** (20 mg, 0.021 mmol) and the headspace evacuated on the high vacuum line. THF-d_8 (*ca.* 400 μL) was admitted via vacuum transfer at -196 °C. The tube was sealed, and the contents thawed and mixed thoroughly, providing a deep red solution. The J. Young tube was submerged in a -78 °C dry ice/acetone bath, and with a heavy counterflow of argon, ^{i}Pr$_3$SiCl (16.6 μL, 0.086 mmol) was admitted via microsyringe. The tube was again sealed and carefully transferred to the NMR probe (pre-chilled to -80 °C).

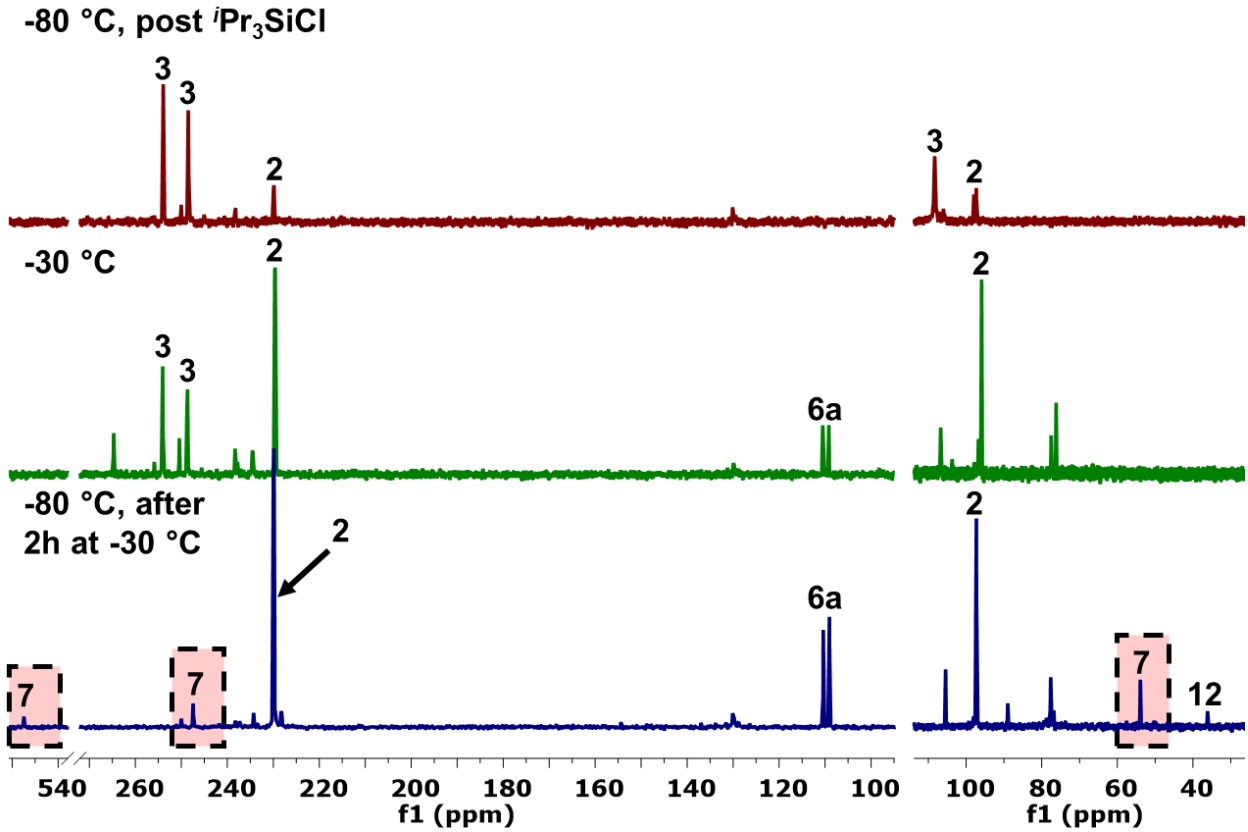

Figure S1—Stacked partial ^{13}C{^{1}H} (126 MHz, left) and ^{31}P{^{1}H} (202 MHz, right) NMR spectra (THF-d_8) of the low temperature addition of 4 equiv. of ^{i}Pr$_3$SiCl to **3-^{13}C**. Immediately after admitting ^{i}Pr$_3$SiCl to the reaction mixture, some oxidation to Mo(0) dicarbonyl **2-^{13}C** was observed (top). Warming the sample to -30 °C in the NMR probe resulted in formation of metal-free C_2O_1 fragment **6a** (middle). Maintaining this temperature (at which coupling occurs slowly) for two hours and then cooling the sample back to -80 °C afforded spectra with features attributable to **7-^{13}C** consistent with the proposed intermediacy of this species in the coupling reaction. Note that with the chosen ratio of reagents, electrons are limiting (0.5 equiv.), and trace formation of silyl carbyne **12-^{13}C** is detected.

Variable Temperature NMR of 9-^{13}C

A J. Young NMR tube was charged with **3-^{13}C** (22 mg, 0.024 mmol) and THF-d_8 (400 µL) was added via vacuum transfer at -78 °C. With an argon counterflow, Me_3SiCl (17 µL, 0.132 mmol) was introduced to the NMR tube via Hamilton syringe. Mixing at low temperature provided a deep red solution of **9-^{13}C**, which was analyzed by multinuclear NMR at a series of temperatures. The experimental NMR spectra were fit using the dNMR module within the TopSpin Software Package.[7] Trace **2-^{13}C** formed following the addition of Me_3SiCl was likewise fit and used to determine the line broadening for the simulation at -100 °C, as it is not involved in exchange processes. Simulations at higher temperatures were derived from the parameters of the -100 °C fit, via iterative variation of the exchange rate, *k*.

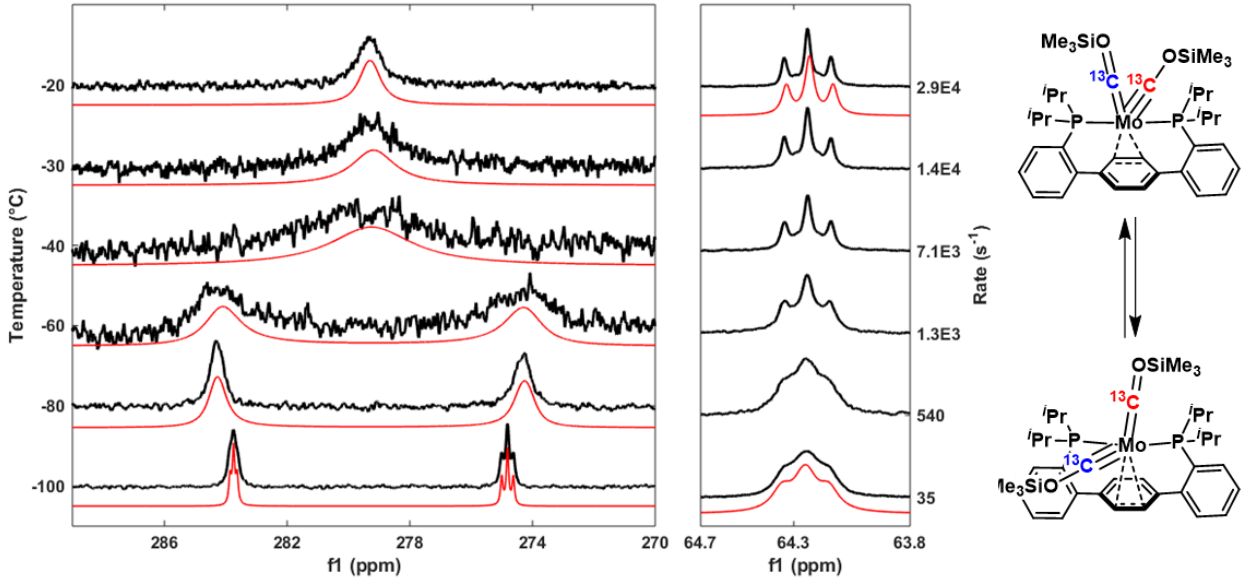

Figure S2: Variable Temperature $^{13}C\{^1H\}$ (left) and $^{31}P\{^1H\}$ (right) NMR Spectra of **9-^{13}C** (only select regions of spectra are shown, for clarity). Sample temperature (in °C) and the calculated rate of exchange for the carbyne carbons (in s^{-1}) are shown on the vertical axes. Experimental spectra and iteratively fit simulations are represented with black and red lines, respectively.

Table S1—Dynamic NMR Fit Parameters for Carbyne Exchange in 9-^{13}C

T [K]	*k* [sec^{-1}]	1/T [K^{-1}]	Ln(*k*)	Ln(*k*/T)	ΔG‡ (kcal/mol)
173.15	34.87	0.0058	3.55	-1.60	8.73
193.15	539.42	0.0052	6.29	1.03	8.73
213.15	1343.35	0.0047	7.20	1.84	9.28
233.15	7103.41	0.0043	8.86	3.42	9.42
243.15	12982.40	0.0041	9.47	3.98	9.56
253.15	28800.20	0.0040	10.27	4.73	9.57

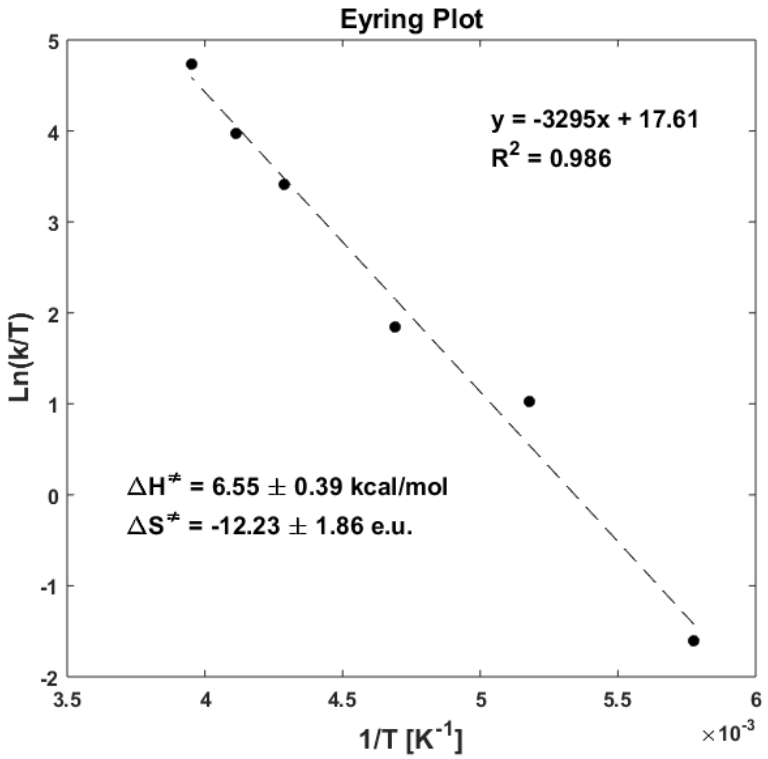

Figure S3—Eyring plot for dicarbyne exchange in **9-^{13}C** (^{13}C{^{1}H}, THF-d_8, 126 MHz).

In Situ Reduction of 10

A J. Young NMR tube was charged with a deep red solution of **3-^{13}C** (28 mg, 0.031 mmol) in THF (400 µL). The contents of the tube were frozen in liquid nitrogen and the headspace evacuated. Me_3SiCl (3.3 cm Hg in 33.4 mL, 0.060 mmol) was condensed into the tube which was then sealed and warmed to -78 °C. The reaction mixture was mixed and left at -78 °C, in a dry ice/acetone slush bath, for 5 days. $^{31}P\{^1H\}$ and $^{13}C\{^1H\}$ NMR spectra collected at this point display significant conversion to bis(siloxy)acetylene **10-^{13}C** (Figure S4, A). With a heavy counterflow of argon, a THF solution of [Na][$C_{10}H_8$] (0.060 mmol in 200 µL) was added via syringe at -78 °C. The tube was sealed, mixed, and the reduction reaction monitored by variable temperature NMR spectroscopy (Figure S4, B-C).

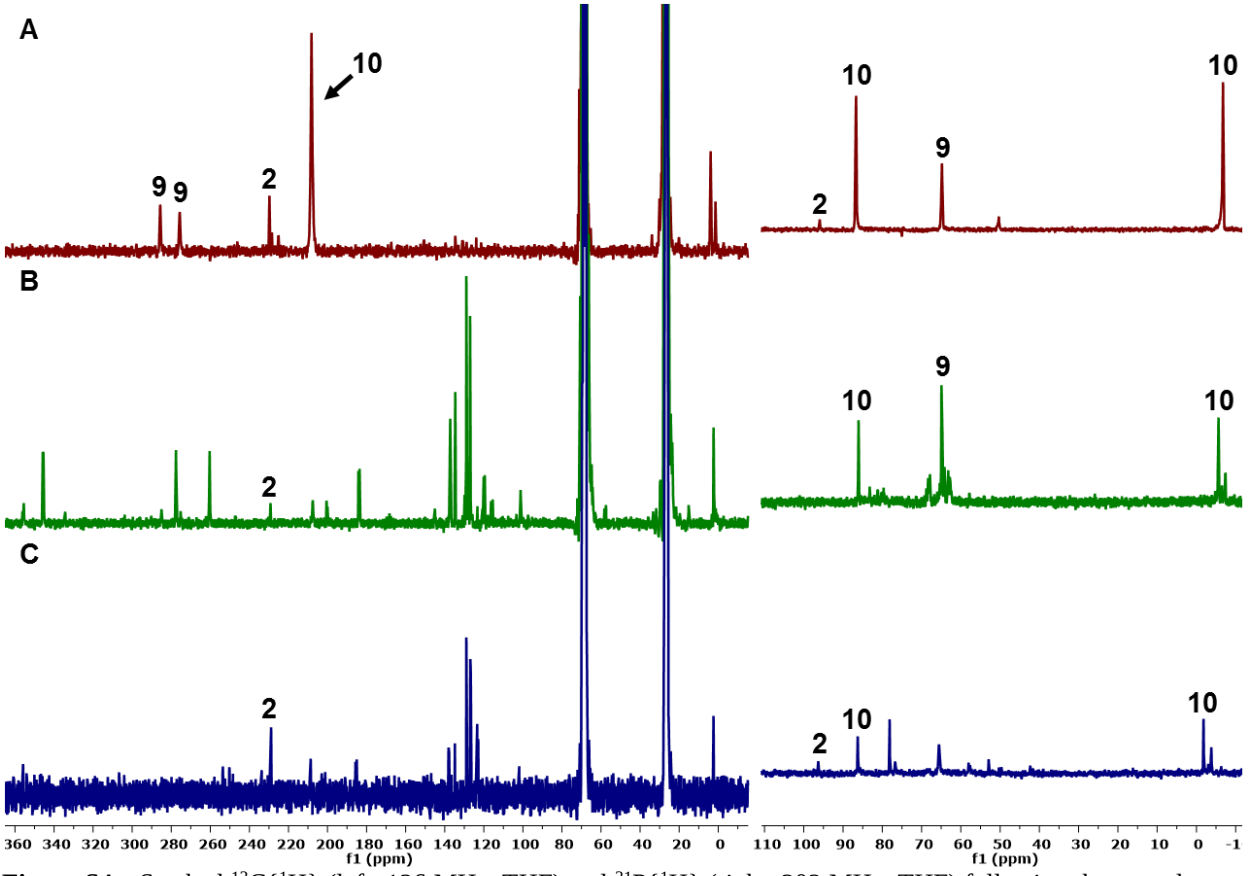

Figure S4—Stacked $^{13}C\{^1H\}$ (left; 126 MHz, THF) and $^{31}P\{^1H\}$ (right; 202 MHz, THF) following the two-electron reduction of **10-^{13}C**. From a reaction mixture comprised of a *ca.* 63:36:1 ratio of **10-^{13}C**, **9-^{13}C**, and **2-^{13}C**, respectively, two-electron reduction at -78 °C leads to an intractable mixture of species. Though downfield resonances at 345.5 and 355.7 ppm (Figure S4, B), attributable to **11-^{13}C** and **8-^{13}C**, respectively, are observed in the $^{13}C\{^1H\}$ NMR spectrum, these are attributed to C–O cleavage chemistry from **9-^{13}C**. Warming the reaction mixture to room temperature (Figure S4, C) did not afford spectra consistent with C–O cleavage chemistry from **10-^{13}C**.

Isomerization of 11 to 8

A J. Young tube was charged with microcrystals from the preparation of **11** (method A, *vide supra*) and THF-d_8 (*ca.* 500 μL) was admitted at -78 °C via vacuum transfer. The contents of the tube were mixed at low temperature, providing a burgundy solution. ^{1}H and ^{31}P{^{1}H} NMR spectroscopy at -80 °C showed a 57:43 mixture of **11** to **8**, respectively. The tube was warmed to room temperature for set time intervals before being returned to the probe for spectral analysis (Figure S5).

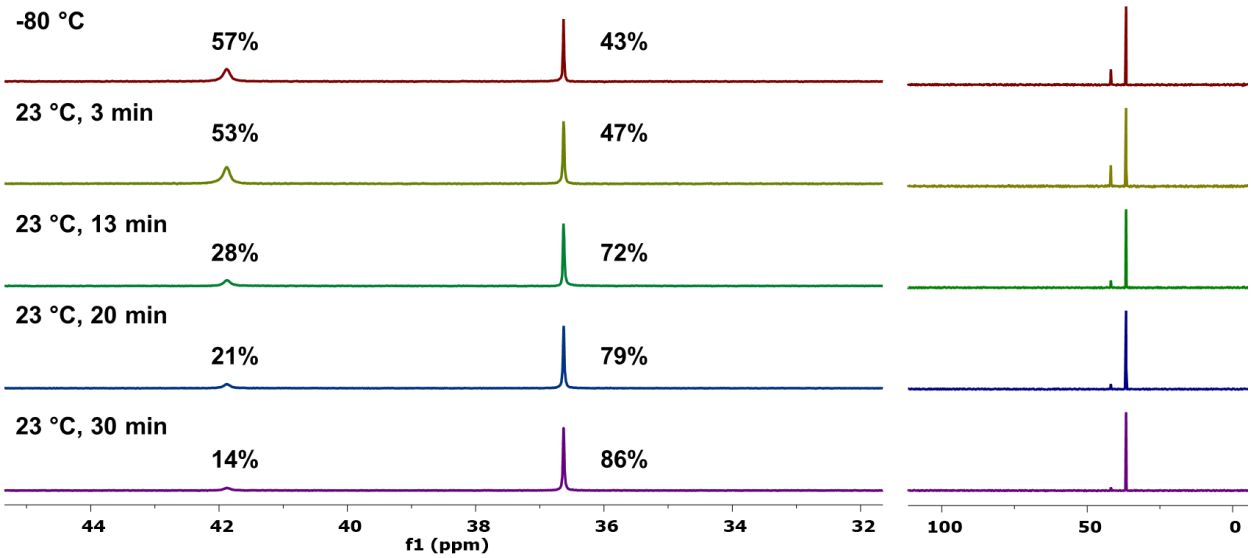

Figure S5—Stacked partial (left) and full (right) ^{31}P{^{1}H} NMR spectra (202 MHz, THF-d_8, -80°C) supporting the conversion of **11** to **8** after warming to room temperature. The resonances at 41.9 ppm and 36.6 ppm correspond to **11** and **8**, respectively.

C–O Bond Cleavage Kinetics Experiments

In a representative reaction (5 equiv. of Me_3SiCl), 0.5 mL of a deep red stock solution of **3-^{13}C** (120 mg, 0.132 mmol) in THF (3 mL)/C_6D_6 (12 drops) was added to a J. Young tube. THF (70 µL) was added via Hamilton syringe to ensure the desired 585 µL approximate sample volume (25 °C) following addition of silyl chloride. The tube was sealed and attached to the high vacuum line, where the contents were freeze-pump-thawed twice. Me_3SiCl (33.4 mL at 2.0 cm Hg, 23 °C, 0.036 mmol) was admitted via condensation from a calibrated gas bulb. The contents of the J. Young were thawed, mixed quickly, and refrozen. Me_3SiCl (33.4 mL at 4.0 cm Hg, 23 °C, 0.072 mmol) was admitted as before. The tube was then sealed and placed in a liquid nitrogen cooled Dewar. Thawing occurred directly prior to placing the NMR tube in a 0 °C NMR probe. $^{13}C\{^1H\}$ NMR spectra were recorded as an array utilizing the pre-acquisition delay mechanism in Agilent's VnmrJ software. Relative concentrations of species in the reaction mixture were determined via integration of their respective resonances against the C_6D_6 triplet at 128.06.

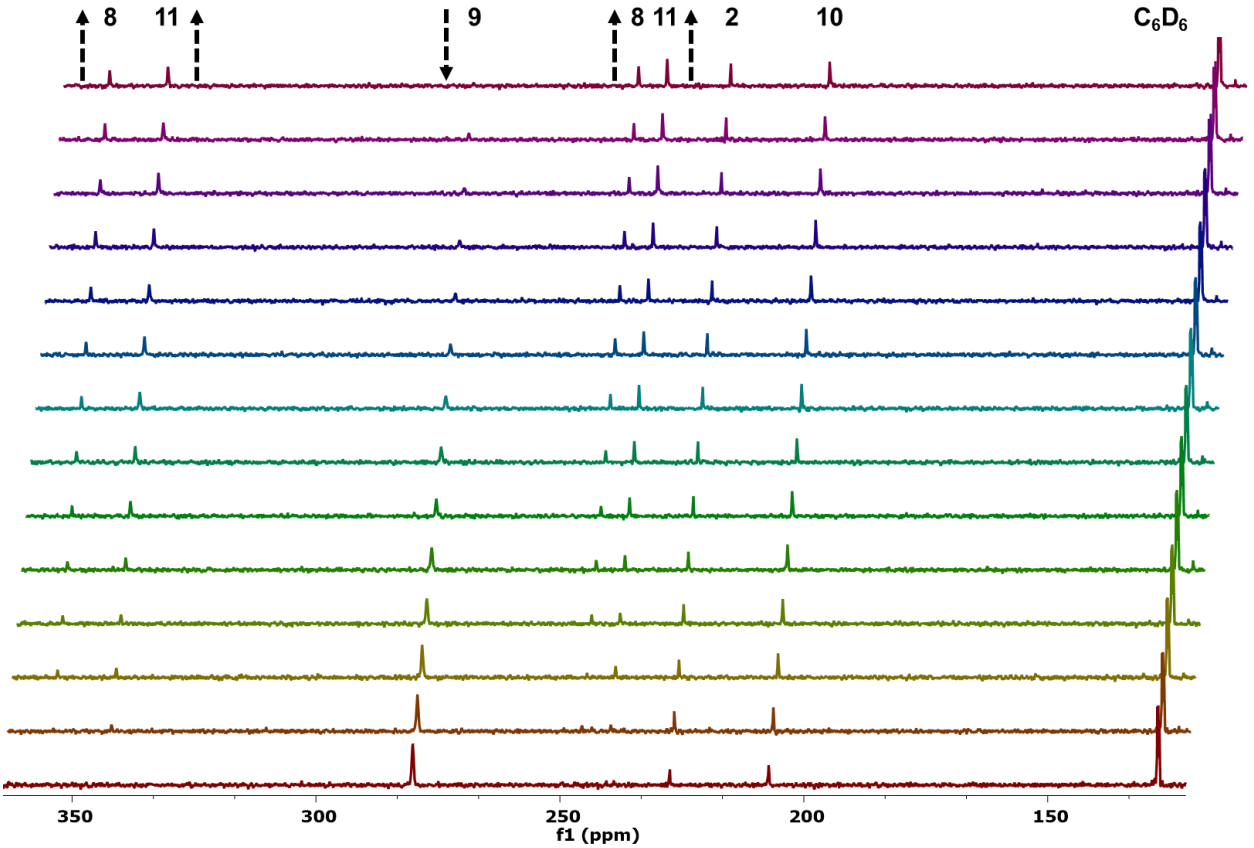

Figure S6—Representative $^{13}C\{^1H\}$ NMR spectrum array (126 MHz, 0 °C, THF) for the conversion of **9-^{13}C** to **11-^{13}C** and **8-^{13}C**. For clarity, every third spectrum collected is displayed. Small amounts of **2-^{13}C** and **10-^{13}C** were formed upon electrophilic quenching, but their concentrations remain constant over the course of the kinetics experiment (Figure S7).

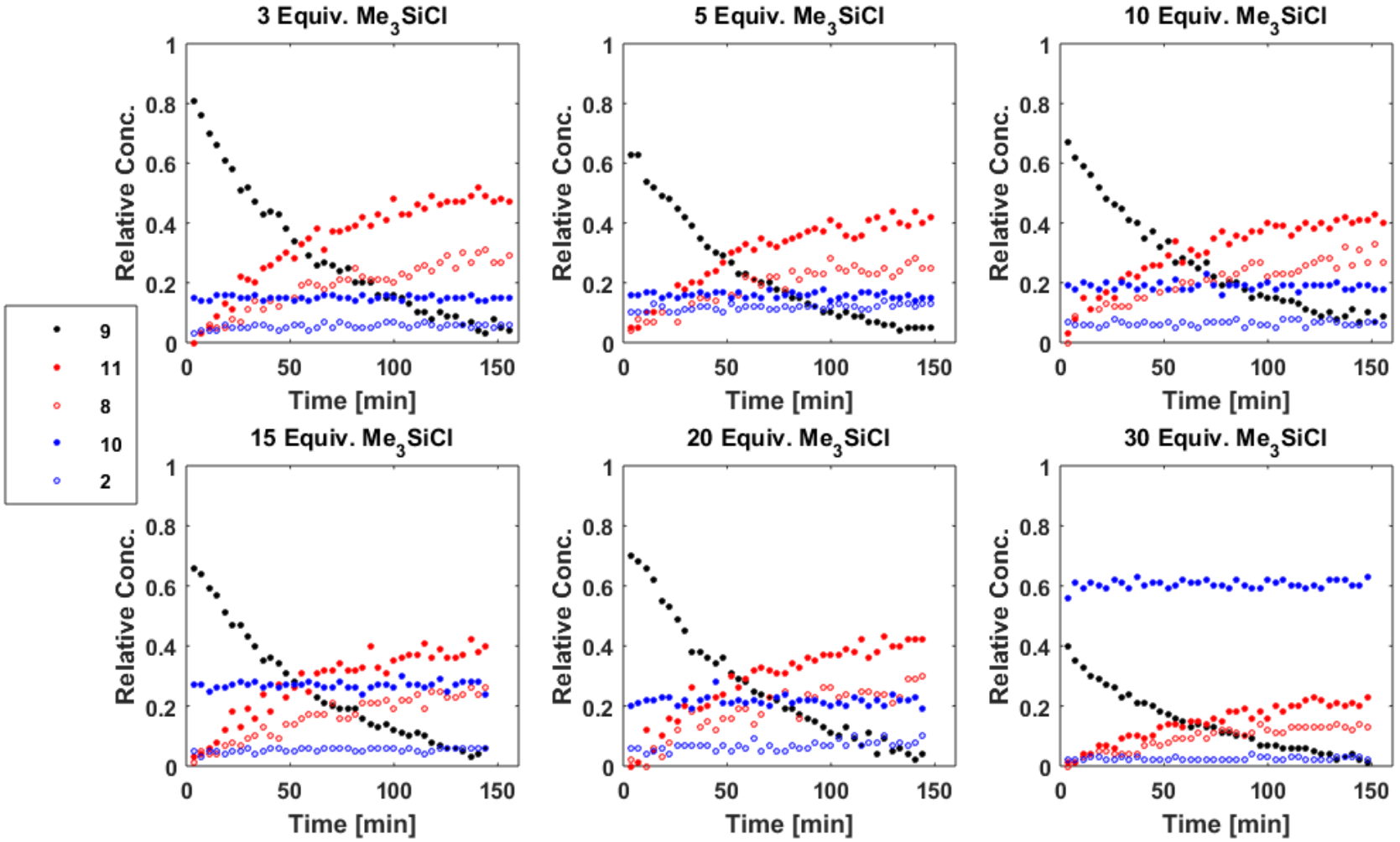

Figure S7—Relative concentration vs. time for species observed during C–O bond cleavage kinetics experiments. Variable amounts of **2-^{13}C** and **10-^{13}C** were formed in the initial addition of Me_3SiCl, but the concentrations of these complexes remain constant, within error, over the course of the reaction. Dicarbyne **9-^{13}C** is consumed and silyl carbynes **11-^{13}C** and **8-^{13}C** are concomitantly observed to grow in.

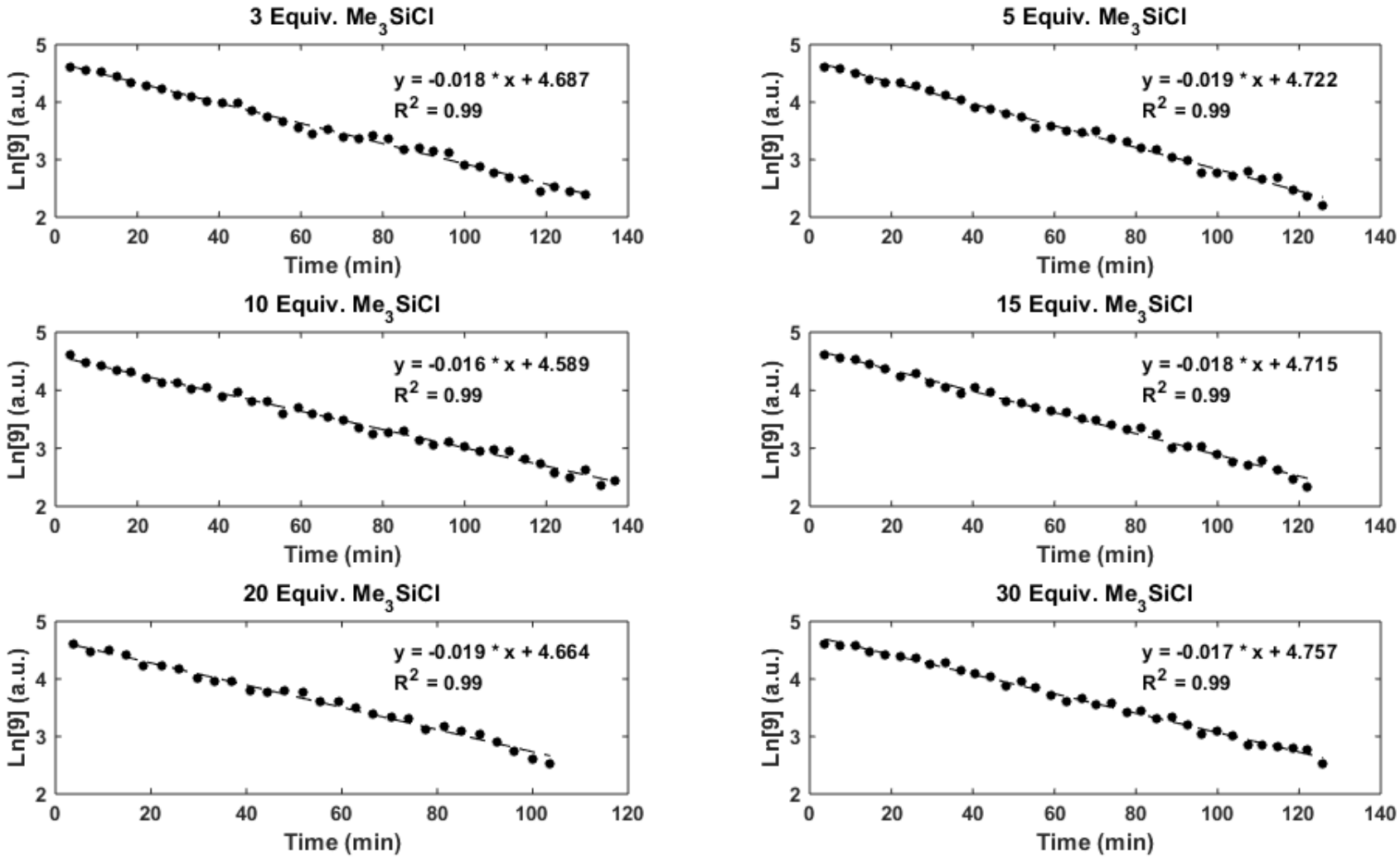

Figure S8— Log plots of [**9-^{13}C**] vs. time for variable silyl chloride concentrations as monitored by $^{13}C\{^{1}H\}$ NMR spectroscopy at 0 °C.

Rate Equations for Elementary C–O Bond Cleavage Steps

Case I: Irreversible Dicarbyne Formation

Path 1—Intramolecular HMDSO Formation from Dicarbyne 9

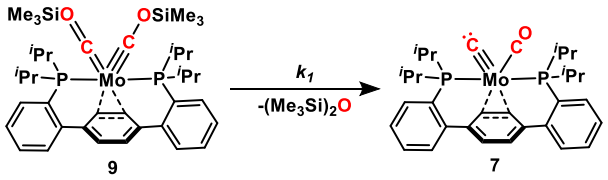

$$\text{Rate} = \frac{\text{d}[\mathbf{7}]}{\text{dt}} = k_1[\mathbf{9}] \qquad (1)$$

Overall: Zeroth order in [Me_3SiCl]

Path 2—External Silyl Electrophile Attack on Dicarbyne 9

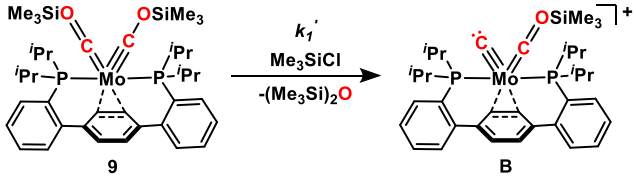

$$\text{Rate} = \frac{\text{d}[\mathbf{7}]}{\text{dt}} = k_1'[\mathbf{9}][\text{Me}_3\text{SiCl}] \qquad (2)$$

Overall: First order in [Me_3SiCl]

Path 3—Siloxide Dissociation from Dicarbyne 9

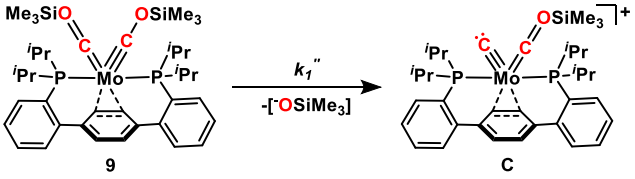

$$\text{Rate} = \frac{\text{d}[\mathbf{7}]}{\text{dt}} = \text{k}_1''[\mathbf{9}] \qquad (3)$$

Overall: Zeroth order in [Me_3SiCl]

Case II: Reversible Dicarbyne Formation—Fast Pre-Equilibrium

Path 4—External Silyl Electrophile Attack on Carbyne Anion A

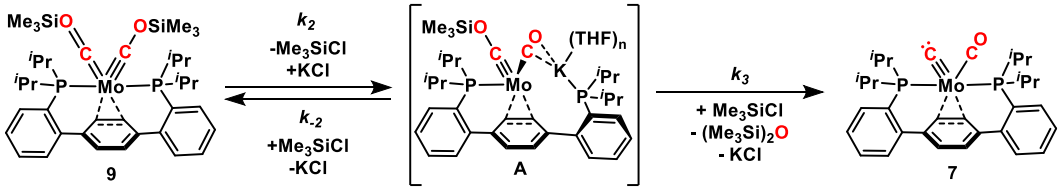

$$\text{Rate} = \frac{d[\mathbf{7}]}{dt} = k_3[\mathbf{A}][Me_3SiCl]$$

Assuming a fast pre-equilibrium between **A** and **9**:

$$K_2 = \frac{k_2}{k_{-2}} = \frac{[\mathbf{A}][Me_3SiCl]}{[\mathbf{9}][KCl]}$$

$$[\mathbf{A}] = \frac{K_2[\mathbf{9}][KCl]}{[Me_3SiCl]} \qquad \text{and let} \qquad [\mathbf{9}] = [Mo]_0 - [\mathbf{A}]$$

$$\Rightarrow [\mathbf{A}] = \frac{K_2[KCl][Mo]_0 - K_2[KCl][\mathbf{A}]}{[Me_3SiCl]}$$

$$\Rightarrow [\mathbf{A}] + \frac{K_2[KCl][\mathbf{A}]}{[Me_3SiCl]} = \frac{K_2[KCl][Mo]_0}{[Me_3SiCl]}$$

$$\Rightarrow [\mathbf{A}]\left(1 + \frac{K_2[KCl]}{[Me_3SiCl]}\right) = \frac{K_2[KCl][Mo]_0}{[Me_3SiCl]}$$

$$\Rightarrow [\mathbf{A}] = \frac{K_2[KCl][Mo]_0}{[Me_3SiCl]\left(1 + \frac{K_2[KCl]}{[Me_3SiCl]}\right)} = \frac{K_2[KCl][Mo]_0}{[Me_3SiCl] + K_2[KCl]}$$

$$\therefore \frac{d[\mathbf{7}]}{dt} = k_3[\mathbf{A}][Me_3SiCl] = \frac{k_3K_2[KCl][Me_3SiCl][Mo]_0}{[Me_3SiCl] + K_2[KCl]} = \frac{\frac{k_2k_3}{k_{-2}}[KCl][Me_3SiCl][Mo]_0}{[Me_3SiCl] + \frac{k_2}{k_{-2}}[KCl]}$$

$$\Rightarrow \frac{d[\mathbf{7}]}{dt} = \frac{k_2k_3[KCl][Me_3SiCl][Mo]_0}{k_{-2}[Me_3SiCl] + k_2[KCl]} \qquad (4)$$

Overall: Complex positive rate dependence on [Me_3SiCl]

Assuming $k_{-2} >> k_2$ (consistent with spectroscopic observation of **9** only):

$$\text{Then} \qquad \frac{d[\mathbf{7}]}{dt} = \frac{k_2k_3[KCl][Me_3SiCl][Mo]_0}{k_{-2}[Me_3SiCl]} = \frac{k_2k_3}{k_{-2}}[KCl][Mo]_0 \qquad (4a)$$

Overall: Zeroth order in [Me_3SiCl]

Path 5—Siloxide Dissociation from Carbyne Anion A

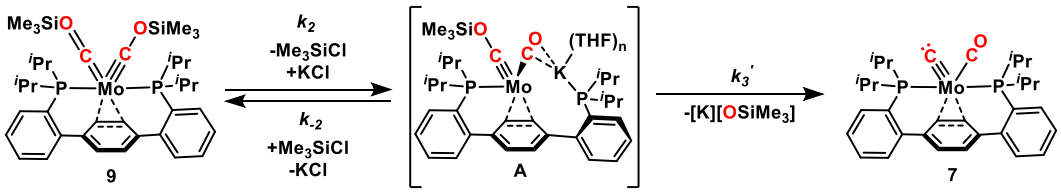

$$\text{Rate} = \frac{d[\mathbf{7}]}{dt} = k_3'[\mathbf{A}]$$

Assuming a fast pre-equilibrium between **A** and **9** (the pre-equilibrium expression is the same as in Path 4 above):

$$\Rightarrow [\mathbf{A}] = \frac{K_2[KCl][Mo]_0}{[Me_3SiCl] + K_2[KCl]}$$

$$\therefore \frac{d[\mathbf{7}]}{dt} = k_3'[\mathbf{A}] = \frac{k_3'K_2[KCl][Mo]_0}{[Me_3SiCl] + K_2[KCl]} = \frac{\frac{k_2k_3'}{k_{-2}}[KCl][Mo]_0}{[Me_3SiCl] + \frac{k_2}{k_{-2}}[KCl]}$$

$$\Rightarrow \frac{d[\mathbf{7}]}{dt} = \frac{k_2k_3'[KCl][Mo]_0}{k_{-2}[Me_3SiCl] + k_2[KCl]} \qquad (5)$$

Assuming $k_{-2} >> k_2$ (consistent with spectroscopic observation of **9** only):

$$\text{Then} \qquad \frac{d[\mathbf{7}]}{dt} = \frac{k_2k_3'[KCl][Mo]_0}{k_{-2}[Me_3SiCl]} = \frac{k_2k_3'[KCl][Mo]_0}{k_{-2}[Me_3SiCl]} \qquad (5a)$$

Overall: Inverse first order in [Me_3SiCl]

Case II: Reversible Dicarbyne Formation—Rate Limiting Formation of A

Path 4—External Silyl Electrophile Attack on Carbyne Anion A

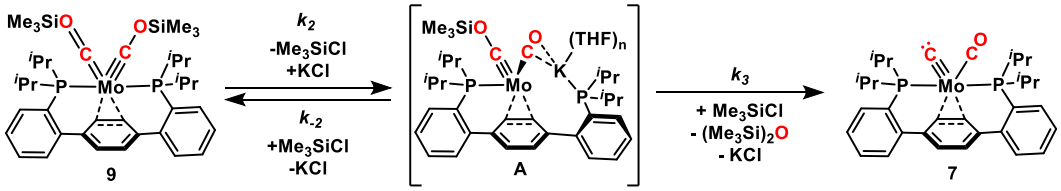

$$\text{Rate} = \frac{d[\mathbf{7}]}{dt} = k_3[\mathbf{A}][Me_3SiCl]$$

Applying the steady-state approximation:

$$\text{Assume} \quad \frac{d[\mathbf{A}]}{dt} = 0 = k_2[\mathbf{9}][KCl] - k_{-2}[\mathbf{A}][Me_3SiCl] - k_3[\mathbf{A}][Me_3SiCl]$$

$$\Rightarrow k_2[\mathbf{9}][KCl] = [\mathbf{A}][Me_3SiCl](k_{-2} + k_3)$$

$$\Rightarrow [\mathbf{A}] = \frac{k_2[\mathbf{9}][KCl]}{[Me_3SiCl](k_{-2} + k_3)}$$

$$\therefore \frac{d[\mathbf{7}]}{dt} = \frac{k_2k_3[\mathbf{9}][KCl][Me_3SiCl]}{[Me_3SiCl](k_{-2} + k_3)} = \frac{k_2k_3}{(k_{-2} + k_3)}[\mathbf{9}][KCl] \qquad (6)$$

Overall: Zeroth order in [Me_3SiCl]

Path 5—Siloxide Dissociation from Carbyne Anion A

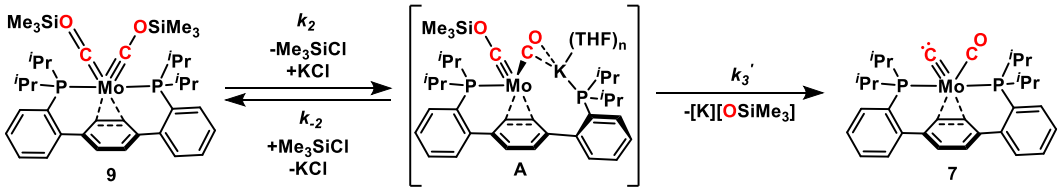

$$\text{Rate} = \frac{d[\mathbf{7}]}{dt} = k_3'[\mathbf{A}]$$

Applying the steady-state approximation:

$$\text{Assume} \quad \frac{d[\mathbf{A}]}{dt} = 0 = k_2[\mathbf{9}][KCl] - k_{-2}[\mathbf{A}][Me_3SiCl] - k_3'[\mathbf{A}]$$

$$\Rightarrow k_2[\mathbf{9}][KCl] = [\mathbf{A}](k_{-2}[Me_3SiCl] - k_3')$$

$$\Rightarrow [\mathbf{A}] = \frac{k_2[\mathbf{9}][KCl]}{k_{-2}[Me_3SiCl] + k_3'}$$

$$\therefore \frac{d[\mathbf{7}]}{dt} = \frac{k_2 k_3'}{k_{-2}[Me_3SiCl] + k_3'}[\mathbf{9}][KCl] \qquad (7)$$

Overall: Complex inverse rate dependence on [Me_3SiCl]

Assuming the rate of C–O bond cleavage is much faster than the rate of resilylation (*ie:* $k_3' >> k_{-2}[Me_3SiCl]$):

$$\frac{d[\mathbf{7}]}{dt} = \frac{k_2 k_3'}{k_3'}[\mathbf{9}] = k_2[\mathbf{9}] \qquad (7a)$$

Overall: Zeroth order in [Me_3SiCl]

Isotopic Labeling Experiments Employing $(CD_3)_3SiCl$

Reactivity of **9-^{13}C** *with Excess* $(CD_3)_3SiCl$

A J. Young NMR tube was charged with 600 μL of a deep red solution of **3-^{13}C** (20 mg, 0.022 mmol) in THF. One drop of C_6D_6 was added as an internal standard for NMR spectroscopy. This tube was degassed thoroughly via three freeze-pump-thaw cycles. Following the third evacuation, the tube was left frozen in liquid nitrogen, and Me_3SiCl was admitted via condensation from a calibrated gas bulb (33.4 mL at 2.5 cm Hg, 0.045 mmol). The tube was sealed and thawed to -80 °C, at which point it was mixed cold and refrozen. $^{13}C\{^1H\}$ and $^{31}P\{^1H\}$ NMR of this sample (-80 °C) showed conversion of the starting material to a mixture of **9-^{13}C** (61%), **10-^{13}C** (10%), **3-^{13}C** (23%) and **2-^{13}C** (6%) (Figure S9). The tube was reattached to the vacuum line and the contents refrozen. To complete the conversion of **3-^{13}C** to **9-^{13}C**, additional Me_3SiCl (33.4 mL at 0.6 cm Hg, 0.011 mmol) was condensed into the J. Young tube as before. The sample was thawed to -78 °C, mixed vigorously, and refrozen.

$(CD_3)_3SiCl$ was admitted, in two portions, via condensation from a calibrated gas bulb (33.4 mL at 6.2 cm Hg per addition, 0.225 mmol total). The tube was thawed, mixed, and the reaction mixture was again analyzed by multinuclear NMR spectroscopy. allowed to warm to room temperature.

During this time, an oven-dried 100 mL Schlenk tube was charged with a stir bar, 4-^{t}Bu-PhONa (56.8 mg, 0.330 mmol), and THF (2 mL). The reaction mixture from the J. Young NMR tube was vacuum transferred into this collection flask. Following the transfer, the contents of the Schlenk tube were stirred at room temperature for 30 minutes and then vacuum transferred a second time into an empty Schlenk tube. Aliquots from this vessel were filtered through alumina and analyzed by GC/MS.

The terminal metal products of the reaction were analyzed via multinuclear NMR spectroscopy following addition of C_6D_6 (ca. 400 μL) to the reaction J. Young NMR tube via vacuum transfer, indicating near exclusive deuteration at the silyl carbyne position (Figure S9).

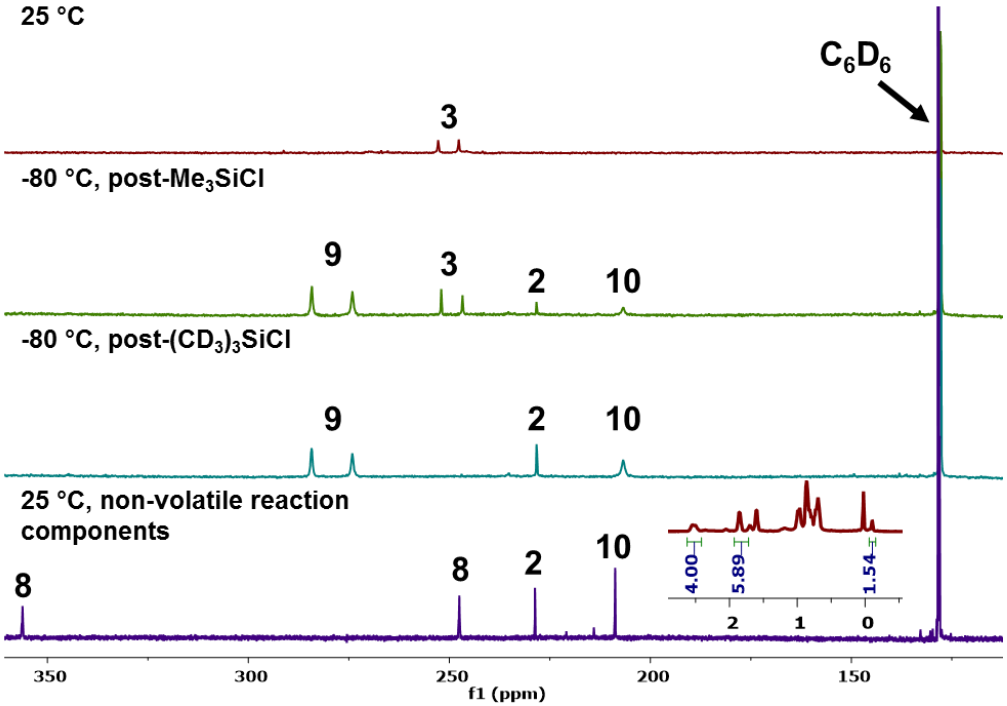

Figure S9—$^{13}C\{^1H\}$ NMR spectra following the addition of proteo- and deutero-silyl electrophiles to **3-^{13}C**. The inset shows the upfield region of the ^1H NMR spectrum (500 MHz, C_6D_6, 25 °C) of the non-volatile reaction components.

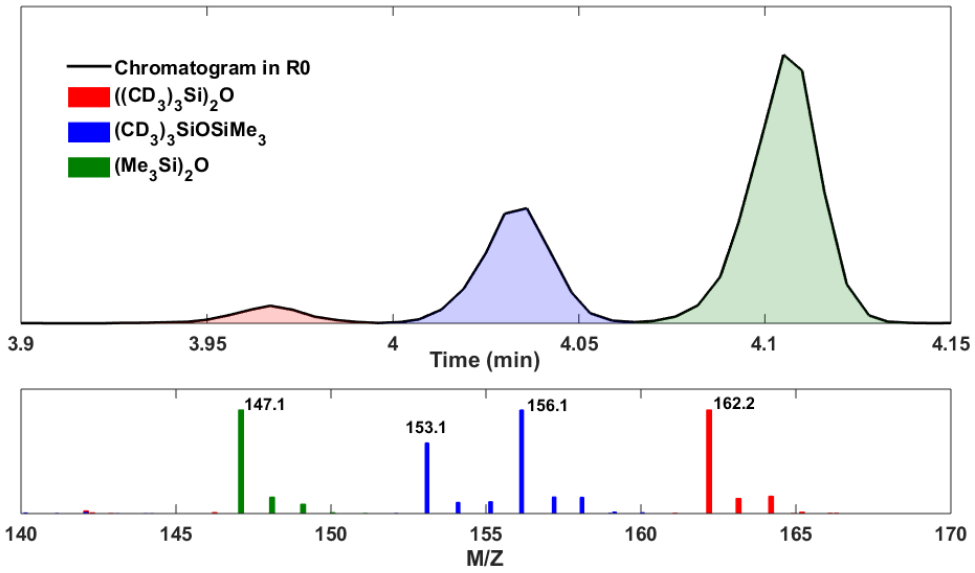

Figure S10—Partial gas chromatogram (top) and mass spectrum (bottom) of the HMDSO generated from warming **9-^{13}C** in the presence of excess $(CD_3)_3SiCl$. The isotopologs of HMDSO were resolved in the GC trace and the normalized mass spectra corresponding to each region are color coded.

Reactivity of **9-^{13}C-*d*$_{18}$** *with Excess* Me_3SiCl

This reaction was conducted analogously to that described for the addition of excess $(CD_3)_3SiCl$ to **9-^{13}C** except the deuterated silyl chloride was added first (2 equiv.) and the proteo silyl electrophile was added second, in excess (10 equiv.). Following addition of $(CD_3)_3SiCl$, the reaction mixture was comprised of **9-^{13}C-*d*$_{18}$** (77%), **10-^{13}C-*d*$_{18}$** (14%), and **2-^{13}C** (9%). The terminal metal products of the reaction were analyzed as described above, and indicate near exclusive protonation at the silyl carbyne position (Figure S11).

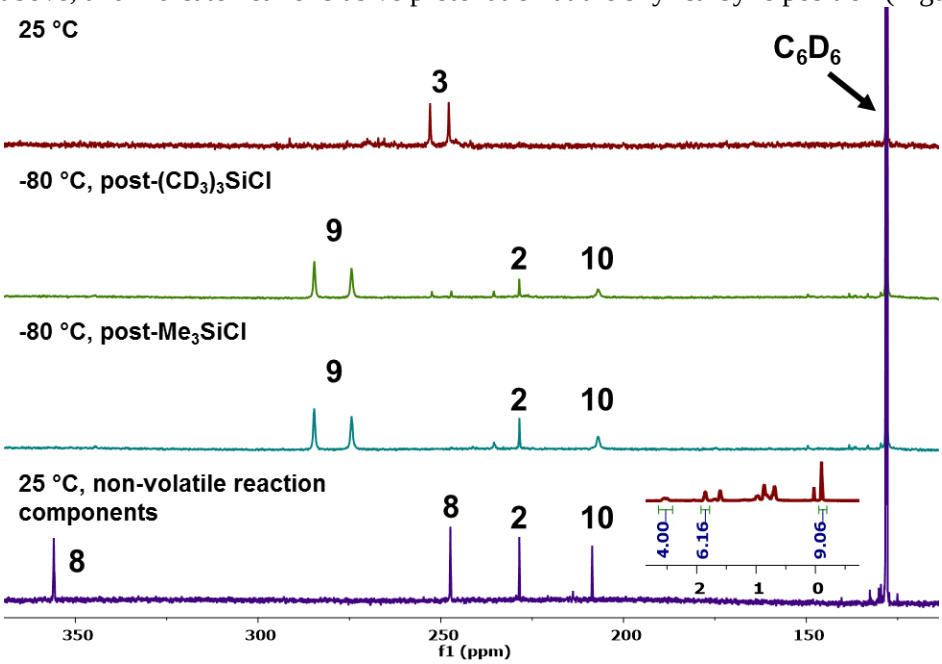

Figure S11—$^{13}C\{^1H\}$ NMR spectra following the addition of deutero- and proteo-silyl electrophiles to **3-^{13}C**. The inset shows the upfield region of the ^1H NMR spectrum (500 MHz, C_6D_6, 25 °C) of the non-volatile reaction components.

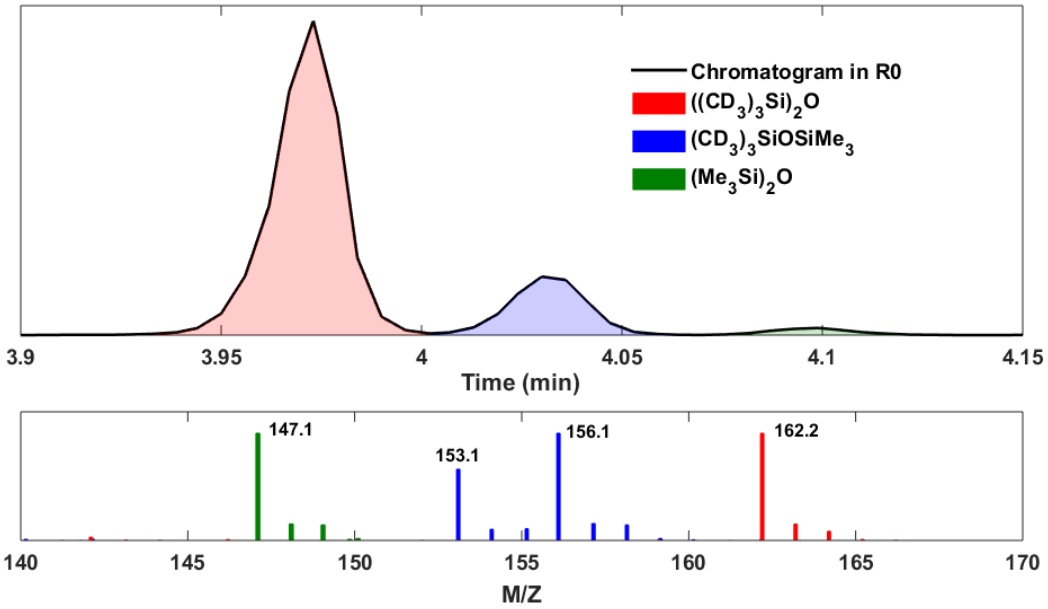

Figure S12—Partial gas chromatogram (top) and mass spectrum (bottom) of the HMDSO generated from warming **9-^{13}C-*d*$_{18}$** in the presence of excess Me_3SiCl. The isotopologs of HMDSO were resolved in the GC trace and the normalized mass spectra corresponding to each region are color coded.

Reaction Monitoring via ^{2}H NMR Spectroscopy

^{2}H NMR spectra of the reaction mixtures at different stages were collected to observe the fate of the deuterated trimethyl silyl fragment. These data are inconsistent with a fast exchange process scrambling the labeled electrophile onto (Figure S13, left) or off of (Firgure S13, right) dicarbyne **9**. Though a small amount of free $(CD_3)_3SiCl$ is observed upon warming the reaction mixture to 0 °C (Figure S13, panel 3, right), a temperature at which C–O cleavage is known to proceed, this is attributed to silyl dissociation from **9** (Scheme 4) rather than an exchange process. In the latter case, a statistical distribution of silyl electrophiles would be expected (83% **9-^{13}C**, 17% **9-^{13}C-*d*$_{18}$**). Moreover, the deuterated label is not observed to be incorporated into the metal complex in the complimentary experiment (Figure S13, left).

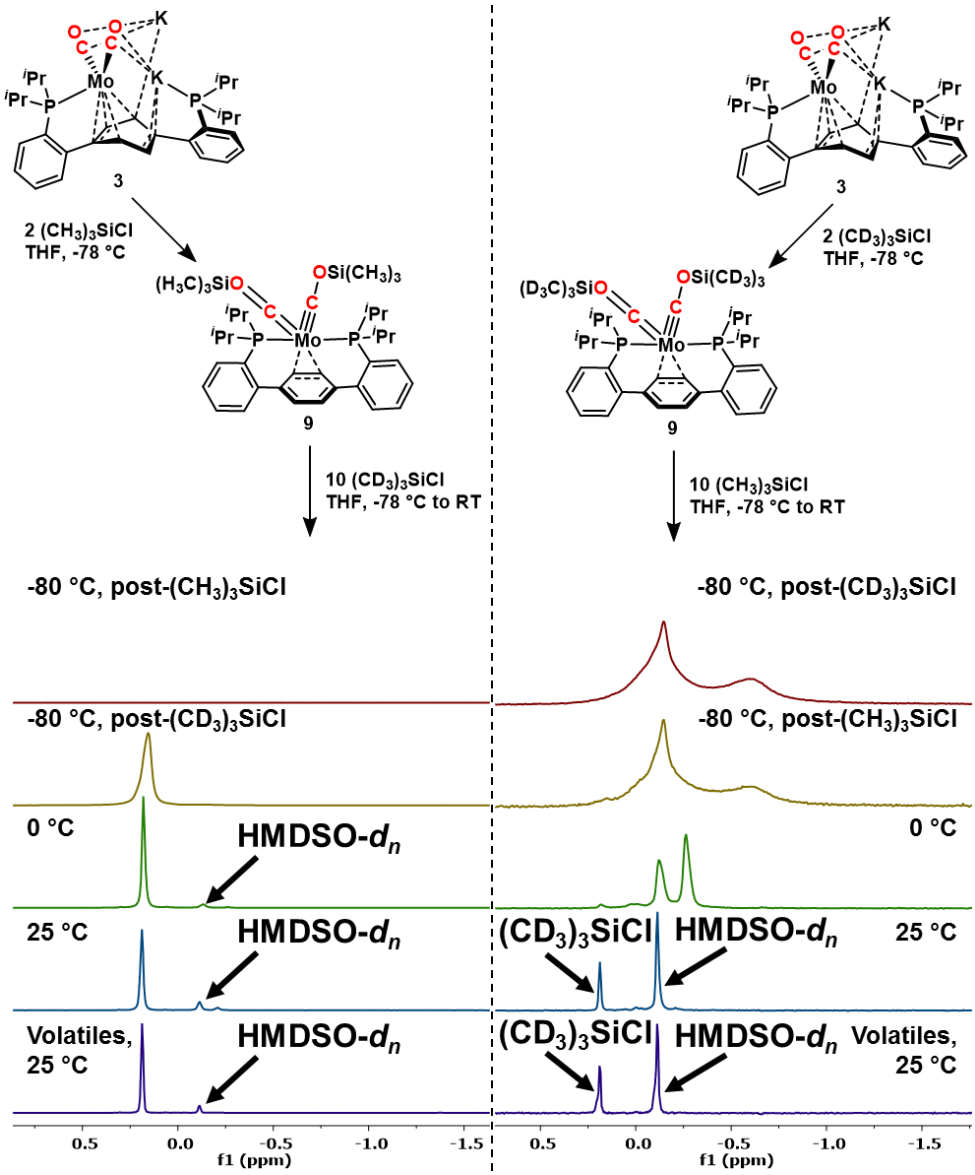

Figure S13—Partial ^{2}H NMR spectra at various stages of the isotopic labeling experiments. A small amount of free $(CD_3)_3SiCl$ is detected when **9-^{13}C-*d*$_{18}$** is warmed to 0 °C in the presence of excess Me_3SiCl (right).

Control Reaction for Sequestration of Excess Silyl Chloride

A concern with HMDSO isotopolog end product analysis was siloxane formation from silyl chloride hydrolysis. To avoid this, the excess trimethylsilyl chloride remaining in the reaction mixture was sequestered with dry 4-^{t}Bu-PhONa (see experimental procedure description). To ensure that the phenoxide was not leading to silyl group redistribution, a control experiment was performed as follows. A J. Young NMR tube was charged with 4-^{t}Bu-PhONa (30 mg, 0.174 mmol) and THF (500 µL). The contents of the tube were degassed via three freeze-pump-thaw cycles and Me_3SiCl (33.4 mL at 4 cm Hg, 0.072 mmol), $(CD_3)_3SiCl$ (33.4 mL at 4 cm Hg, 0.072 mmol), and $(Me_3Si)_2O$ (33.4 mL at 4 cm Hg, 0.072 mmol) were sequentially condensed into the reaction vessel. The J. Young tube was sealed, the contents thawed, and the reaction mixed via inversion for 30 minutes. The reaction volatiles were vacuum transferred to a Schlenk tube and an aliquot was removed, filtered through alumina, and analyzed by GC/MS—$(Me_3Si)_2O$, 4-^{t}Bu-$PhOSiMe_3$, and 4-^{t}Bu-$PhOSi(CD_3)_3$ were observed (Figure S14).

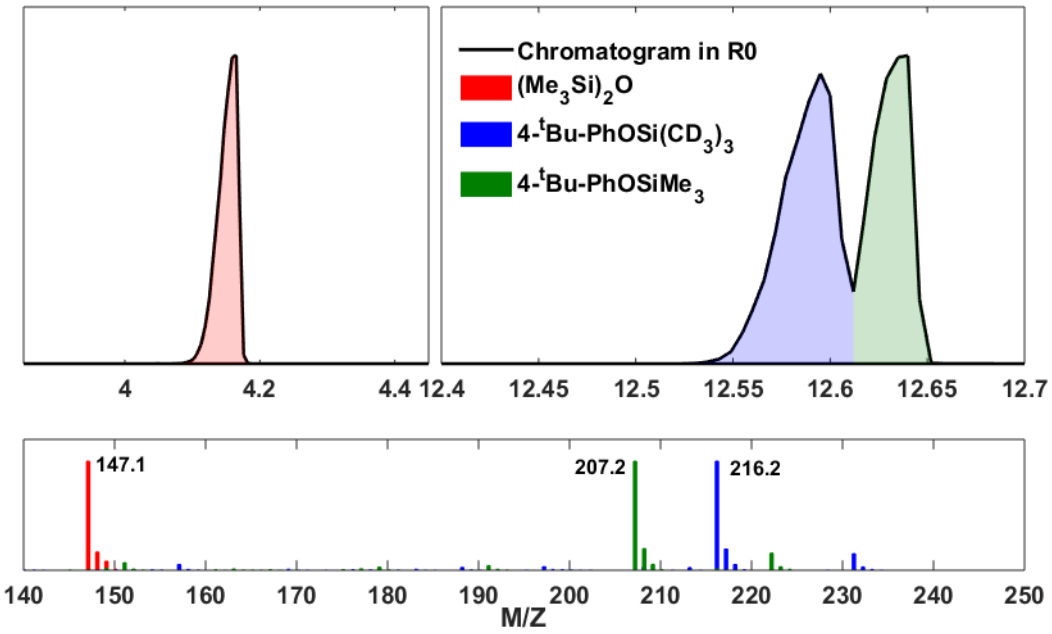

Figure S14—Partial gas chromatogram (top) and mass spectrum (bottom) of the control reaction for silyl chloride sequestration by 4-^{t}Bu-PhONa.

$NaOSiMe_3$ *Mediated Silyl Scrambling*

The possibility of silyl group scrambling via siloxide initiated substitution chemistry was likewise explored. In an attempt to mimic reaction conditions, sodium trimethyl siloxide and HMDSO were present in a ten-fold subcess with respect to silyl chloride.

A J. Young NMR tube was charged with 500 μL of a THF solution of $NaOSiMe_3$ (5 mg, 0.045 mmol). The tube was degassed via three freeze-pump-thaw cycles. Following the third evacuation, the contents of the tube were left frozen and HMDSO (33.4 mL at 2.5 cm Hg, 0.045 mmol) was added via condensation from a calibrated gas bulb. Still without thawing, $(CD_3)_3SiCl$ was admitted, in two portions, via condensation from a calibrated gas bulb (33.4 mL at 12.6 cm Hg twice, 0.450 mmol total). The tube was sealed and the contents thawed; the reaction was mixed vigorously immediately upon thawing.

The resulting clear reaction mixture was vacuum transferred into a dry Schlenk tube charged with 4-^{t}Bu-PhONa (100 mg, 0.581 mmol) and a stir bar and mixed for 30 minutes. The volatiles were again vacuum transferred, this time to an empty Schlenk tube, and an aliquot was removed, filtered through alumina, and analyzed by GC/MS (Figure S15).

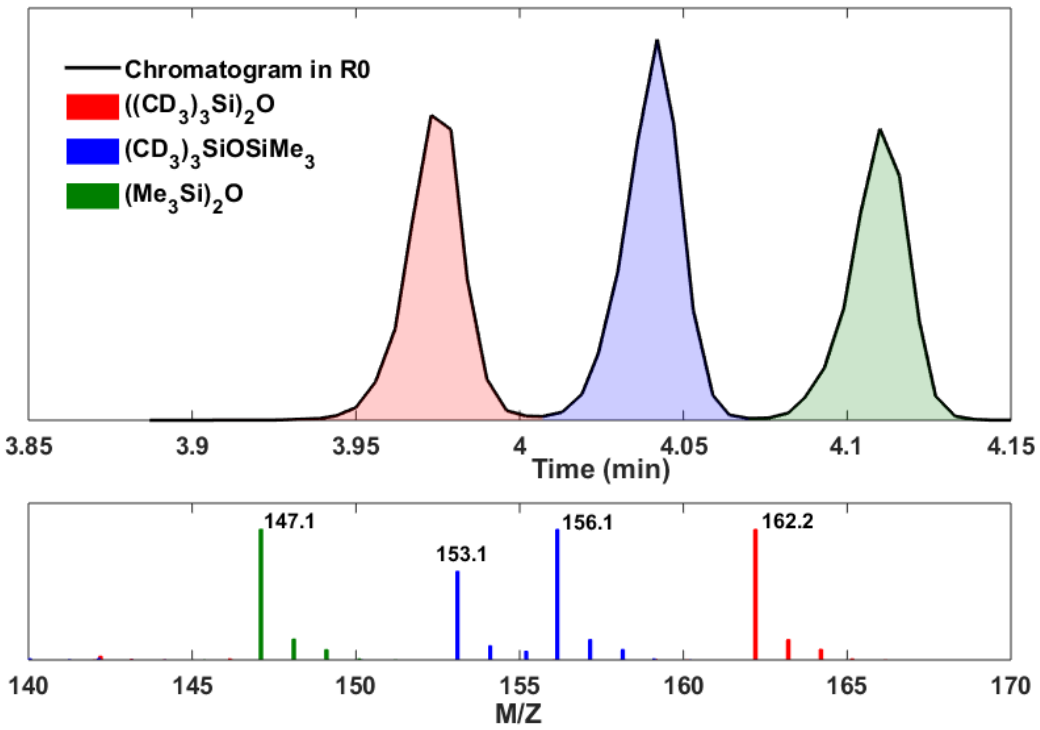

Figure S15—Partial gas chromatogram (top) and mass spectrum (bottom) supporting siloxide mediated silyl group scrambling.

Addition of 1 Equiv. of Me_3SiCl to Dianion **3-^{13}C**

A J. Young NMR tube was charged with a deep red THF solution (600 µL) of **3-^{13}C** (20 mg, 0.022 mmol). The tube was degassed via three freeze-pump-thaw cycles. Following the third evacuation, the tube was left immersed in the liquid nitrogen cooling bath and Me_3SiCl (33.4 mL at 1.24 cm Hg, 0.023 mmol) was condensed onto the frozen reaction mixture. The tube was thawed, mixed thoroughly whilst cold, and placed in a -78 °C dry ice/acetone cold bath. $^{13}C\{^1H\}$ and $^{31}P\{^1H\}$ NMR spectra were collected at -80 °C (Figure S16), ensuring the sample remained cold. Resonances in the $^{13}C\{^1H\}$ NMR spectrum at 263.6 and 232.7 ppm are within the range of Mo siloxycarbyne and Mo carbonyl carbons, respectively. This new species likewise shows $^{31}P\{^1H\}$ resonances at 97.6 and -2.8 ppm, leading to assignment of this complex as carbyne anion **A**.

In this same sample, dianion **3-^{13}C** and dicarbyne **9-^{13}C** were present, presumably due to rapid disilylation of starting material, even at low temperature. The resonances for **3-^{13}C** in the $^{13}C\{^1H\}$ NMR spectrum are in excellent agreement with an authentic sample; however, the $^{31}P\{^1H\}$ resonances shift to 99.6 and -2.8 ppm for the bound and free phosphine arms, respectively. The upfield shifted phosphine signal is attributed to breaking of the dimeric structure of **3-^{13}C** upon partial silylation. The free phosphine resonances for both **3** and **A** coincide at -80 °C but start to separate at -70 °C (Figure S16, inset); integration supports both species having a high-field phosphine resonance consistent with an arm-on/arm-off structure. We disfavor a silyl exchange process leading to the upfield shift observed for the Mo-bound phosphine for **3** in these samples, as resonances at both 107.3 and 99.6 ppm are observed simultaneously in some samples (*cf.* Figure S17, panels 2 and 3).

Following NMR spectroscopy, the tube was refrozen and a second addition of Me_3SiCl (33.4 mL at 1.24 cm Hg, 0.023 mmol) was added. The tube was thawed, mixed thoroughly whilst cold, and placed in a -78 °C dry ice/acetone cold bath. $^{13}C\{^1H\}$ and $^{31}P\{^1H\}$ NMR spectra were collected at -80 °C (Figure S16), and

demonstrate conversion to **9-^{13}C**. This reactivity is both consistent with the assignment of **A** as a siloxycarbyne carbonyl anion as well as the assignment of the $^{31}P\{^{1}H\}$ resonance at 99.7 ppm to dianion **3**.

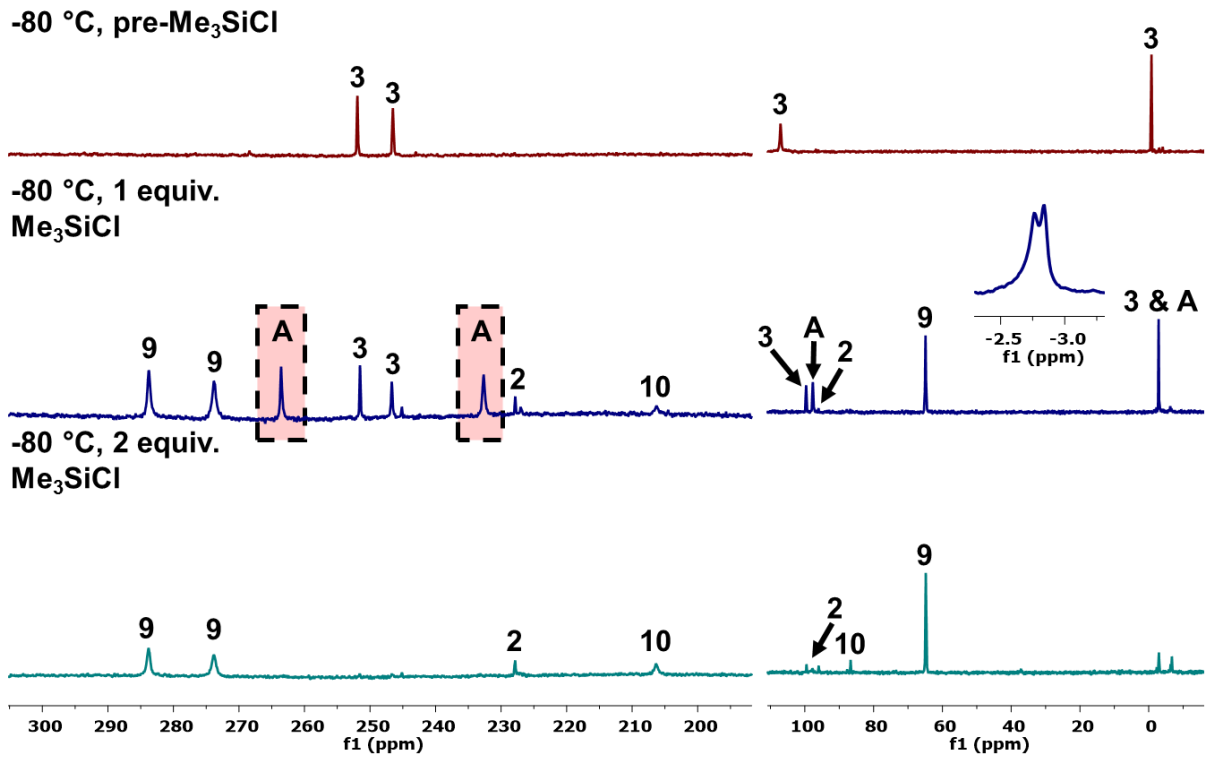

Figure S16—Stacked $^{13}C\{^{1}H\}$ (left) and $^{31}P\{^{1}H\}$ (right) spectra supporting the formation of an anionic siloxycarbyne complex, **A**. The downfield region of the $^{13}C\{^{1}H\}$ NMR spectra show formation of an intermediate (denoted **A**, highlighted in red) upon treating dianion **3** with a single equiv. of Me_3SiCl at low temperature. Starting material (**3**) and the bis(siloxycarbyne) complex (**9**) are also observed in this reaction mixture. The inset shows the decoalescence of the resonances assigned to the free phosphine arms in **3** and **A** observed at -70 °C. Following addition of a second equiv. of Me_3SiCl, **9** is formed as the major species.

C–O Bond Cleavage from a Mixture of **3**, **9**, *and* **A**

A J. Young NMR tube was charged with a deep red THF solution (600 μL) of **3-^{13}C** (10 mg, 0.011 mmol). The tube was degassed via three freeze-pump-thaw cycles. Following the third evacuation, the tube was left immersed in the liquid nitrogen cooling bath and Me_3SiCl (2.8 mL at 2.4 cm Hg, 0.004 mmol) was condensed into the frozen reaction mixture. The tube was thawed, mixed thoroughly whilst cold, and refrozen. Two more Me_3SiCl additions (2.8 mL at 2.4 cm Hg, 0.004 mmol) were made in the same manner (0.012 mmol total), again mixing the contents of the tube between additions. The tube was submerged in liquid nitrogen to freeze the contents and thawed immediately before transfer to an NMR probe pre-cooled to -80 °C, demonstrating a mixture of **3-^{13}C**, **A-^{13}C**, and **9-^{13}C** by $^{13}C\{^{1}H\}$ and $^{31}P\{^{1}H\}$ NMR spectroscopy (Figure S17, top panel). This mixture was warmed in 10 °C increments in the NMR probe; $^{13}C\{^{1}H\}$ and $^{31}P\{^{1}H\}$ NMR spectra were collected at each temperature step (Figure S17). Upon reaching -50 °C, complete consumption of putative carbyne anion **A** was observed.

The resulting mixture demonstrated several carbonyl resonances in the $^{13}C\{^{1}H\}$ NMR spectrum from 225 to 235 ppm (Figure S17, panels 4 and 5). The $^{31}P\{^{1}H\}$ NMR spectrum displayed new resonances upfield of 65 ppm, consistent with higher valent Mo species. However, these spectroscopic features did not match the expected product of C–O bond cleavage in the absence of excess silyl electrophile, carbide **7**. Hypothesizing

that **7** may have been reduced *in situ* by remaining dianion **3**, the mixture was removed from the NMR probe and refrozen. Excess Me_3SiCl (2.8 mL at 10.8 cm Hg, thrice, 0.066 mmol total) was condensed into the J. Young tube which was resealed, mixed at low temperature, and returned to the NMR probe. At both -80 °C and -20 °C, C–O cleavage products **8-^{13}C**, **11-^{13}C**, and **15-^{13}C** were observed. Dicarbyne **9-^{13}C**, oxidation byproduct **2-^{13}C**, and bis(siloxy)acetylene adduct **10-^{13}C** account for the balance of the Mo species in solution (Figure S17, bottom panel).

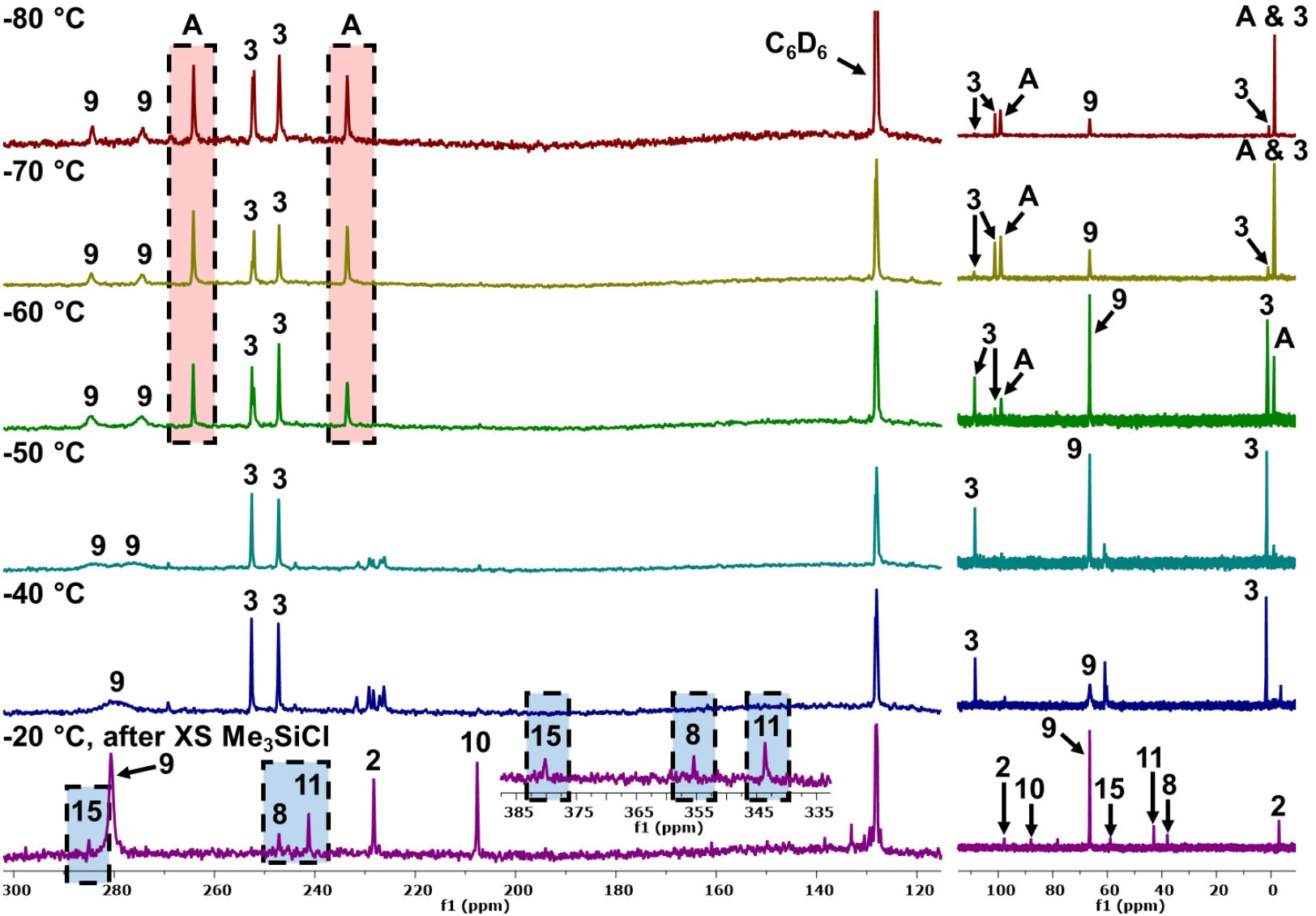

Figure S17—Partial $^{13}C\{^{1}H\}$ and $^{31}P\{^{1}H\}$ NMR spectra monitoring the formation and C–O bond cleavage reactivity of proposed siloxycarbyne anion **A**. Complete consumption of **A** is observed upon warming to -50 °C. Though this provided an intractable mixture, low temperature silylation resulted in the formation of three C–O cleaved products—silyl carbynes **8** and **11** as well as mixed dicarbyne **15**.

Reactions from Carbide 7 and Mixed Dicarbynes

Silylation Reactions: Me_3SiCl

A J. Young NMR tube was charged with **8-^{13}C** (15 mg, 0.021 mmol) and $^{n}Bu_4NF$ (7.3 mg, 0.028 mmol). The headspace of the NMR tube was evacuated and THF-d_8 (400 µL) admitted at -196 °C via vacuum transfer. The contents of the J. Young tube were thawed to -78 °C and mixed. Warming to -20 °C in the NMR probe for 15 minutes showed complete conversion to **7-^{13}C** by $^{13}C\{^{1}H\}$ and $^{31}P\{^{1}H\}$ NMR spectroscopy (Figure S18, top).

The tube was returned to a -78 °C acetone/dry ice slush and a with a heavy argon counterflow, a THF (100 µL) solution of Me_3SiCl was added via syringe. The J. Young tube was inverted quickly to mix and returned to the -80 °C NMR spectrometer, showing complete conversion to **11-^{13}C** (71%) and **8-^{13}C** (29%) by $^{13}C\{^{1}H\}$ and $^{31}P\{^{1}H\}$ NMR spectroscopies (Figure S18, middle).

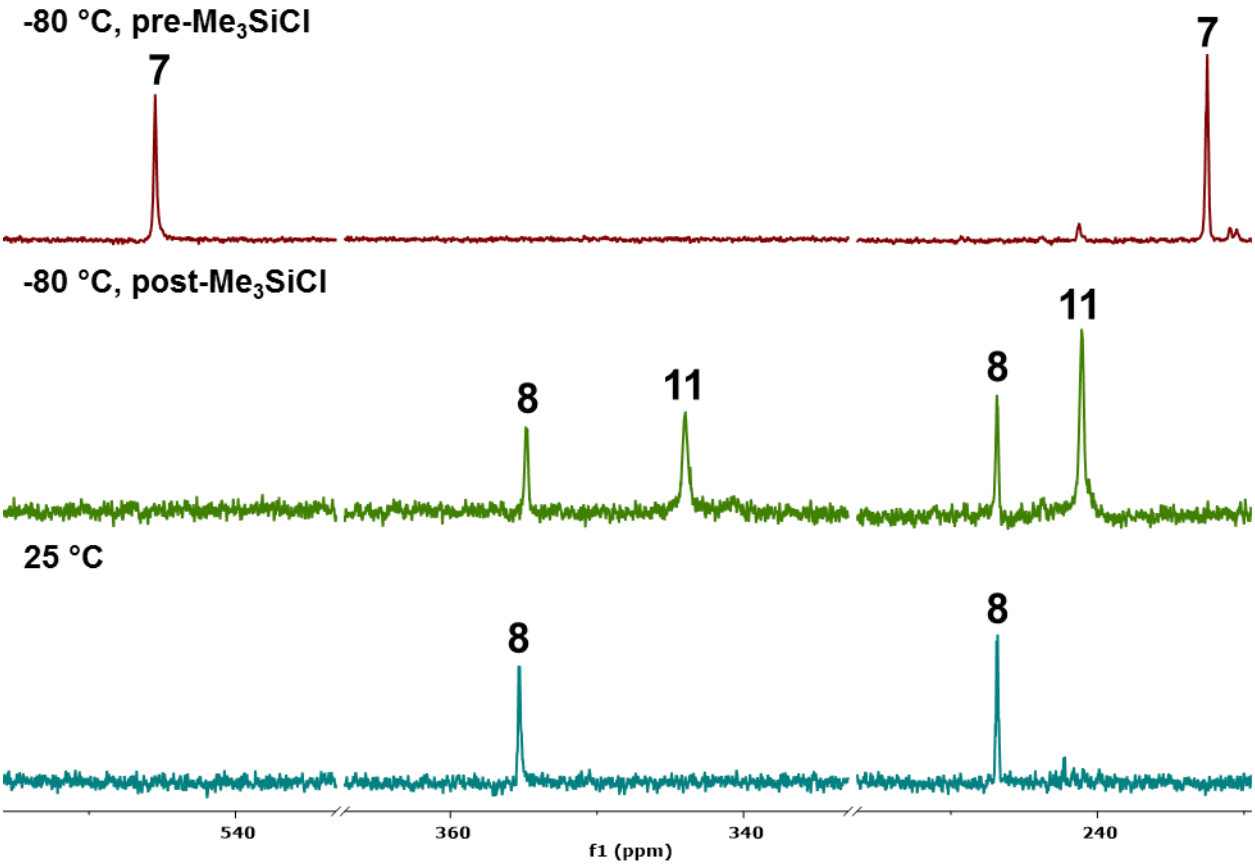

Figure S18—Partial $^{13}C\{^{1}H\}$ NMR spectra of the *in situ* generation and silylation of **7-^{13}C** with Me_3SiCl.

Silylation Reactions: $^{i}Pr_3SiCl$

A J. Young NMR tube was charged with **8-^{13}C** (17 mg, 0.024 mmol) and $^{n}Bu_4NF$ (6.9 mg, 0.026 mmol). The headspace of the NMR tube was evacuated and THF-d_8 (400 µL) admitted at -196 °C via vacuum transfer. The contents of the J. Young tube were thawed to -78 °C and mixed. Warming to -20 °C in the NMR probe for 15 minutes showed complete conversion to **7-^{13}C** by $^{13}C\{^{1}H\}$ and $^{31}P\{^{1}H\}$ NMR spectroscopy (Figure S19, top).

The tube was returned to a -78 °C acetone/dry ice slush and a with a heavy argon counterflow, a THF (100 µL) solution of $^{i}Pr_3SiCl$ (14.5 µL, 0.114 mmol) was added via syringe. The J. Young tube was

inverted quickly to mix and returned to the -80 °C NMR spectrometer. $^{13}C\{^{1}H\}$ and $^{31}P\{^{1}H\}$ NMR spectra were collected from -80 °C to 10 °C, monitoring the conversion of **7-^{13}C** to **12-^{13}C**.

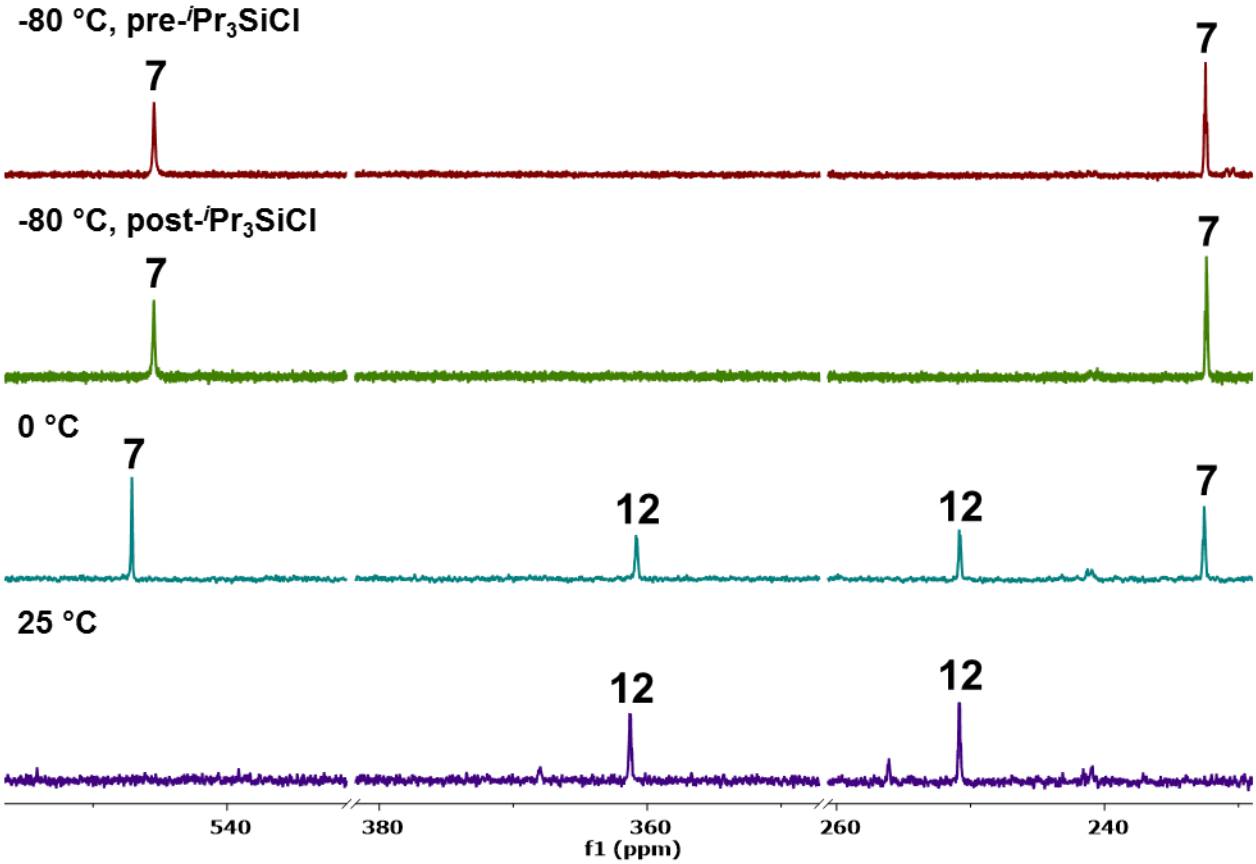

Figure S19— Partial $^{13}C\{^{1}H\}$ NMR spectra of the *in situ* generation and silylation of **7-^{13}C** with ^{i}Pr$_3$SiCl.

Reduction Prior to Silylation

Carbide **7-^{13}C** was prepared *in situ* from **8-^{13}C** (20 mg, 0.028 mmol) and ^{n}Bu$_4$NF (8.1 mg, 0.031 mmol) as described above and characterized by $^{13}C\{^{1}H\}$ and $^{31}P\{^{1}H\}$ NMR spectroscopy at -20 °C (Figure S20, A). The J. Young tube was cooled to -78 °C and a solution of ^{i}Pr$_3$SiCl (10.8 mg, 0.056 mmol) in THF (100 µL) was added via syringe with a heavy argon counterflow. The $^{13}C\{^{1}H\}$ NMR spectrum at -80 °C showed no change to the characteristic carbide resonance at 546.2 ppm (Figure S20, B). The tube was once again chilled to -78 °C and a deep green solution of [Na][C$_{10}$H$_8$] (0.056 mmol) in THF (200 µL) was added via syringe with a heavy argon counterflow. $^{13}C\{^{1}H\}$ NMR spectroscopy at -80 °C showed quantitative conversion to a new species characterized by a broad resonance at 327.92 ppm (Figure S20, D). Cooling this solution to -100 °C in the NMR probe resulted in broadening of this signal and warming to -60 °C resulted in decoalescence to two broad triplets (Figure S20 C and E, respectively). The chemical shifts of this species in both the $^{13}C\{^{1}H\}$ and $^{31}P\{^{1}H\}$ NMR spectra are consistent with an assignment as the silylcarbyne/oxycarbyne complex **13-^{13}C**.

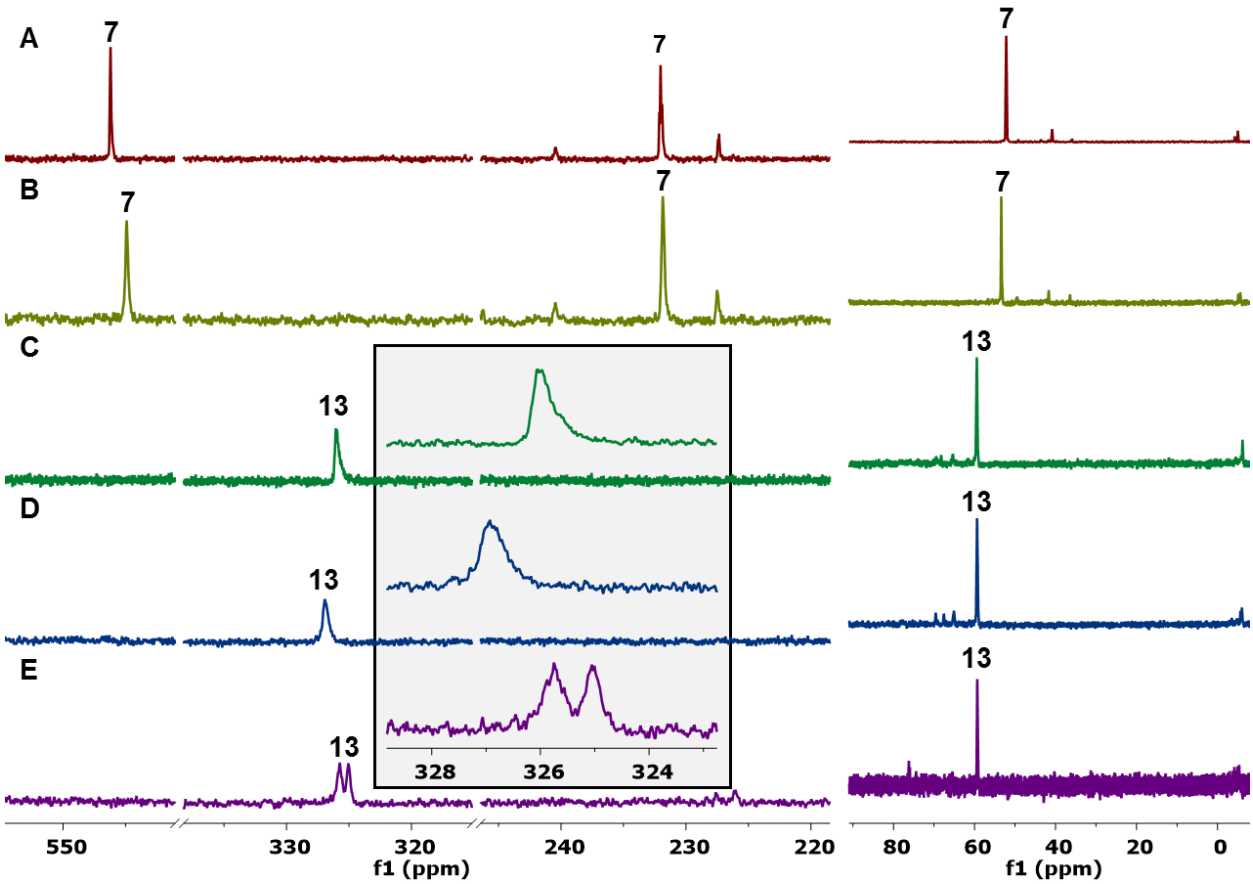

Figure S20— Partial $^{13}C\{^{1}H\}$ (left) and full $^{31}P\{^{1}H\}$ NMR spectra of the *in situ* generation of **7-^{13}C** (A), addition of $^{i}Pr_3SiCl$ (B), and subsequent reduction with $[Na][C_{10}H_8]$ (C-E). The shaded inset shows an enlargement of the resonances attributed to the silylcarbyne and oxycabyne carbons of **13-^{13}C**—only at -60 °C are the two carbon resonances resolved; warming the sample to higher temperatures resulted in reaction (*vide infra*).

Independent Synthesis of a Silylcarbyne/Oxycarbyne Complex

If the proposed assignment of **13** is indeed correct, it should be directly accessible via the two-electron reduction of **8**. To investigate this, a J. Young NMR tube was charged with a deep red THF (400 µL) solution of **8-^{13}C** (20 mg, 0.028 mmol). $^{13}C\{^{1}H\}$ NMR spectroscopy (Figure S21, A) showed the characteristic resonances at 355.8 and 247.5 attributable to the silyl alkylidyne and carbonyl carbons, respectively. The tube was chilled to -80 °C and a deep green solution of $[Na][C_{10}H_8]$ (0.059 mmol) in THF (200 µL) was added via syringe with a heavy argon counterflow. The $^{13}C\{^{1}H\}$ NMR spectrum (-80 °C) showed quantitative conversion of **8-^{13}C** to a new species characterized by a broad triplet at 338.7 ppm and a broad resonance at 58.49 ppm in the $^{13}C\{^{1}H\}$ and $^{31}P\{^{1}H\}$ NMR spectra, respectively (Figure S21, C). Cooling this mixture to -100 °C showed decoalescence of the $^{13}C\{^{1}H\}$ NMR resonance to two triplets (Figure S21, B). Warming the sample to -60 °C likewise resulted in decoalescence, with the broader resonance now shifting downfield (Figure S21, D). These spectral features are consistent with those observed for **13**, leading to the assignment of this complex as the trimethylsilyl analog, **14**. Further warming resulted in C–C coupling chemistry and formation of dinitrogen complex **5** (*vide infra*).

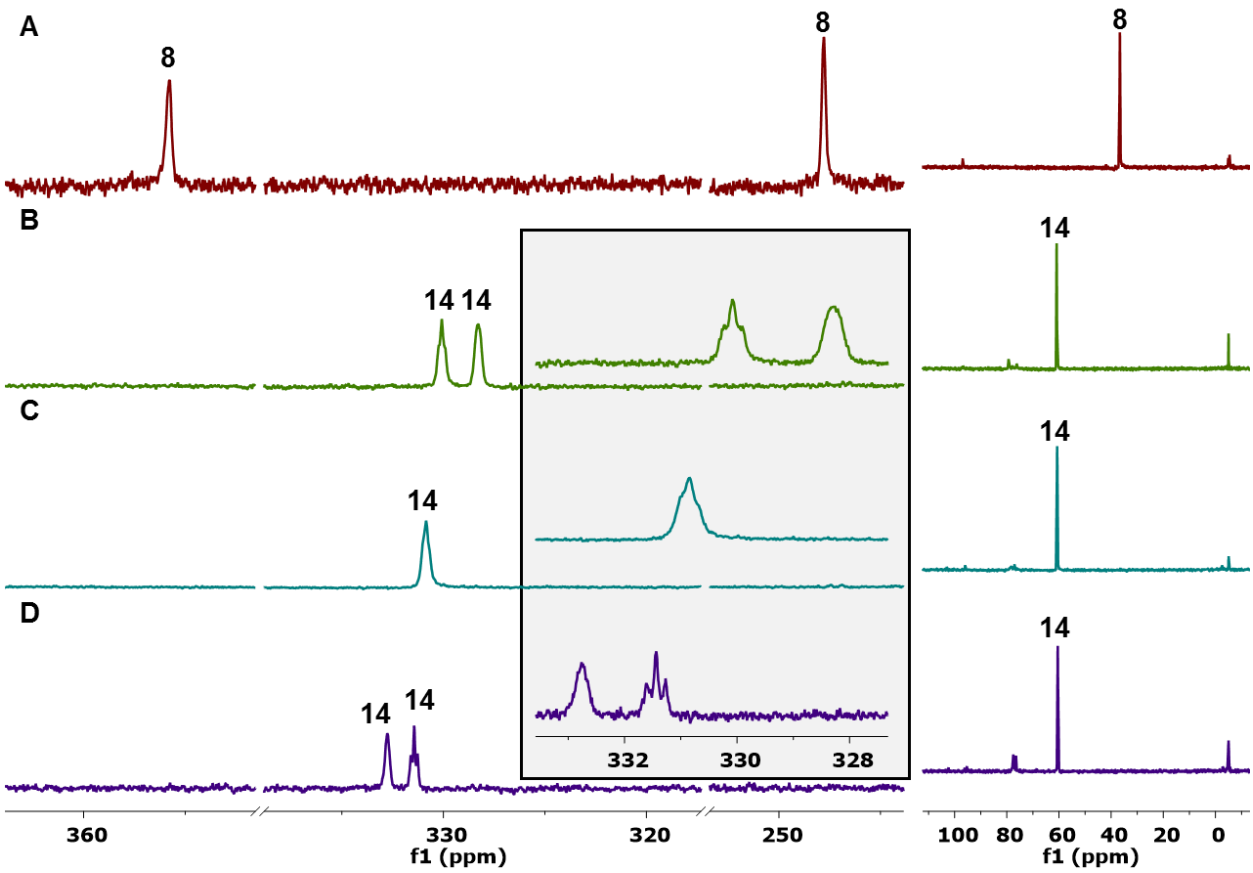

Figure S21—Partial $^{13}C\{^{1}H\}$ (left) and full $^{31}P\{^{1}H\}$ (right) NMR spectra of the reduction of **8-^{13}C**. The shaded inset shows an enlargement of the resonances attributed to the silylcarbyne and oxycabyne carbons of **14-^{13}C** at -100°C (B), -80 °C (C), and -60 °C (D); warming the sample to higher temperatures resulted in reaction (*vide infra*).

*Demonstration of C–C Bond Formation and Organic Fragment Release from **14***

Warming either of the above samples of **13** or **14** to -60 °C resulted in C–C coupling, release of the resulting silyl ethynolate, and adventitious binding of dinitrogen (Figure S22). For **13-^{13}C** doublets (δ = 107.7, 23.98, ^{1}J(C,C) = 168.8 Hz) characteristic of **6a** were observed in the $^{13}C\{^{1}H\}$ NMR spectrum, with simultaneous observation of complex **5** in the $^{31}P\{^{1}H\}$ NMR spectrum (Figure S22, A). The resonance for the second acetylenic carbon (δ = 23.98 ppm) is obscured, overlapping with the upfield side of the THF solvent residual.

Samples of **14-^{13}C** showed two coupling doublets in the $^{13}C\{^{1}H\}$ NMR spectrum—assigned as the silyl ethynolate **6b** based on chemical shift and $^{1}J_{CC}$ coupling constant[8]—at -60 °C (Figure S22, B); these resonances grow in as the sample is warmed to -30 °C (Figure S22, B-E). Freezing the contents of the J. Young NMR tube, evacuating the headspace, and adding of one equiv. of Me_3SiCl (33.4 mL at 1.8 cm Hg, 0.030 mmol) via condensation at -196 °C resulted in formation of disilyl ketene **6c** upon thawing to -78 °C by $^{13}C\{^{1}H\}$ NMR spectroscopy (Figure S22, F). This is the thermodynamically preferred isomer of oxyacetylenes bearing small silyl substituents.[9,10]

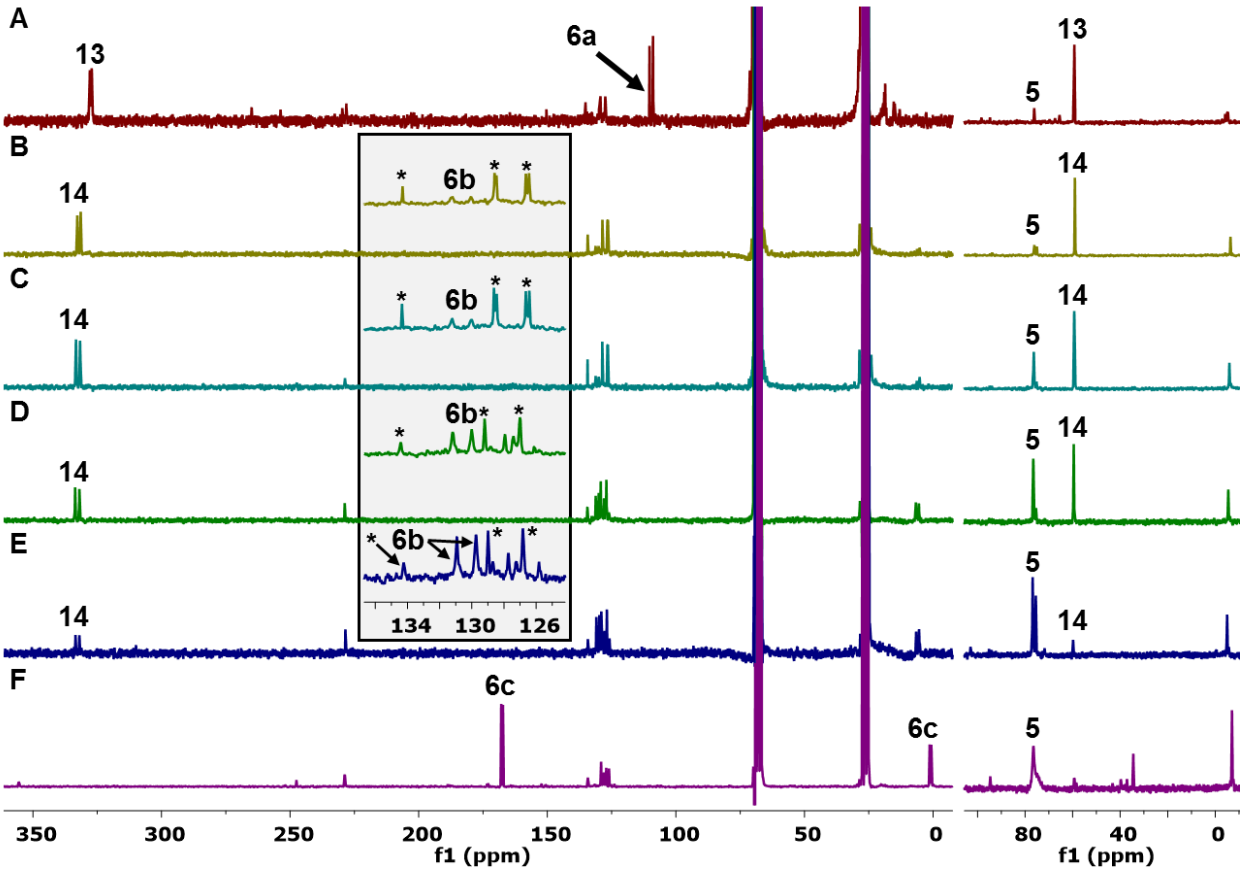

Figure S22—$^{13}C\{^{1}H\}$ NMR spectra supporting the formation of silylated oxyacetylenes from mixed carbynes **13** and **14**. Warming **13-^{13}C** (as prepared, a second equivalent of $^{i}Pr_3SiCl$ is present in solution) affords **6a** ($^{13}C\{^{1}H\}$ NMR (126 MHz, -60 °C, THF) δ = 107.72, 23.98, $^{1}J_{CC}$ = 168.83 Hz) at -60 °C. Warming **14-^{13}C** likewise results in formation of the metal free organic, ethynolate **6b** ($^{13}C\{^{1}H\}$ NMR (126 MHz, 25 °C, THF) δ = 131.34, 5.94, $^{1}J_{CC}$ = 139.6 Hz), as observed at -60 °C, -50 °C, -40 °C and -30 °C (B-E, respectively). Addition of Me_3SiCl to this mixture yields ketene **6c** ($^{13}C\{^{1}H\}$ NMR (126 MHz, -80 °C, THF) δ = 167.54, 1.13, $^{1}J_{CC}$ = 82.3 Hz). The shaded inset shows an enlargement of the 125-135 ppm region of the $^{13}C\{^{1}H\}$ NMR spectrum; the starred resonances correspond to naphthalene.

*Silylation of **14**: Formation of Mixed Silyl/Siloxy Dicarbyne **15***

Complex **14-^{13}C** was prepared *in situ*, as described above, from the reduction of **8-^{13}C** (20 mg, 0.028 mmol) with [Na][$C_{10}H_8$] (0.028 mmol in 100 μL of THF) in THF (500 μL) in a J. Young NMR tube (Figure S23, A). The contents of this tube were frozen by immersion in liquid nitrogen and Me_3SiCl (33.4 mL at 1.7 mL Hg, 0.031 mmol) was added via condensation from a calibrated bulb. The tube was sealed, the contents thawed and mixed, and placed in a -78 °C dry ice/acetone slush bath. NMR spectroscopy studies at -80 °C show new resonances in the $^{13}C\{^{1}H\}$ (δ = 378.9, 283.8 ppm) and $^{31}P\{^{1}H\}$ (δ = 57.0 ppm) spectra were assigned to the mixed dicarbyne **15** (Figures S23, B). Warming this sample to -40 °C resolved the scalar coupling between the trans-spanning phosphines and carbyne carbons—$^{13}C\{^{1}H\}$ δ = 378.1 ppm (t, ^{2}J(P,C) = 18.79 Hz, *C*$SiMe_3$), 301.3 ppm (t, ^{2}J(P,C) = 13.55 Hz, *C*O$SiMe_3$); $^{31}P\{^{1}H\}$ δ = 57.4 ppm (dd, ^{2}J(P,C) = 18.79, 13.55 Hz). Further warming to 0 °C resulted in formation of disilylketene **6c** (Figure S23, B-D) and concomitant generation of **5**, as evidenced by $^{31}P\{^{1}H\}$ NMR spectroscopy.

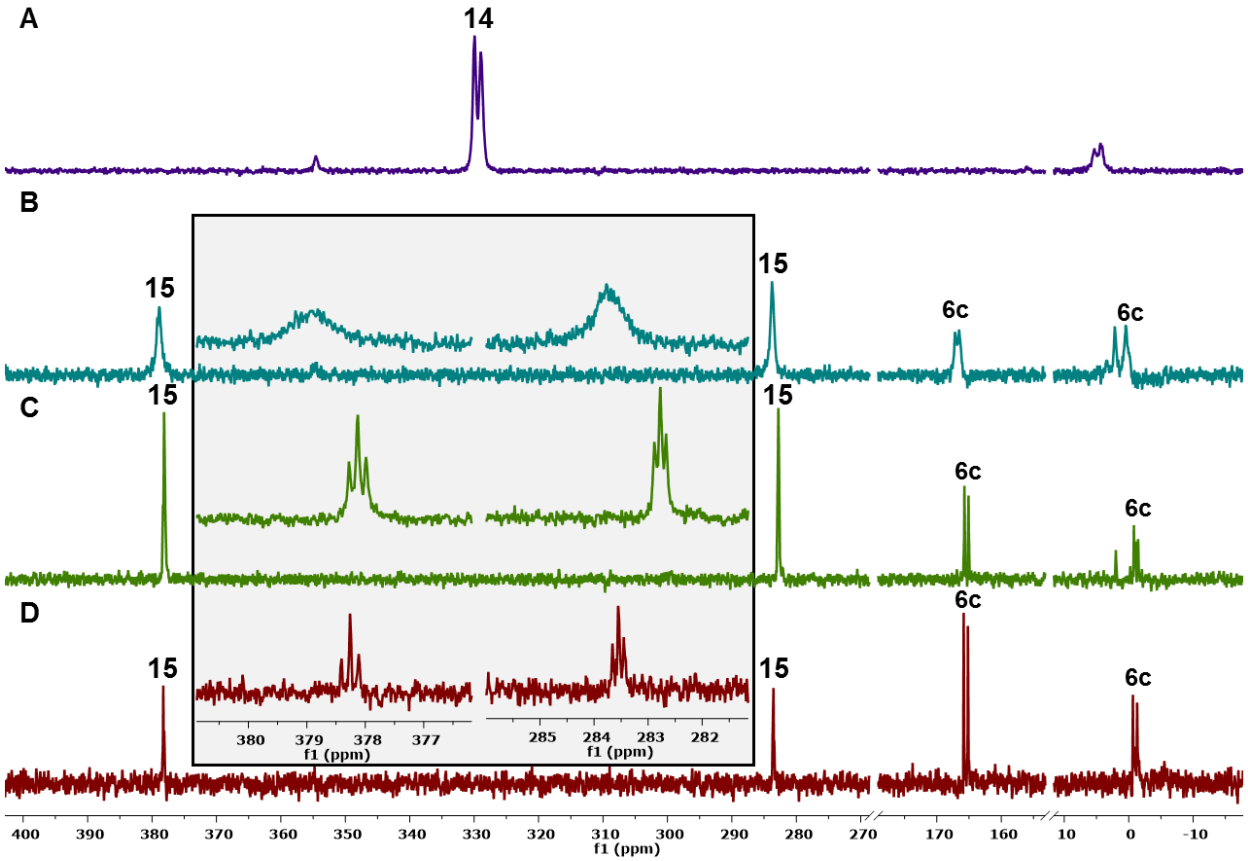

Figure S23—Partial $^{13}C\{^{1}H\}$ NMR spectra following the formation of and C–C coupling from mixed dicarbyne **15-^{13}C**. The shaded inset shows an enlargement of the silyl- and siloxycarbyne resonances of **15-^{13}C**.

Crossover Experiments

To rule out the possibility of a bimetallic pathway for C–C bond formation, crossover experiments were conducted. Both one-pot reduction and coupling from dicarbonyl dication precursors **1**/**1-^{13}C** as well as silyl ethynolate formation from **8**/**8-^{13}C** showed no evidence for label scrambling.

One-Pot Reduction and Silylation

A 20 mL scintillation vial was charged with **1** (52 mg, 0.057 mmol), **1-^{13}C** (70 mg, 0.077 mmol), THF (4 mL), and a stir bar. Stirring was initiated and KC_8 (127 mg, 0.938 mmol) was added in a single portion to the yellow suspension. An immediate darkening of the mixture resulted; stirring continued for 30 minutes. At this time, the vial was placed in a liquid nitrogen cooled cold well and the dark purple mixture frozen solid. While thawing, a solution of $^{i}Pr_3SiCl$ (103 mg, 0.536 mmol) in THF (1 mL) was added dropwise, with stirring. Following the addition, the vial was allowed to warm to room temperature. An aliquot was removed, filtered through a Celite plug, and analyzed by $^{13}C\{^1H\}$ and $^{31}P\{^1H\}$ NMR spectroscopies, indicating no formation of monolabeled **6a** (Figure S24, top).

Silyl Carbyne Reductive Coupling

A 20 mL scintillation vial was charged with **8** (15 mg, 0.021 mmol), **8-^{13}C** (17 mg, 0.024 mmol), THF (3 mL), and a stir bar. The deep burgundy solution was frozen in a liquid nitrogen cooled cold well and, while thawing, KC_8 (20 mg, 0.148 mmol) was added in a single portion with stirring. An aliquot was removed, filtered through a Celite plug, and analyzed by $^{13}C\{^1H\}$ and $^{31}P\{^1H\}$ NMR spectroscopies, indicating no formation of monolabeled **6b** (Figure S24, bottom).

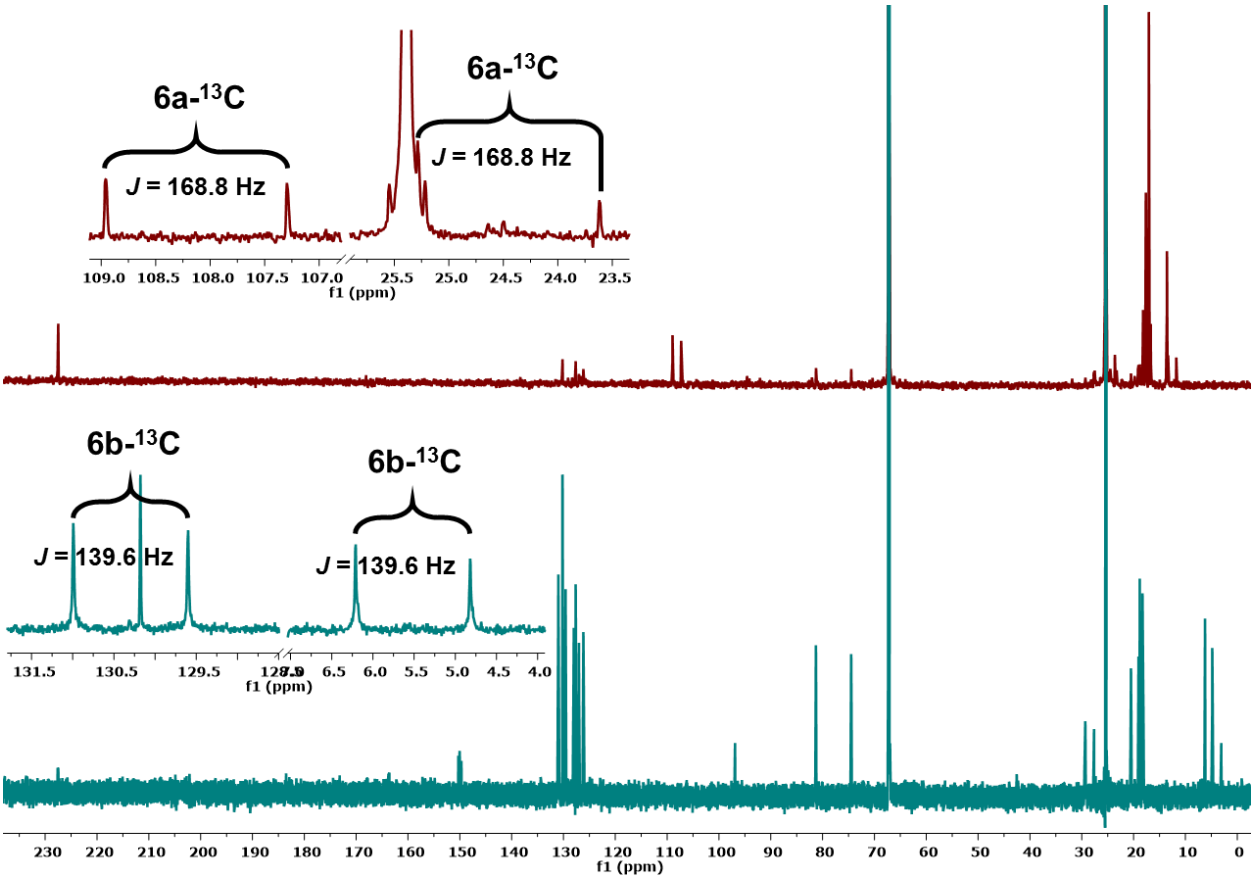

Figure S24—$^{13}C\{^{1}H\}$ (126 MHz, THF, 23 °C) NMR spectra of aliquots of crossover experiment reaction mixtures. In both cases, no monolabeled C–C coupled products were observed; these would resonate as singlets midway between the doublets of the coupled products. The insets show enlargements of the C_2O_1 organic product carbon resonances.

NMR Spectra

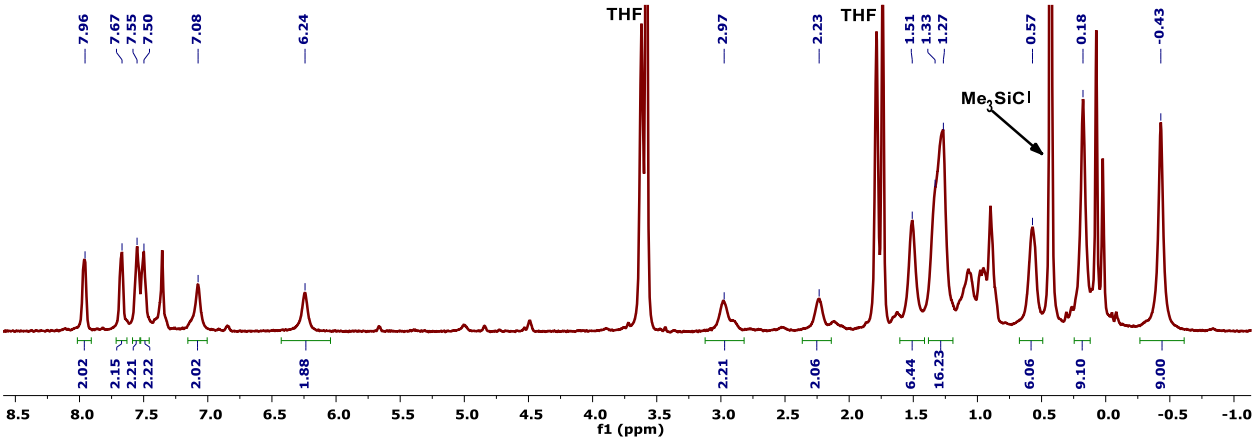

Figure S25—^{1}H NMR spectrum (500 MHz, THF-d_8, -80°C) of a mixture of **2-^{13}C** (3%), **9-^{13}C** (10%), and **11-^{13}C** (87%).

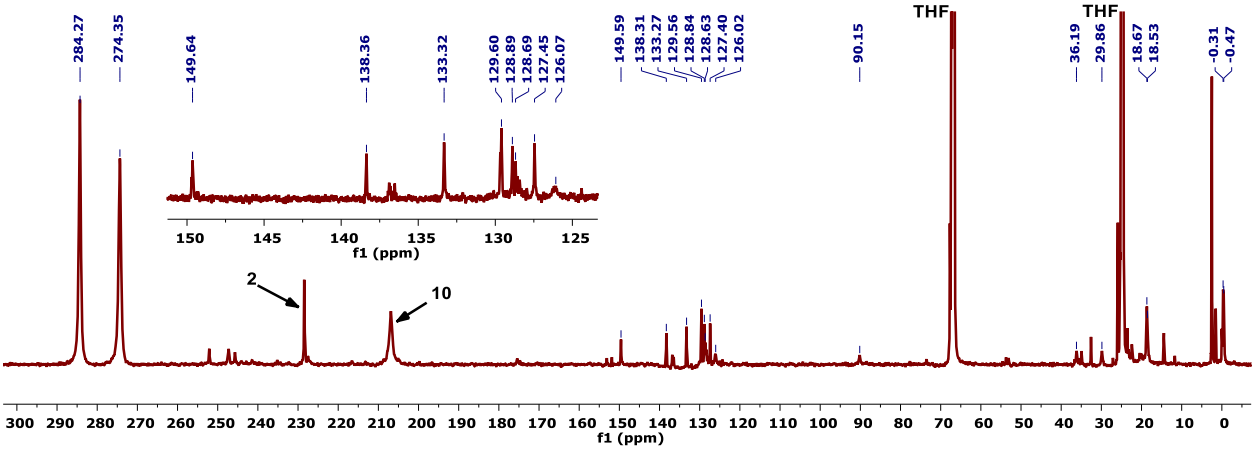

Figure S26—^{13}C{^{1}H} NMR spectrum (126 MHz, THF-d_8, -80°C) of a mixture of **2-^{13}C** (3%), **9-^{13}C** (10%), and **11-^{13}C** (87%). The inset shows an enlargement of the aryl region.

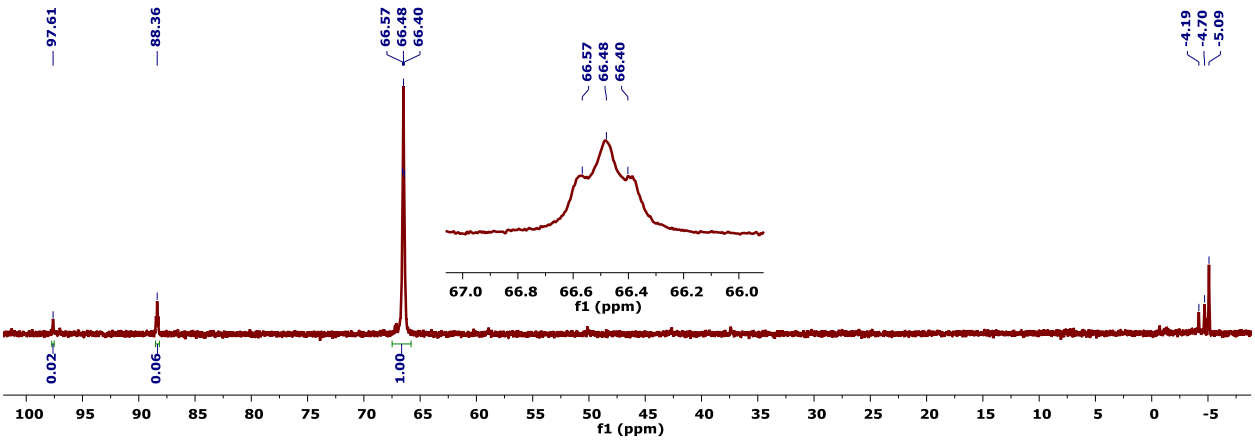

Figure S27—^{31}P{^{1}H} NMR spectrum (202 MHz, THF-d_8, -80°C) of a mixture of **2-^{13}C** (3%), **9-^{13}C** (10%), and **11-^{13}C** (87%). The inset shows and enlargement of the doublet of doublets assigned to **9-^{13}C**.

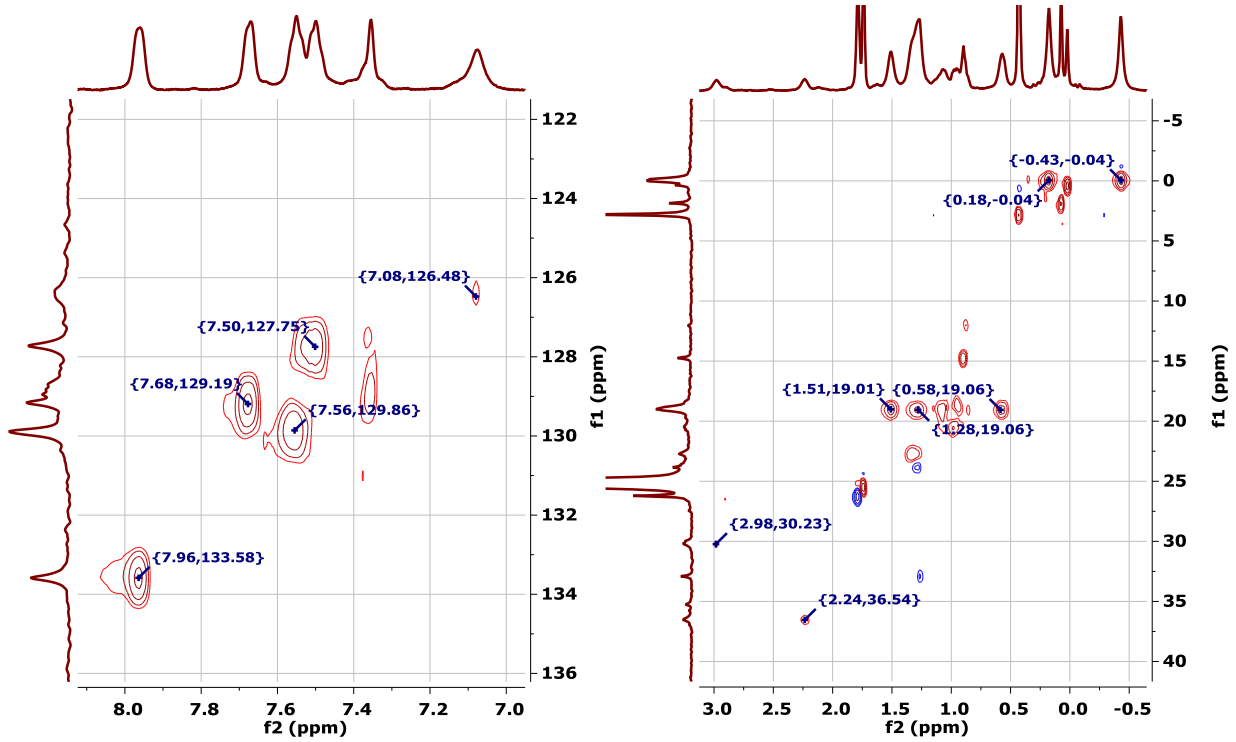

Figure S28—Partial $^{1}H/^{13}C$ HSQC NMR spectra (500/126 MHz, THF-d_8, -80°C) of a mixture of **2-^{13}C** (3%), **9-^{13}C** (10%), and **11-^{13}C** (87%). The cross peaks attributable to the aryl (left) and alkyl (right) resonances of **9-^{13}C** are labeled.

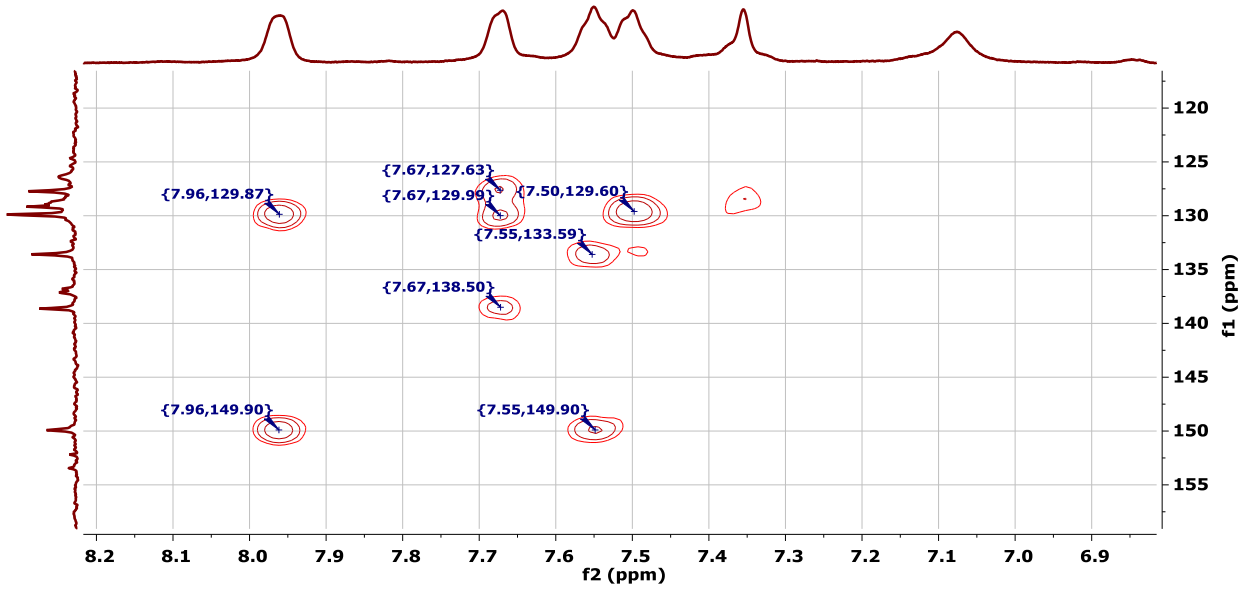

Figure S29—Partial $^{1}H/^{13}C$ HMBC NMR spectrum (500/126 MHz, THF-d_8, -80°C) of a mixture of **2-^{13}C** (3%), **9-^{13}C** (10%), and **11-^{13}C** (87%). The cross peaks attributable to the aryl resonances of **9-^{13}C** are labeled.

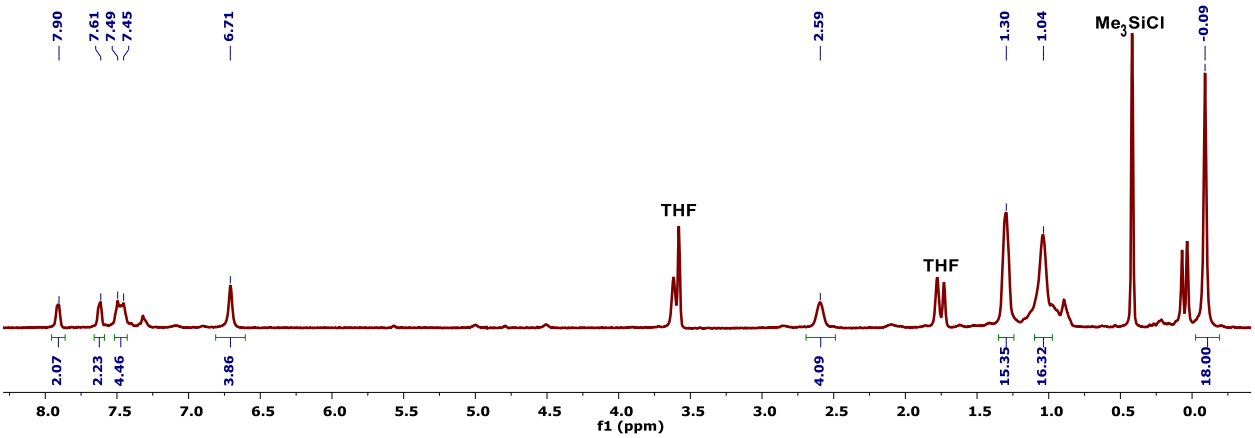

Figure S30—^{1}H NMR Spectrum (500 MHz, THF-d_8, -20°C) of a mixture of **2-^{13}C** (5%), **9-^{13}C** (13%), and **11-^{13}C** (82%).

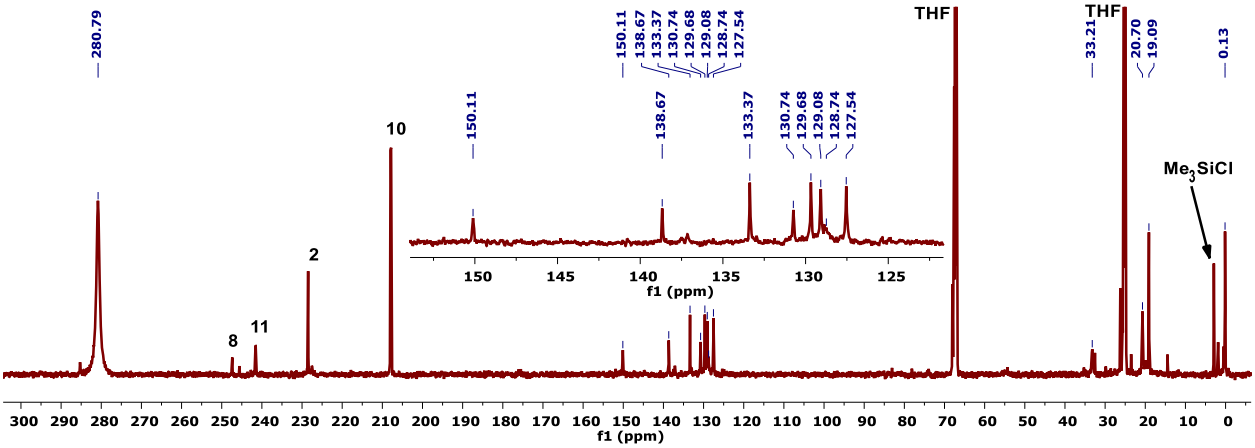

Figure S31—^{13}C{^{1}H} NMR Spectrum (126 MHz, THF-d_8, -20°C) of a mixture of **2-^{13}C** (5%), **9-^{13}C** (13%), and **11-^{13}C** (82%). Over the course of the NMR experiment, trace amounts of **11-^{13}C** and **8-^{13}C** were formed. The inset shows and enlargement of the aryl region.

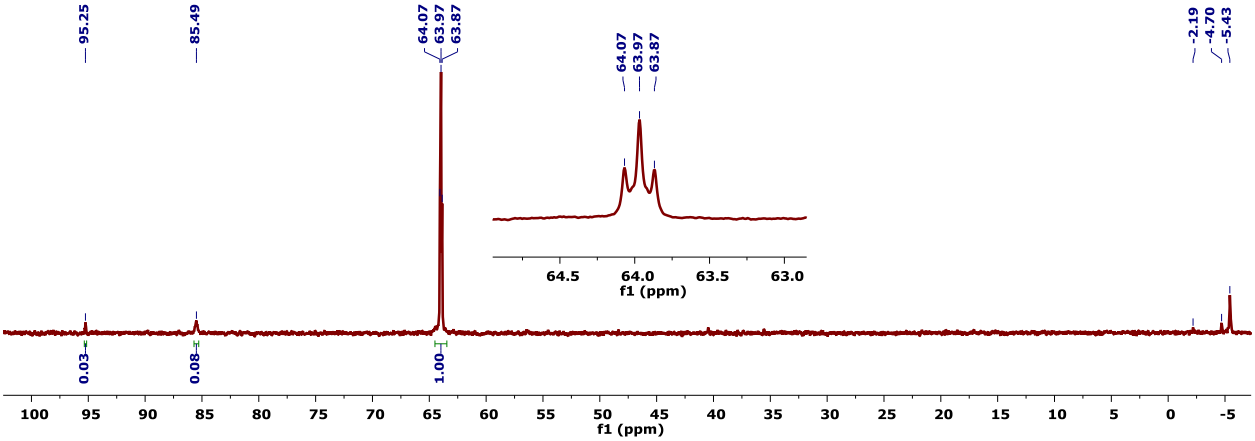

Figure S32—^{31}P{^{1}H} NMR Spectrum (202 MHz, THF-d_8, -20°C) of a mixture of **2-^{13}C** (5%), **9-^{13}C** (13%), and **11-^{13}C** (82%). The inset shows and enlargement of the triplet assigned to **9-^{13}C**.

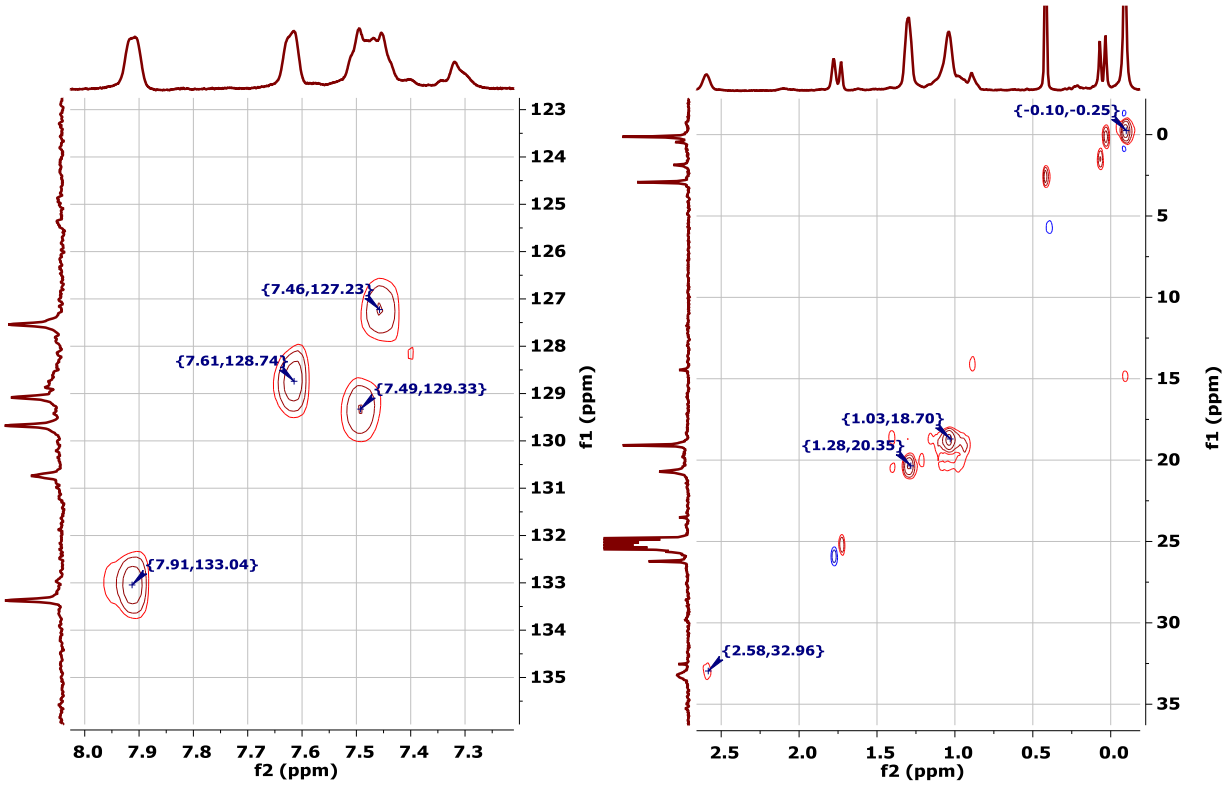

Figure S33—Partial $^{1}H/^{13}C$ HSQC NMR spectra (500/126 MHz, THF-d_8, -80°C) of a mixture of **2-^{13}C** (3%), **9-^{13}C** (10%), and **11-^{13}C** (87%). The cross peaks attributable to the aryl (left) and alkyl (right) resonances of **9-^{13}C** are labeled.

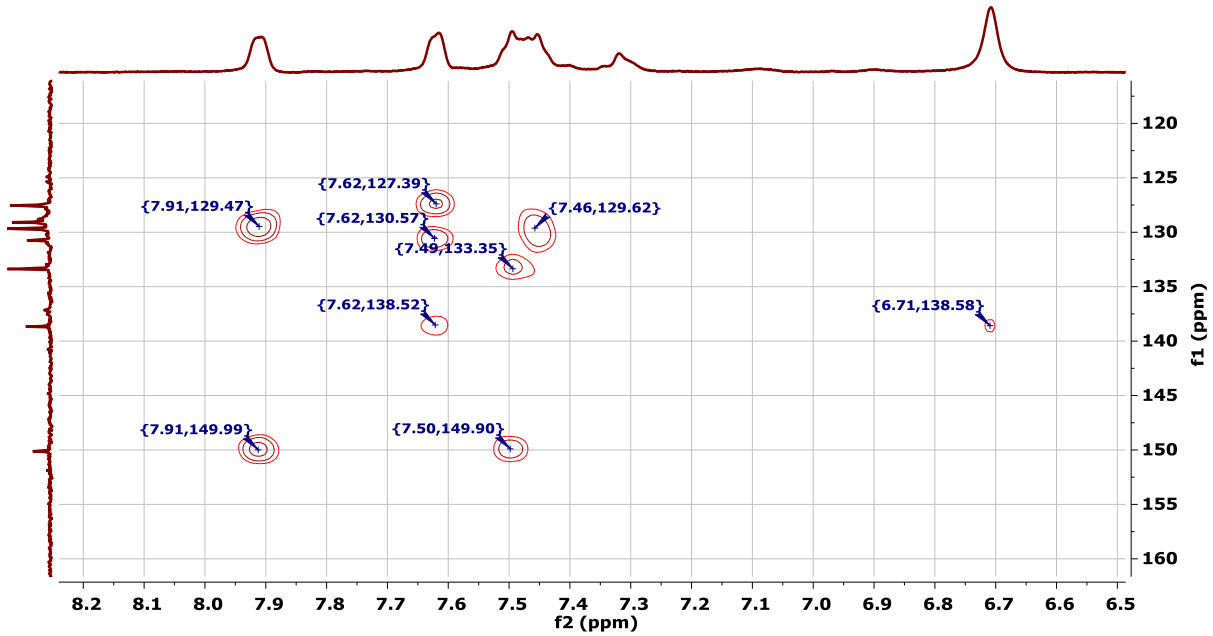

Figure S34—Partial $^{1}H/^{13}C$ HMBC NMR spectrum (500/126 MHz, THF-d_8, -80°C) of a mixture of **2-^{13}C** (3%), **9-^{13}C** (10%), and **11-^{13}C** (87%). The cross peaks attributable to the aryl resonances of **9-^{13}C** are labeled.

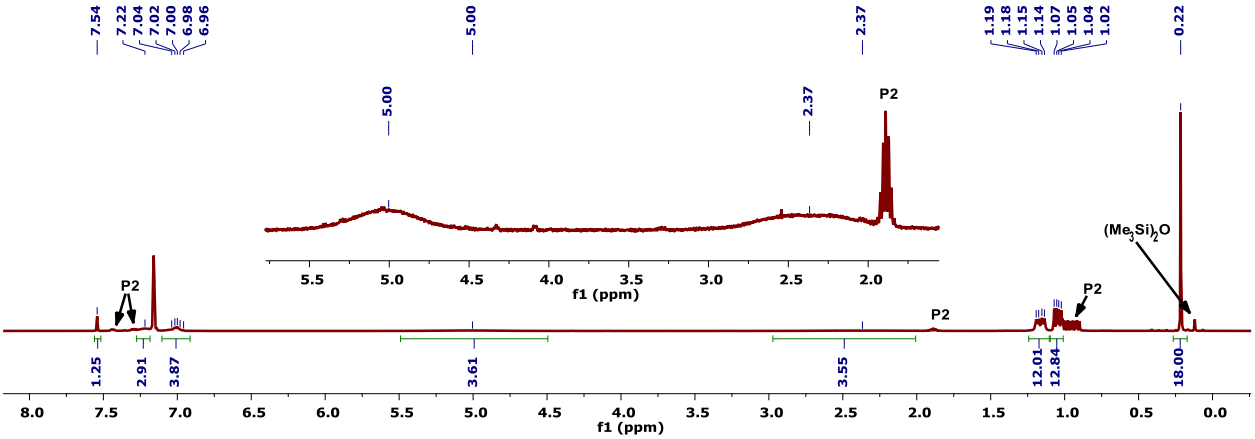

Figure S35—^{1}H NMR Spectrum (400 MHz, C_6D_6, 23°C) of a 75:25 mixture of **10** and free diphosphine (P2). The inset shows broad resonances associated with the central arene and isopropyl methine resonances of **10** at 5.00 and 2.37 ppm, respectively. The shaper multiplet centered at 1.89 ppm is the isopropyl methine resonance of the free diphosphine ligand.

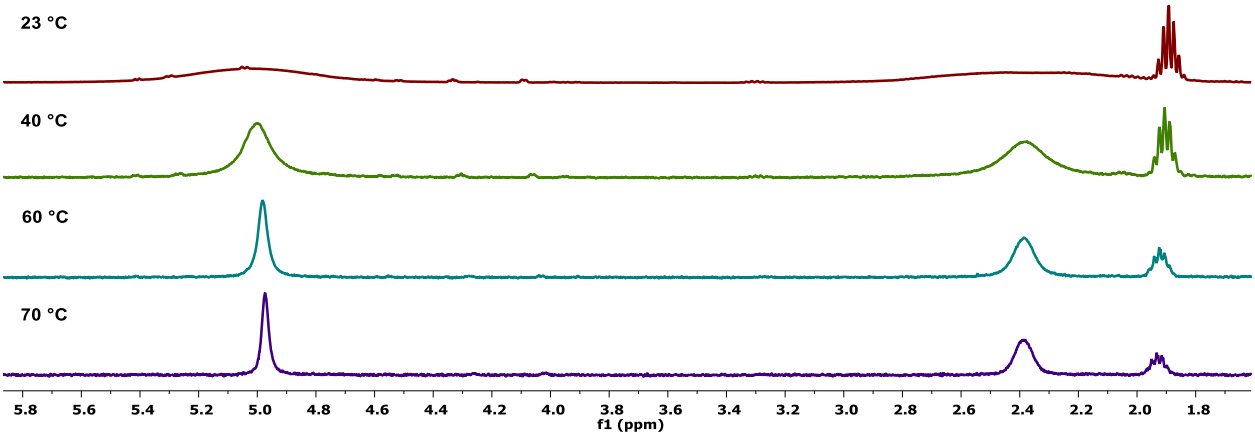

Figure S36—Partial ^{1}H NMR Spectra (400 MHz, C_6D_6) of a 75:25 mixture of **10** and free diphosphine (P2) from 23 to 70 °C., showing the temperature dependent breadth of the central arene and isopropyl methine resonances.

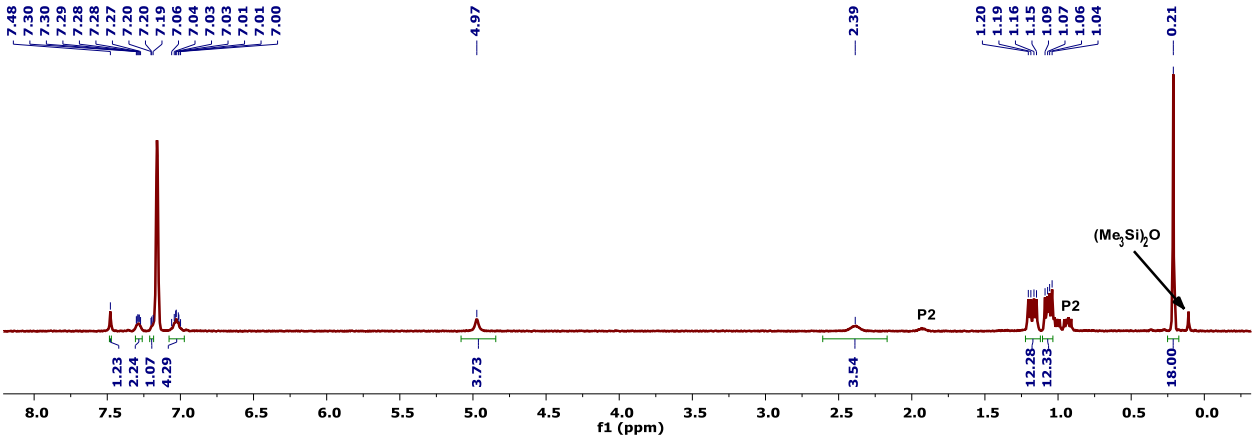

Figure S37—^{1}H NMR Spectrum (400 MHz, C_6D_6, 70°C) of a 75:25 mixture of **10** and free diphosphine (P2).

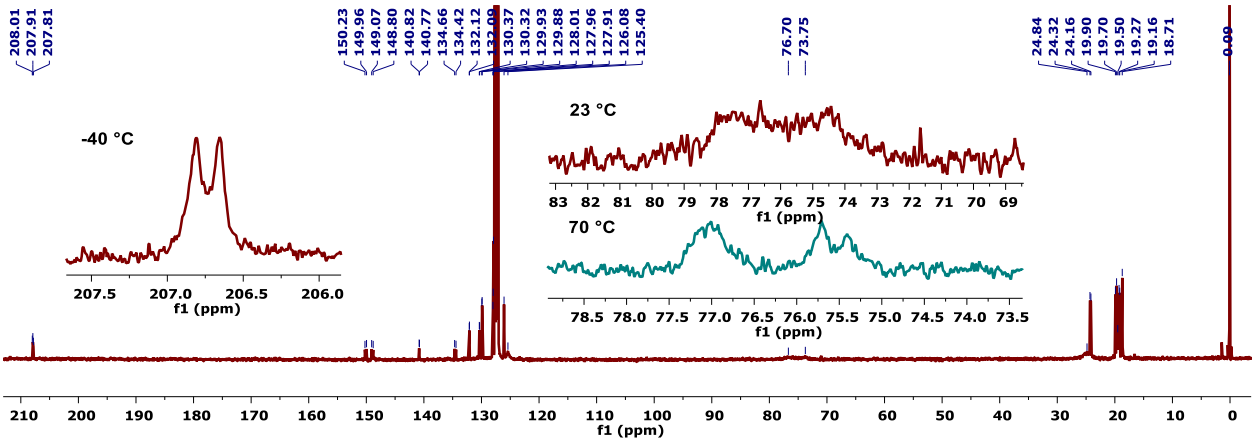

Figure S38—$^{13}C\{^{1}H\}$ NMR Spectrum (162 MHz, C_6D_6, 23°C) of a 75:25 mixture of **10** and free diphosphine (P2). The left inset shows the resolved $^{31}P/^{13}C$ scalar coupling in **10-^{13}C** at -40 °C. The right inset shows the central arene carbon resonances of **10** at 23 (top right) and 70 (bottom right) °C.

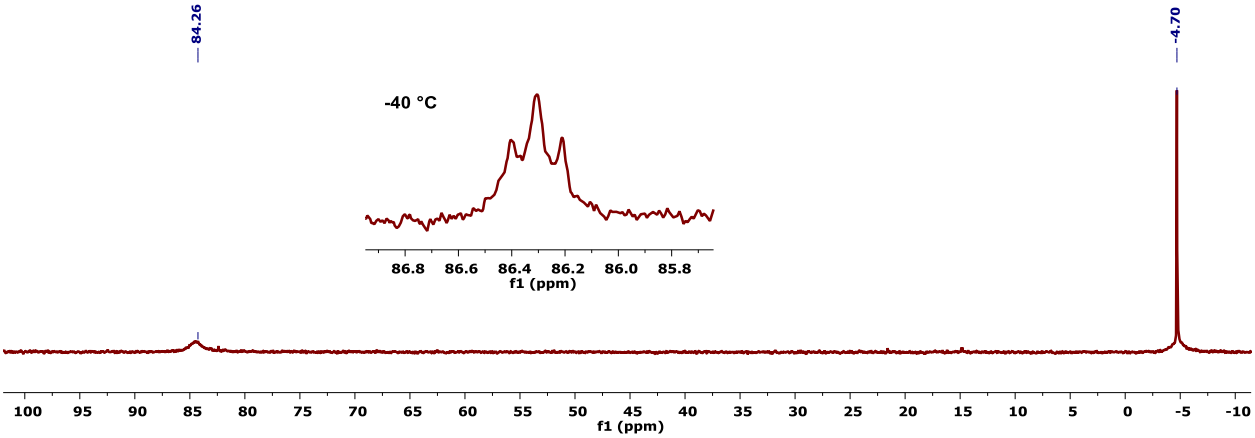

Figure S39—$^{31}P\{^{1}H\}$ NMR Spectrum (162 MHz, C_6D_6, 23°C) of a 75:25 mixture of **10** and free diphosphine (P2). The resonance for the free phosphine arm of **10** coincides with that of the free ligand. The inset shows the triplet assigned to the bound phosphine arm of **10-^{13}C** (202.4 MHz, THF, -40 °C) displaying a ^{2}J(P,C) of 19.57 Hz.

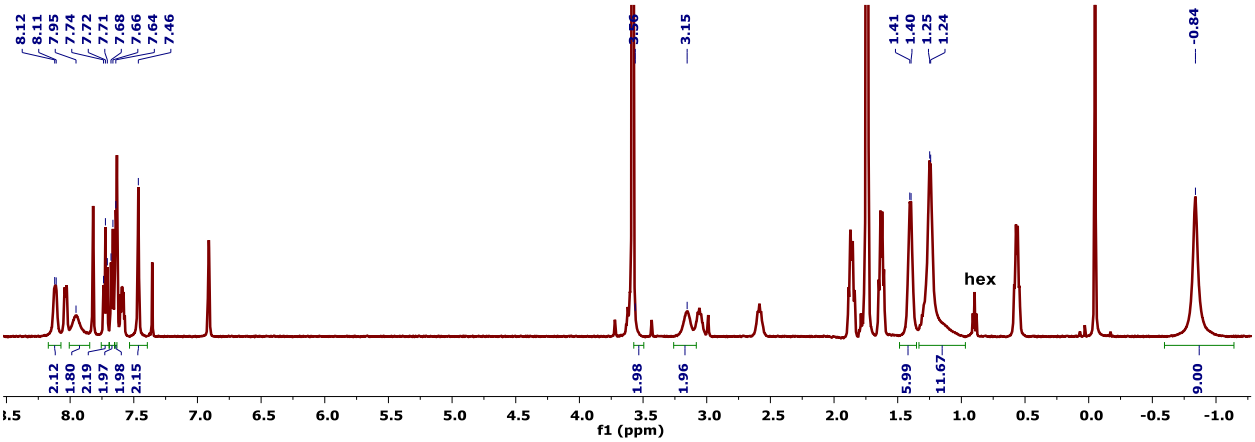

Figure S40—^{1}H NMR Spectrum (500 MHz, THF-d_8, -80°C) of a mixture of **11** (56%) and **8** (44%).

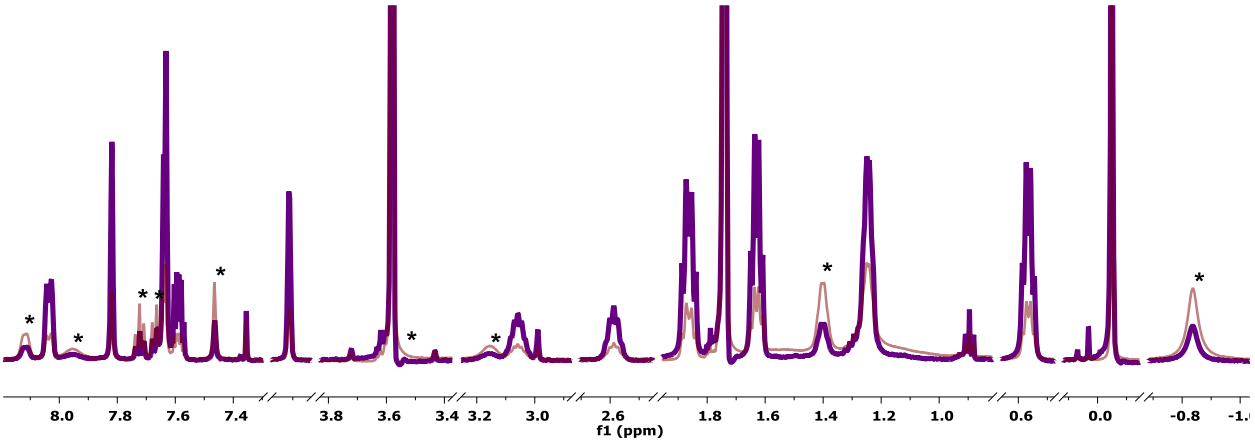

Figure S41—Stacked ^{1}H NMR Spectrum (500 MHz, THF-d_8, -80°C) of the same mixture of **11** (56%) and **8** (44%) after 30 minutes at room temperature (14% **11**/86% **8**). The asterisks denote peaks unambiguously assigned to **11**.

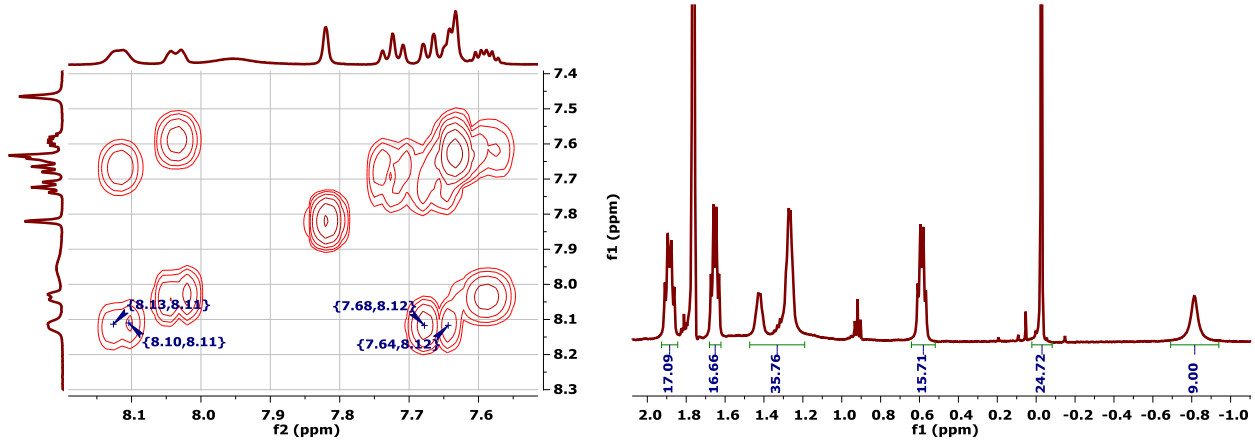

Figure S42—Partial ^{1}H/^{1}H COSY NMR spectrum showing a correlation between the aryl proton signal of **11** at 8.12 ppm and a proton resonance of **11** at 7.64 ppm; this proton's chemical shift coincides with that of an aryl proton in **8** (7.63 ppm) (left). Partial ^{1}H NMR spectrum showing that the isopropyl methyl protons of **11** resonate as two multiplets (1.42 and 1.27 ppm). The integration of these resonances sums to *ca.* 18H relative to the trimethylsilyl group after subtracting the coincidental isopropyl methyl resonance of **8** at 1.27 ppm (16-17H in the same relative integration scale, right).

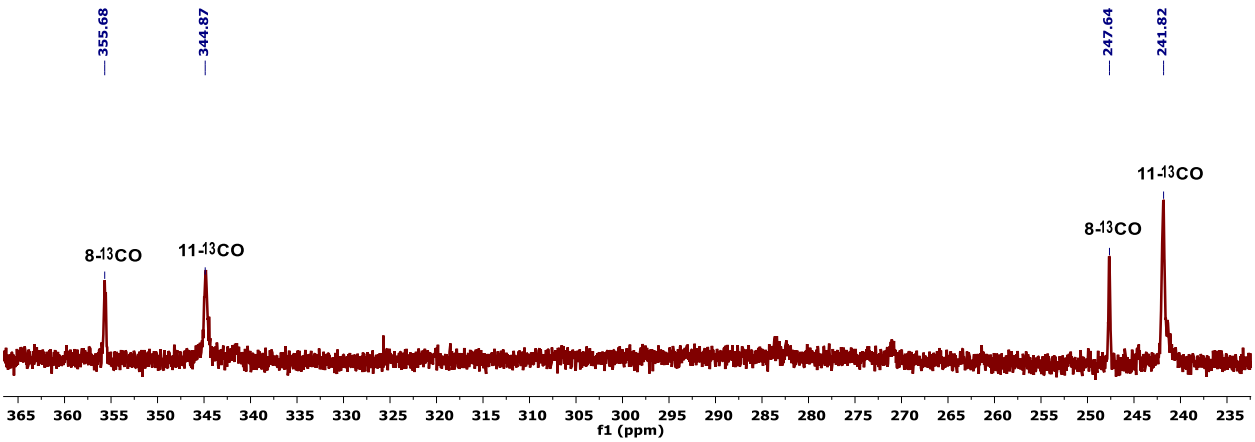

Figure S43—Partial $^{13}C\{^{1}H\}$ NMR Spectrum (202 MHz, THF, -80°C) of a mixture of **11** (74%) and **8** (26%). At this temperature, the resonances are broad and the ^{2}J(P,C) cannot be resolved.

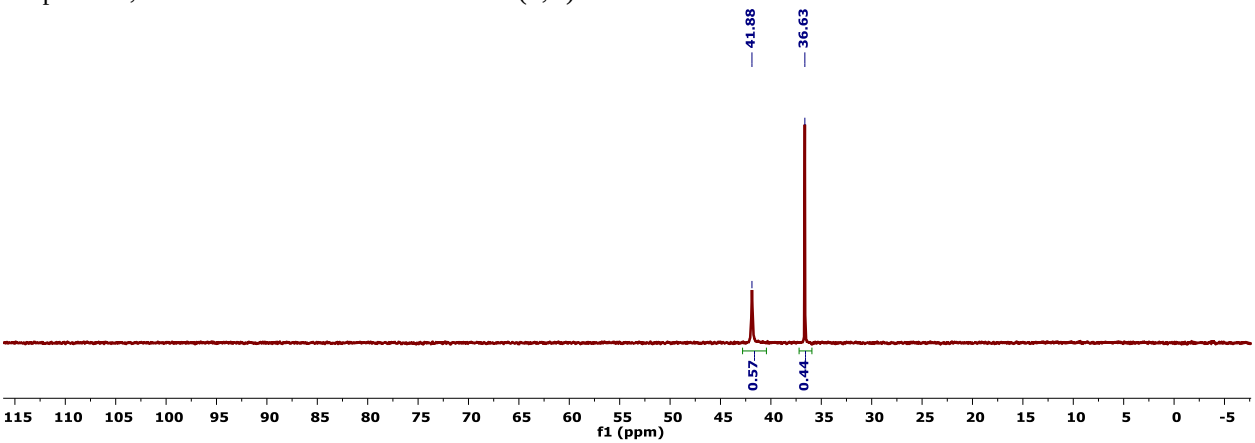

Figure S44—$^{31}P\{^{1}H\}$ NMR Spectrum (202 MHz, THF-d_8, -80°C) of a mixture of **11** and **8**.

Quantum Mechanics Data

Computational Details

All calculations were performed with DFT as implemented in Gaussian 09 Revision C.01.[11] Geometry optimizations and electronic structure calculations were performed with revised TPSS exchange and correlation functionals.[12,13] The LANL2DZ basis set[14-17] was used for all atoms. No solvent corrections were employed. All optimizations were performed ignoring molecular symmetry—crystallographic coordinates were used as a starting point when possible. Energetic minima were confirmed with subsequent frequency calculations which did not return imaginary frequencies. Structures optimized in this manner showed good agreement with bond lengths and angles determined via single crystal X-ray diffraction (Table S4). To further validate the application of these calculations, ^{13}C NMR shifts were calculated using the GIAO method.[18,19] The trends observed in the calculated spectroscopic data (NMR and IR) are in good agreement with those established experimentally. In instances when the single-point energy was of interest, DFTD3 single-point dispersion corrections[20] with BJ-damping[21] were conducted. All molecular orbital illustrations were generated using GaussView, the GUI component of the Gaussian software package, and depicted with a 0.04 e/Å^3 isosurface value.

Cartesian Coordinates for 2

Mo	-0.693000	-0.926000	0.013000
P	-3.169000	-0.841000	0.068000
P	3.889000	2.179000	0.151000
O	-0.696000	-3.304000	-2.083000
O	-0.568000	-3.150000	2.269000
C	-1.109000	1.376000	-0.069000
C	-0.423000	1.130000	1.179000
H	-0.886000	1.415000	2.119000
C	0.846000	0.445000	1.168000
H	1.335000	0.219000	2.112000
C	1.508000	0.088000	-0.063000
C	0.799000	0.340000	-1.295000
H	1.254000	0.038000	-2.235000
C	-0.468000	1.033000	-1.316000
H	-0.962000	1.247000	-2.259000
C	-2.509000	1.922000	-0.063000
C	-3.605000	1.015000	0.002000
C	-4.929000	1.514000	0.010000
H	-5.774000	0.827000	0.060000
C	-5.169000	2.905000	-0.046000
H	-6.191000	3.281000	-0.040000
C	-4.081000	3.805000	-0.112000
H	-4.262000	4.878000	-0.156000
C	-2.757000	3.315000	-0.120000
H	-1.916000	4.006000	-0.169000
C	2.876000	-0.537000	-0.069000
C	3.002000	-1.947000	-0.186000
H	2.093000	-2.544000	-0.246000
C	4.270000	-2.562000	-0.207000
H	4.345000	-3.646000	-0.293000
C	5.435000	-1.770000	-0.110000
H	6.421000	-2.236000	-0.123000
C	5.318000	-0.369000	0.004000
H	6.226000	0.230000	0.076000
C	4.052000	0.268000	0.026000
C	-4.200000	-1.571000	-1.358000
H	-5.265000	-1.331000	-1.238000
C	-4.150000	-1.460000	1.579000
H	-4.009000	-2.544000	1.662000
C	4.917000	2.659000	-1.404000
H	5.077000	3.747000	-1.399000
C	5.226000	2.534000	1.487000
H	5.318000	3.623000	1.602000
C	-0.703000	-2.403000	-1.276000
C	-0.626000	-2.310000	1.401000
H	-5.220000	-1.231000	1.476000
H	-3.751000	-0.980000	2.480000
H	-4.063000	-2.659000	-1.362000
H	-3.829000	-1.162000	-2.304000
H	4.900000	2.105000	2.443000
H	5.890000	2.148000	-1.424000
H	6.209000	2.119000	1.223000
H	4.350000	2.391000	-2.304000

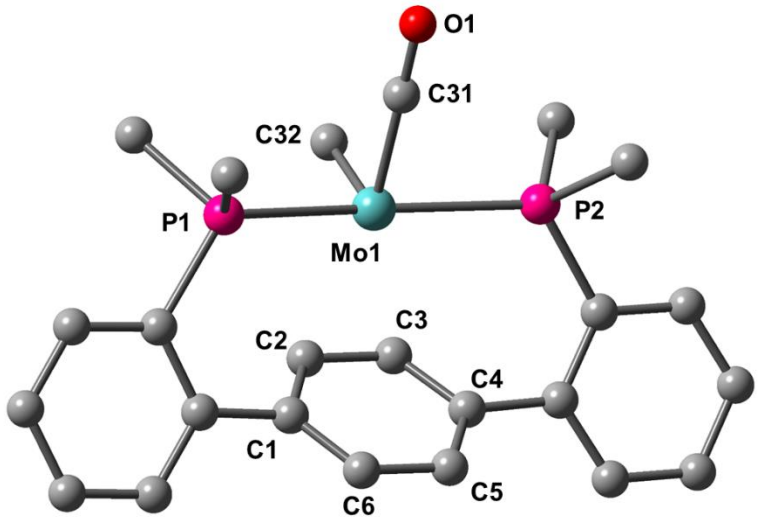

Figure S45—Geometry optimized structure of carbide **7** with atom radii scaled by 50%. Hydrogen atoms are omitted for clarity. Selected bond lengths [Å] and angles [°]: C1–C2 1.445, C2–C3 1.430, C3–C4 1.445, C4–C5 1.403, C5–C6 1.428, C6–C1 1.403, Mo1–C2 2.492, Mo1–C3 2.492, Mo1–C31 1.979, C31–O1 1.210, Mo1–C32 1.771, C31-Mo1-C32 89.09.

Cartesian Coordinates for 7

Mo	-1.110000	-0.242000	-0.000000
P	-1.118000	0.039000	2.568000
P	-1.118000	0.039000	-2.568000
O	-3.927000	1.253000	-0.000000
C	1.867000	-0.052000	1.435000
C	1.130000	-1.065000	0.715000
H	0.779000	-1.945000	1.251000
C	1.130000	-1.065000	-0.715000
H	0.779000	-1.945000	-1.251000
C	1.867000	-0.052000	-1.435000
C	2.630000	0.879000	-0.714000
H	3.182000	1.653000	-1.248000
C	2.630000	0.879000	0.714000
H	3.182000	1.653000	1.248000
C	1.774000	-0.012000	2.923000
C	0.505000	-0.053000	3.578000
C	0.458000	-0.043000	4.993000
H	-0.505000	-0.069000	5.505000
C	1.638000	0.010000	5.765000
H	1.579000	0.006000	6.853000
C	2.892000	0.076000	5.118000
H	3.810000	0.122000	5.703000
C	2.954000	0.066000	3.710000
H	3.921000	0.088000	3.206000
C	1.774000	-0.012000	-2.923000
C	0.505000	-0.053000	-3.578000
C	0.458000	-0.043000	-4.993000
H	-0.505000	-0.069000	-5.505000
C	1.638000	0.010000	-5.765000
H	1.579000	0.006000	-6.853000
C	2.892000	0.076000	-5.118000
H	3.810000	0.122000	-5.703000
C	2.954000	0.066000	-3.710000
H	3.921000	0.088000	-3.206000
C	-1.833000	1.673000	3.248000
H	-2.847000	1.799000	2.847000
C	-2.224000	-1.243000	3.428000
H	-2.301000	-1.061000	4.508000
C	-1.833000	1.673000	-3.248000
H	-2.847000	1.799000	-2.847000
C	-2.224000	-1.243000	-3.428000
H	-2.301000	-1.061000	-4.508000
C	-2.851000	0.699000	-0.000000
C	-1.977000	-1.786000	-0.000000
H	-1.207000	2.506000	2.907000
H	-1.863000	1.663000	4.346000
H	-1.811000	-2.239000	3.237000
H	-3.215000	-1.184000	2.963000
H	-3.215000	-1.184000	-2.963000
H	-1.811000	-2.239000	-3.237000
H	-1.207000	2.506000	-2.907000
H	-1.863000	1.663000	-4.346000

Cartesian Coordinates for 8

Mo	-0.000000	0.993000	0.072000
Cl	0.001000	1.347000	2.617000
P	2.584000	0.890000	0.220000
P	-2.584000	0.883000	0.223000
Si	-0.026000	4.330000	-1.458000
O	-0.001000	-0.069000	-2.924000
C	1.437000	-2.192000	0.053000
C	0.710000	-1.556000	1.098000
H	1.231000	-1.098000	1.936000
C	-0.702000	-1.558000	1.098000
H	-1.225000	-1.101000	1.937000
C	-1.427000	-2.196000	0.053000
C	-0.700000	-2.926000	-0.918000
H	-1.233000	-3.425000	-1.728000
C	0.712000	-2.924000	-0.918000
H	1.246000	-3.421000	-1.728000
C	2.918000	-2.043000	-0.011000
C	3.552000	-0.769000	0.129000
C	4.968000	-0.705000	0.112000
H	5.470000	0.256000	0.225000
C	5.758000	-1.861000	-0.060000
H	6.845000	-1.781000	-0.063000
C	5.130000	-3.114000	-0.234000
H	5.727000	-4.014000	-0.373000
C	3.725000	-3.196000	-0.209000
H	3.237000	-4.165000	-0.308000
C	-2.909000	-2.051000	-0.010000
C	-3.546000	-0.779000	0.131000
C	-4.963000	-0.720000	0.115000
H	-5.469000	0.239000	0.229000
C	-5.749000	-1.878000	-0.057000
H	-6.836000	-1.803000	-0.060000
C	-5.118000	-3.129000	-0.233000
H	-5.712000	-4.032000	-0.374000
C	-3.713000	-3.207000	-0.209000
H	-3.221000	-4.175000	-0.310000
C	3.418000	1.853000	-1.194000
H	3.095000	1.422000	-2.148000
C	3.357000	1.710000	1.754000
H	4.452000	1.733000	1.680000
C	-3.423000	1.844000	-1.188000
H	-3.099000	1.417000	-2.144000
C	-3.358000	1.698000	1.759000
H	-2.964000	2.718000	1.832000
C	-0.000000	0.305000	-1.772000
C	-0.002000	2.627000	-0.666000
H	-1.237000	5.081000	-1.036000
H	1.171000	5.110000	-1.054000
H	-0.036000	4.219000	-2.939000
H	-3.040000	1.148000	2.651000
H	-4.454000	1.717000	1.687000
H	-4.517000	1.799000	-1.112000
H	-3.093000	2.888000	-1.128000
H	4.512000	1.814000	-1.117000
H	3.081000	2.895000	-1.135000
H	3.042000	1.160000	2.647000
H	2.958000	2.729000	1.826000

Cartesian Coordinates for 8-Me_3Si

Mo	0.571000	0.092000	0.000000
Cl	0.820000	2.667000	0.000000
P	0.436000	0.202000	2.589000
P	0.436000	0.202000	-2.589000
Si	4.195000	-0.521000	0.000000
O	-0.236000	-2.984000	-0.000000
C	-2.625000	-0.007000	1.430000
C	-2.028000	1.061000	0.706000
H	-1.598000	1.913000	1.229000
C	-2.028000	1.061000	-0.706000
H	-1.598000	1.913000	-1.229000
C	-2.625000	-0.007000	-1.430000
C	-3.308000	-1.015000	-0.706000
H	-3.772000	-1.843000	-1.242000
C	-3.308000	-1.015000	0.706000
H	-3.772000	-1.843000	1.242000
C	-2.492000	-0.048000	2.913000
C	-1.227000	0.130000	3.553000
C	-1.173000	0.138000	4.969000
H	-0.218000	0.274000	5.477000
C	-2.332000	-0.040000	5.753000
H	-2.262000	-0.022000	6.840000
C	-3.577000	-0.250000	5.119000
H	-4.479000	-0.396000	5.712000
C	-3.648000	-0.254000	3.713000
H	-4.611000	-0.383000	3.218000
C	-2.492000	-0.048000	-2.913000
C	-1.227000	0.130000	-3.553000
C	-1.173000	0.138000	-4.969000
H	-0.218000	0.274000	-5.477000
C	-2.332000	-0.040000	-5.753000
H	-2.262000	-0.022000	-6.840000
C	-3.577000	-0.250000	-5.119000
H	-4.479000	-0.396000	-5.712000
C	-3.648000	-0.254000	-3.713000
H	-4.611000	-0.383000	-3.218000
C	1.333000	-1.251000	3.430000
H	2.354000	-1.299000	3.037000
C	1.293000	1.708000	3.375000
H	1.221000	1.687000	4.471000
C	1.333000	-1.251000	-3.430000
H	2.354000	-1.299000	-3.037000
C	1.293000	1.708000	-3.375000
H	1.221000	1.687000	-4.471000
C	0.048000	-1.806000	-0.000000
C	2.301000	-0.381000	0.000000
C	4.806000	-1.462000	-1.547000
H	5.896000	-1.612000	-1.486000
H	4.599000	-0.900000	-2.469000
H	4.334000	-2.452000	-1.631000
C	4.866000	1.273000	0.000000
H	5.485000	1.465000	-0.890000
H	5.485000	1.465000	0.890000
H	4.034000	1.992000	0.000000
C	4.806000	-1.462000	1.547000
H	4.334000	-2.452000	1.631000
H	4.599000	-0.900000	2.469000
H	5.896000	-1.612000	1.486000
H	0.808000	-2.179000	-3.171000
H	1.355000	-1.129000	-4.520000
H	0.834000	2.618000	-2.974000
H	2.345000	1.694000	-3.068000
H	0.808000	-2.179000	3.171000
H	1.355000	-1.129000	4.520000
H	2.345000	1.694000	3.068000
H	0.834000	2.618000	2.974000

Cartesian Coordinates for 8-^{i}Pr$_2$P-Me$_3$Si

Mo	2.727000	7.609000	8.530000
Cl	0.732000	6.963000	10.050000
P	3.302000	9.597000	10.219000
P	2.297000	5.397000	7.097000
Si	1.138000	9.843000	6.050000
O	5.510000	8.021000	7.066000
C	5.267000	7.045000	10.902000
C	3.963000	6.479000	10.839000
H	3.164000	6.866000	11.468000
C	3.701000	5.370000	10.008000
H	2.707000	4.929000	10.016000
C	4.736000	4.795000	9.219000
C	6.051000	5.301000	9.357000
H	6.858000	4.874000	8.762000
C	6.313000	6.412000	10.189000
H	7.319000	6.829000	10.225000
C	5.482000	8.272000	11.717000
C	4.616000	9.404000	11.612000
C	4.818000	10.493000	12.500000
H	4.154000	11.354000	12.459000
C	5.864000	10.494000	13.446000
H	5.988000	11.344000	14.117000
C	6.749000	9.395000	13.512000
H	7.567000	9.387000	14.232000
C	6.549000	8.296000	12.656000
H	7.199000	7.424000	12.731000
C	4.399000	3.688000	8.283000
C	3.279000	3.770000	7.400000
C	2.953000	2.633000	6.616000
H	2.088000	2.661000	5.955000
C	3.724000	1.453000	6.663000
H	3.443000	0.596000	6.052000
C	4.860000	1.394000	7.499000
H	5.471000	0.492000	7.540000
C	5.185000	2.503000	8.303000
H	6.034000	2.450000	8.985000
C	4.072000	11.092000	9.203000
H	3.586000	10.959000	8.227000
C	5.601000	10.907000	9.019000
H	6.134000	11.060000	9.967000
H	5.967000	11.655000	8.297000
H	5.853000	9.915000	8.629000
C	3.758000	12.514000	9.731000
H	2.681000	12.707000	9.823000
H	4.169000	13.250000	9.021000
H	4.234000	12.702000	10.705000
C	1.832000	10.402000	11.208000
H	2.204000	11.376000	11.565000
C	1.421000	9.542000	12.431000
H	1.056000	8.561000	12.101000
H	0.606000	10.052000	12.969000
H	2.255000	9.401000	13.133000
C	0.631000	10.636000	10.257000
H	0.895000	11.281000	9.406000
H	-0.184000	11.125000	10.815000
H	0.265000	9.676000	9.871000
C	2.776000	5.761000	5.224000
H	2.598000	6.842000	5.165000
C	4.285000	5.495000	4.980000
H	4.919000	5.990000	5.725000
H	4.562000	5.886000	3.988000
H	4.501000	4.418000	4.995000
C	1.923000	5.047000	4.146000
H	2.072000	3.958000	4.163000
H	2.242000	5.405000	3.154000
H	0.849000	5.257000	4.244000
C	0.476000	4.715000	6.997000
H	0.453000	4.047000	6.122000
C	0.094000	3.902000	8.261000
H	0.771000	3.050000	8.418000
H	-0.927000	3.507000	8.137000
H	0.109000	4.545000	9.150000
C	-0.505000	5.892000	6.764000
H	-0.485000	6.572000	7.626000
H	-1.527000	5.498000	6.648000
H	-0.256000	6.465000	5.858000
C	4.453000	7.852000	7.639000
C	2.008000	8.700000	7.296000
C	1.333000	9.189000	4.265000
H	0.868000	9.898000	3.561000
H	0.843000	8.214000	4.129000
H	2.392000	9.085000	3.986000
C	-0.716000	9.923000	6.495000
H	-1.248000	10.581000	5.790000
H	-0.864000	10.318000	7.510000
H	-1.179000	8.928000	6.452000
C	1.878000	11.604000	6.102000
H	2.958000	11.596000	5.890000
H	1.721000	12.084000	7.078000
H	1.390000	12.230000	5.338000

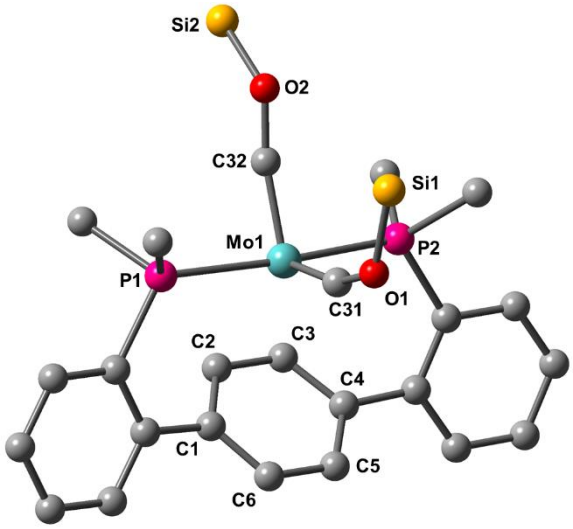

Figure S46—Geometry optimized structure of bis(siloxycarbyne) **9** with atom radii scaled by 50%. Hydrogen atoms are omitted for clarity. Selected bond lengths [Å] and angles [°]: C1–C2 1.437, C2–C3 1.425, C3–C4 1.437, C4–C5 1.411, C5–C6 1.415, C6–C1 1.411, Mo1–C2 2.593, Mo1–C3 2.593, Mo1–C31 1.850, C31–O1 1.360, Mo1–C32 1.850, C32–O2 1.381, C31-Mo1-C32 109.94, Mo1-C31-O1 160.57, Mo1-C32-O2 161.49.

Cartesian Coordinates for 9

Mo	-0.000000	0.573000	-0.101000
P	-2.553000	0.600000	-0.251000
P	2.553000	0.601000	-0.251000
C	-1.434000	-2.415000	-0.299000
C	-0.712000	-1.631000	-1.264000
H	-1.246000	-1.187000	-2.103000
C	0.712000	-1.631000	-1.264000
H	1.246000	-1.187000	-2.103000
C	1.434000	-2.415000	-0.300000
C	0.707000	-3.270000	0.557000
H	1.241000	-3.867000	1.295000
C	-0.707000	-3.270000	0.557000
H	-1.241000	-3.867000	1.295000
C	-2.914000	-2.300000	-0.193000
C	-3.563000	-1.027000	-0.193000
C	-4.974000	-0.973000	-0.084000
H	-5.481000	-0.007000	-0.078000
C	-5.750000	-2.146000	0.033000
H	-6.835000	-2.078000	0.110000
C	-5.108000	-3.405000	0.052000
H	-5.694000	-4.319000	0.142000
C	-3.706000	-3.474000	-0.059000
H	-3.210000	-4.445000	-0.071000
C	2.914000	-2.300000	-0.193000
C	3.563000	-1.027000	-0.193000
C	4.974000	-0.973000	-0.084000
H	5.481000	-0.007000	-0.078000
C	5.750000	-2.146000	0.032000
H	6.835000	-2.078000	0.110000
C	5.108000	-3.404000	0.051000
H	5.694000	-4.319000	0.142000
C	3.706000	-3.474000	-0.059000
H	3.210000	-4.445000	-0.071000
C	-3.443000	1.660000	1.055000
H	-2.968000	2.648000	1.053000
C	-3.258000	1.360000	-1.855000
H	-4.356000	1.326000	-1.863000
C	3.443000	1.660000	1.055000
H	2.968000	2.648000	1.053000
C	3.257000	1.360000	-1.855000
C	0.000000	0.603000	1.749000
C	-0.000000	2.302000	-0.758000
H	-2.868000	0.803000	-2.716000
H	-2.909000	2.398000	-1.920000
H	-3.299000	1.193000	2.036000
H	-4.516000	1.764000	0.845000
H	4.356000	1.327000	-1.863000
H	2.868000	0.803000	-2.716000
H	3.299000	1.193000	2.036000
H	4.516000	1.764000	0.845000
O	-0.000000	3.682000	-0.811000
O	0.000000	1.076000	3.025000
Si	-0.000000	4.615000	-2.295000
H	-0.000000	6.021000	-1.850000
H	1.211000	4.317000	-3.096000
H	-1.211000	4.317000	-3.095000
Si	0.000000	2.773000	3.518000
H	0.000000	2.720000	4.993000
H	1.213000	3.456000	3.017000
H	-1.213000	3.456000	3.017000
H	2.909000	2.398000	-1.920000

Cartesian Coordinates for 10

Mo	0.619000	0.325000	0.131000
P	3.139000	0.281000	0.052000
P	-3.884000	-2.288000	-0.983000
Si	-2.566000	2.690000	-1.747000
Si	1.777000	5.010000	-0.046000
O	-1.117000	3.084000	-0.847000
O	2.042000	3.304000	0.294000
C	1.218000	-1.989000	0.164000
C	0.794000	-1.567000	1.481000
H	1.428000	-1.747000	2.343000
C	-0.484000	-0.904000	1.650000
H	-0.829000	-0.659000	2.649000
C	-1.408000	-0.800000	0.518000
C	-0.898000	-1.077000	-0.811000
H	-1.513000	-0.877000	-1.681000
C	0.420000	-1.663000	-1.003000
H	0.752000	-1.949000	-1.995000
C	2.625000	-2.479000	-0.012000
C	3.681000	-1.527000	-0.048000
C	5.023000	-1.952000	-0.181000
H	5.834000	-1.223000	-0.208000
C	5.320000	-3.329000	-0.286000
H	6.354000	-3.657000	-0.390000
C	4.273000	-4.280000	-0.261000
H	4.500000	-5.342000	-0.345000
C	2.932000	-3.857000	-0.123000
H	2.125000	-4.587000	-0.097000
C	-2.764000	-0.213000	0.758000
C	-2.883000	0.885000	1.657000
H	-1.972000	1.309000	2.079000
C	-4.130000	1.461000	1.964000
H	-4.184000	2.308000	2.648000
C	-5.299000	0.951000	1.359000
H	-6.272000	1.394000	1.572000
C	-5.201000	-0.148000	0.479000
H	-6.117000	-0.539000	0.037000
C	-3.957000	-0.761000	0.179000
C	4.126000	1.007000	1.504000
H	3.870000	2.070000	1.566000
C	4.011000	1.091000	-1.431000
H	5.098000	0.942000	-1.374000
C	-3.361000	-3.615000	0.310000
H	-3.398000	-4.604000	-0.167000
C	-5.742000	-2.755000	-1.088000
H	-6.217000	-2.818000	-0.098000
C	-0.183000	2.173000	-0.384000
C	1.054000	2.326000	0.159000
H	-2.334000	-3.410000	0.631000
H	-4.029000	-3.598000	1.182000
H	-6.285000	-2.035000	-1.714000
H	-5.801000	-3.739000	-1.574000
H	5.206000	0.879000	1.345000
H	3.821000	0.500000	2.426000
H	3.622000	0.646000	-2.354000
H	3.778000	2.162000	-1.410000
H	0.707000	5.556000	0.817000
H	3.079000	5.621000	0.286000
H	1.453000	5.229000	-1.474000
H	-2.751000	3.856000	-2.635000
H	-2.361000	1.457000	-2.539000
H	-3.723000	2.554000	-0.840000

Cartesian Coordinates for 11

Mo	0.000000	-0.983000	0.017000
Cl	-0.000000	-2.043000	-2.379000
P	-2.582000	-1.055000	-0.097000
P	2.582000	-1.055000	-0.098000
Si	0.000000	0.255000	3.497000
O	0.000000	-3.926000	1.207000
C	-1.437000	1.971000	-0.448000
C	-0.711000	1.070000	-1.301000
H	-1.232000	0.521000	-2.084000
C	0.711000	1.070000	-1.301000
H	1.231000	0.521000	-2.084000
C	1.437000	1.971000	-0.448000
C	0.711000	2.918000	0.298000
H	1.240000	3.610000	0.953000
C	-0.711000	2.918000	0.298000
H	-1.241000	3.610000	0.953000
C	-2.918000	1.856000	-0.355000
C	-3.562000	0.583000	-0.260000
C	-4.977000	0.532000	-0.201000
H	-5.483000	-0.432000	-0.128000
C	-5.759000	1.705000	-0.223000
H	-6.846000	1.637000	-0.185000
C	-5.122000	2.964000	-0.292000
H	-5.714000	3.879000	-0.309000
C	-3.718000	3.032000	-0.356000
H	-3.225000	4.001000	-0.443000
C	2.918000	1.856000	-0.355000
C	3.562000	0.583000	-0.261000
C	4.977000	0.532000	-0.201000
H	5.483000	-0.432000	-0.128000
C	5.759000	1.705000	-0.223000
H	6.846000	1.637000	-0.185000
C	5.122000	2.965000	-0.291000
H	5.714000	3.880000	-0.309000
C	3.718000	3.032000	-0.356000
H	3.225000	4.001000	-0.443000
C	-3.394000	-1.822000	1.442000
H	-3.155000	-1.204000	2.314000
C	-3.330000	-2.110000	-1.488000
H	-4.427000	-2.071000	-1.457000
C	3.394000	-1.823000	1.441000
H	2.972000	-2.825000	1.585000
C	3.330000	-2.110000	-1.489000
H	4.427000	-2.071000	-1.458000
C	0.000000	-2.812000	0.752000
C	0.000000	-0.329000	1.706000
H	2.982000	-3.141000	-1.359000
H	2.957000	-1.746000	-2.452000
H	4.483000	-1.896000	1.325000
H	3.156000	-1.204000	2.314000
H	-2.957000	-1.747000	-2.451000
H	-2.982000	-3.141000	-1.358000
H	-2.972000	-2.825000	1.586000
H	-4.483000	-1.895000	1.326000
H	0.003000	1.740000	3.547000
H	-1.204000	-0.228000	4.224000
H	1.202000	-0.231000	4.225000

Cartesian Coordinates for 11-Me_3Si

Mo	-0.004000	-1.026000	-0.215000
Cl	0.001000	-2.292000	-2.523000
P	-2.584000	-1.117000	-0.349000
P	2.576000	-1.115000	-0.342000
O	0.002000	-3.843000	1.250000
C	-1.440000	1.874000	-0.953000
C	-0.715000	0.891000	-1.713000
H	-1.234000	0.269000	-2.441000
C	0.707000	0.890000	-1.715000
H	1.223000	0.267000	-2.443000
C	1.435000	1.874000	-0.959000
C	0.710000	2.895000	-0.317000
H	1.241000	3.655000	0.256000
C	-0.712000	2.895000	-0.314000
H	-1.240000	3.654000	0.263000
C	-2.919000	1.768000	-0.840000
C	-3.564000	0.507000	-0.632000
C	-4.978000	0.464000	-0.557000
H	-5.485000	-0.489000	-0.400000
C	-5.760000	1.632000	-0.671000
H	-6.847000	1.568000	-0.618000
C	-5.123000	2.880000	-0.853000
H	-5.714000	3.791000	-0.944000
C	-3.720000	2.940000	-0.936000
H	-3.228000	3.897000	-1.112000
C	2.915000	1.766000	-0.853000
C	3.558000	0.506000	-0.642000
C	4.973000	0.460000	-0.574000
H	5.479000	-0.493000	-0.414000
C	5.756000	1.626000	-0.698000
H	6.843000	1.561000	-0.650000
C	5.121000	2.875000	-0.882000
H	5.713000	3.784000	-0.979000
C	3.717000	2.937000	-0.957000
H	3.226000	3.893000	-1.135000
C	-3.427000	-1.798000	1.214000
C	-3.313000	-2.251000	-1.688000
C	3.414000	-1.772000	1.235000
C	3.310000	-2.268000	-1.662000
C	-0.001000	-2.776000	0.691000
C	-0.003000	-0.233000	1.417000
H	2.942000	-3.283000	-1.470000
H	3.209000	-1.080000	2.059000
Si	0.012000	0.427000	3.198000
C	-1.586000	1.416000	3.541000
H	-2.475000	0.768000	3.505000
H	-1.547000	1.878000	4.541000
H	-1.726000	2.217000	2.801000
C	0.120000	-1.053000	4.401000
H	1.036000	-1.638000	4.233000
H	0.126000	-0.703000	5.446000
H	-0.736000	-1.731000	4.274000
C	1.519000	1.575000	3.452000
H	1.492000	2.423000	2.753000
H	1.529000	1.977000	4.477000
H	2.467000	1.040000	3.290000
H	2.975000	-2.750000	1.468000
H	4.498000	-1.879000	1.100000
H	2.947000	-1.958000	-2.647000
H	4.408000	-2.245000	-1.628000
H	-2.948000	-1.927000	-2.667000
H	-2.946000	-3.268000	-1.510000
H	-4.411000	-2.227000	-1.656000
H	-3.229000	-1.116000	2.049000
H	-4.510000	-1.907000	1.073000
H	-2.986000	-2.778000	1.437000

Cartesian Coordinates for 11-^{i}Pr$_2$-Me$_3$Si

Mo	5.076000	1.570000	4.018000
Cl	2.923000	2.724000	5.033000
P	4.644000	-0.128000	6.032000
P	5.115000	3.515000	2.209000
Si	7.988000	-0.347000	2.696000
O	3.364000	-0.046000	1.891000
C	7.361000	1.716000	6.380000
C	6.184000	2.494000	6.098000
H	5.322000	2.428000	6.750000
C	6.222000	3.538000	5.136000
H	5.367000	4.208000	5.059000
C	7.449000	3.867000	4.467000
C	8.621000	3.195000	4.858000
H	9.567000	3.433000	4.371000
C	8.574000	2.125000	5.792000
H	9.486000	1.560000	5.988000
C	7.284000	0.484000	7.213000
C	6.181000	-0.435000	7.142000
C	6.247000	-1.627000	7.911000
H	5.438000	-2.352000	7.854000
C	7.344000	-1.920000	8.747000
H	7.355000	-2.845000	9.324000
C	8.417000	-1.007000	8.832000
H	9.265000	-1.208000	9.485000
C	8.379000	0.173000	8.068000
H	9.198000	0.888000	8.146000
C	7.436000	4.894000	3.393000
C	6.409000	4.924000	2.396000
C	6.414000	5.981000	1.450000
H	5.629000	6.035000	0.698000
C	7.414000	6.976000	1.454000
H	7.384000	7.779000	0.718000
C	8.449000	6.921000	2.413000
H	9.230000	7.681000	2.426000
C	8.451000	5.891000	3.371000
H	9.221000	5.868000	4.142000
C	4.069000	-1.916000	5.527000
H	4.029000	-2.509000	6.452000
C	5.073000	-2.581000	4.560000
H	5.192000	-1.982000	3.648000
H	4.700000	-3.577000	4.273000
H	6.056000	-2.704000	5.031000
C	2.642000	-1.861000	4.920000
H	1.905000	-1.446000	5.620000
H	2.325000	-2.884000	4.661000
H	2.619000	-1.260000	4.004000
C	3.266000	0.310000	7.372000
H	2.409000	0.580000	6.739000
C	2.895000	-0.876000	8.303000
H	2.056000	-0.558000	8.942000
H	3.730000	-1.142000	8.965000
H	2.569000	-1.773000	7.762000
C	3.622000	1.543000	8.242000
H	4.596000	1.427000	8.742000
H	2.857000	1.650000	9.027000
H	3.605000	2.462000	7.644000
C	5.536000	2.808000	0.423000
H	5.116000	1.793000	0.481000
C	7.069000	2.705000	0.242000
H	7.515000	3.699000	0.095000
H	7.299000	2.091000	-0.643000
H	7.539000	2.243000	1.117000
C	4.902000	3.539000	-0.787000
H	3.807000	3.582000	-0.734000
H	5.168000	2.987000	-1.704000
H	5.293000	4.560000	-0.898000
C	3.496000	4.546000	1.883000
H	3.702000	5.084000	0.943000
C	2.281000	3.606000	1.667000
H	2.463000	2.853000	0.886000
H	1.412000	4.209000	1.361000
H	2.035000	3.086000	2.600000
C	3.225000	5.588000	2.997000
H	3.019000	5.085000	3.950000
H	2.338000	6.181000	2.721000
H	4.070000	6.280000	3.124000
C	3.992000	0.550000	2.733000
C	6.540000	0.692000	3.388000
C	8.532000	-1.743000	3.886000
H	8.498000	-1.424000	4.937000
H	9.569000	-2.031000	3.651000
H	7.904000	-2.637000	3.779000
C	7.414000	-1.130000	1.049000
H	6.512000	-1.743000	1.195000
H	8.205000	-1.782000	0.644000
H	7.183000	-0.366000	0.294000
C	9.570000	0.691000	2.396000
H	9.388000	1.646000	1.886000
H	10.265000	0.103000	1.774000
H	10.074000	0.908000	3.349000

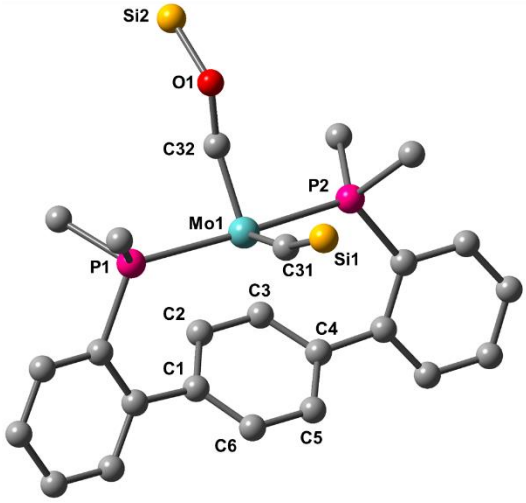

Figure S47—Geometry optimized structure of mixed dicarbyne **15** with atom radii scaled by 50%. Hydrogen atoms are omitted for clarity. Selected bond lengths [Å] and angles [°]: C1–C2 1.433, C2–C3 1.421, C3–C4 1.433, C4–C5 1.411, C5–C6 1.415, C6–C1 1.411, Mo1–C2 2.645, Mo1–C3 2.646, Mo1–C31 1.823, Mo1–C32 1.860, C32–O2 1.382, C31-Mo1-C32 109.27, Mo1-C32-O1 153.39.

Cartesian Coordinates for 15

Mo	-0.002000	0.711000	0.073000
P	-2.571000	0.722000	-0.063000
P	2.565000	0.731000	-0.083000
C	-1.435000	-2.270000	-0.540000
C	-0.715000	-1.373000	-1.395000
H	-1.252000	-0.796000	-2.148000
C	0.707000	-1.370000	-1.401000
H	1.236000	-0.792000	-2.158000
C	1.437000	-2.265000	-0.553000
C	0.714000	-3.216000	0.198000
H	1.251000	-3.901000	0.854000
C	-0.702000	-3.219000	0.204000
H	-1.231000	-3.906000	0.865000
C	-2.915000	-2.168000	-0.406000
C	-3.564000	-0.909000	-0.218000
C	-4.974000	-0.876000	-0.081000
H	-5.481000	0.078000	0.071000
C	-5.747000	-2.055000	-0.123000
H	-6.831000	-2.001000	-0.021000
C	-5.104000	-3.302000	-0.293000
H	-5.688000	-4.221000	-0.326000
C	-3.704000	-3.351000	-0.429000
H	-3.207000	-4.309000	-0.584000
C	2.918000	-2.158000	-0.431000
C	3.564000	-0.896000	-0.248000
C	4.975000	-0.857000	-0.124000
H	5.479000	0.099000	0.024000
C	5.752000	-2.033000	-0.173000
H	6.836000	-1.975000	-0.081000
C	5.113000	-3.282000	-0.338000
H	5.700000	-4.200000	-0.378000
C	3.712000	-3.338000	-0.462000
H	3.218000	-4.298000	-0.613000
C	-3.426000	1.584000	1.399000
H	-2.901000	2.532000	1.566000
C	-3.295000	1.696000	-1.534000
H	-4.394000	1.661000	-1.529000
C	3.428000	1.593000	1.376000
H	2.898000	2.537000	1.550000
C	3.275000	1.711000	-1.557000
C	0.006000	0.587000	1.892000
C	-0.007000	2.506000	-0.417000
H	-2.919000	1.269000	-2.472000
H	-2.947000	2.732000	-1.456000
H	-3.313000	0.954000	2.289000
H	-4.490000	1.774000	1.205000
H	4.373000	1.681000	-1.560000
H	2.893000	1.285000	-2.493000
H	3.326000	0.959000	2.264000
H	4.489000	1.789000	1.173000
H	2.923000	2.746000	-1.473000
Si	0.014000	0.961000	3.736000
H	-1.190000	0.383000	4.400000
H	1.202000	0.346000	4.398000
H	0.038000	2.412000	4.086000
O	-0.007000	3.860000	-0.142000
Si	-0.016000	5.100000	-1.381000
H	-0.010000	6.374000	-0.637000
H	1.189000	4.986000	-2.237000
H	-1.233000	4.987000	-2.220000

Qualitative Molecular Orbital Diagrams of Complexes 7-9, 11, and 15

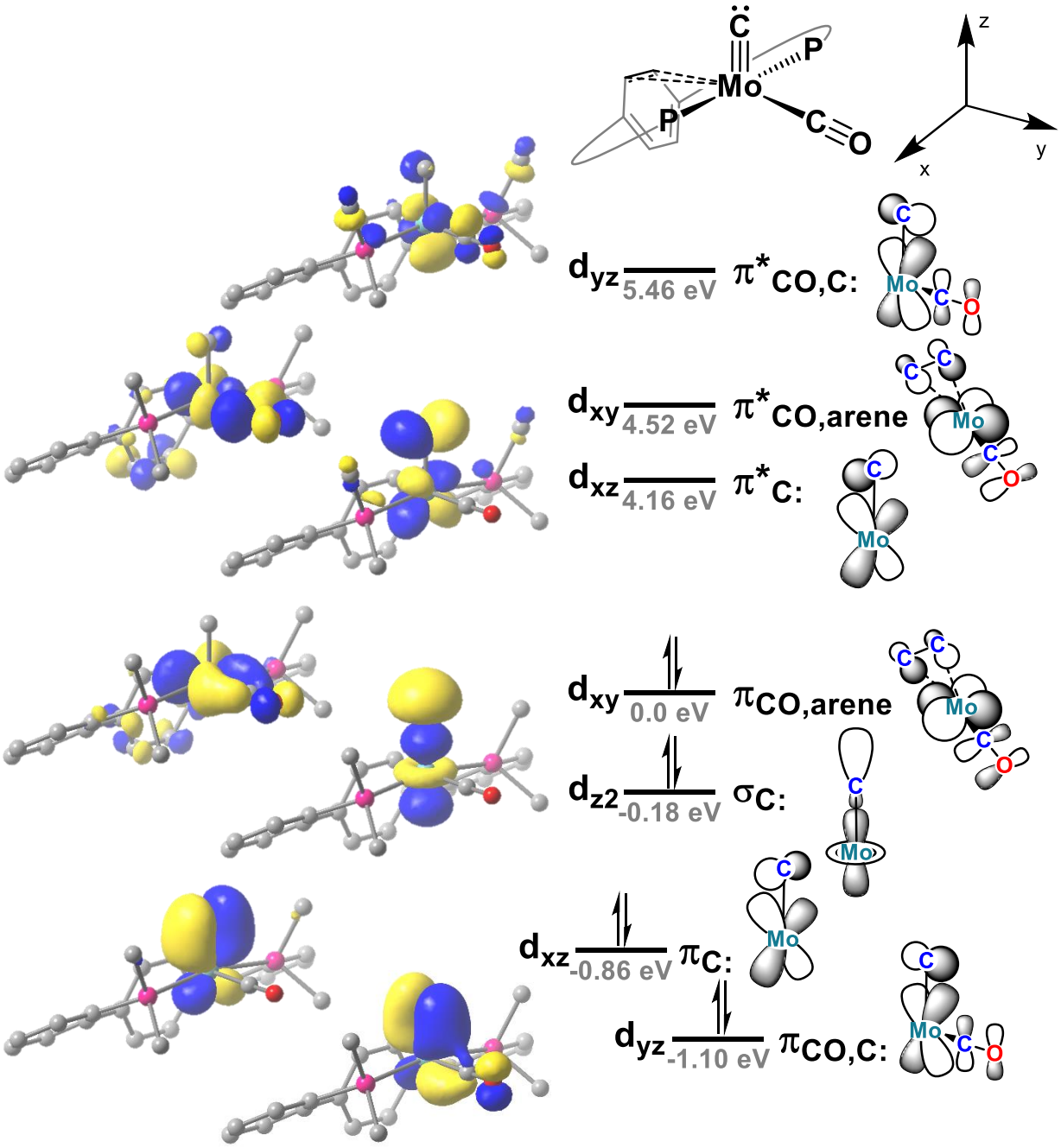

Figure S48—Partial qualitative MO diagram outlining the bonding interactions with the carbide and π-bonding interactions with the carbonyl, and η^2-arene ligands in **7**. Orbital energies relative to the HOMO are given in eV and calculated MOs are depicted with a 0.04 e/Å^3 isosurface value. In the depiction of the molecule's orientation, the phosphine ligands and the terphenyl linker have been truncated for clarity.

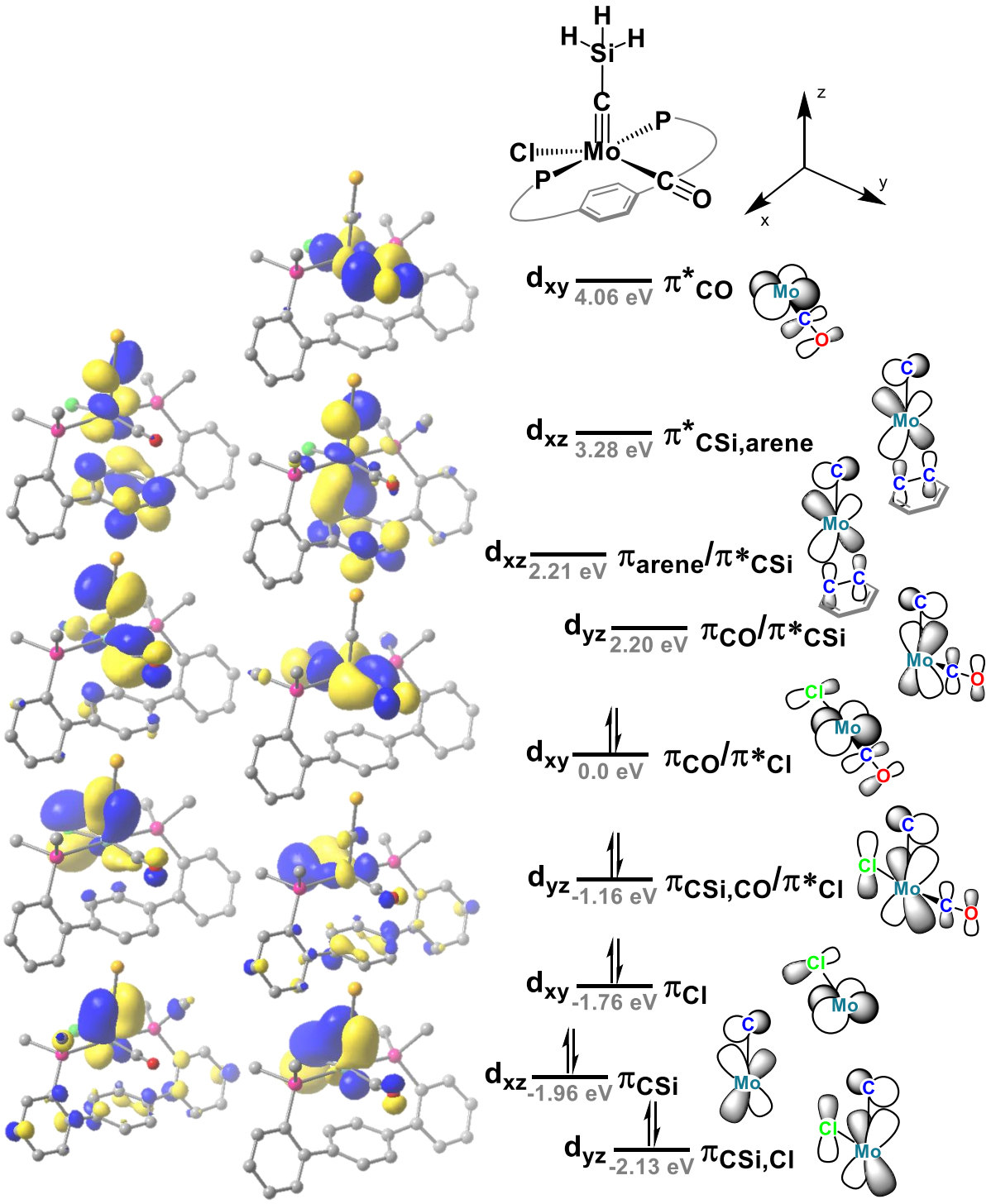

Figure S49—Partial qualitative MO diagram outlining the π-bonding interactions with the carbyne, carbonyl, and chloride ligands in **8**. Orbital energies relative to the HOMO are given in eV and calculated MOs are depicted with a 0.04 e/Å^3 isosurface value. In the depiction of the molecule's orientation, the phosphine ligands and the terphenyl linker have been truncated for clarity.

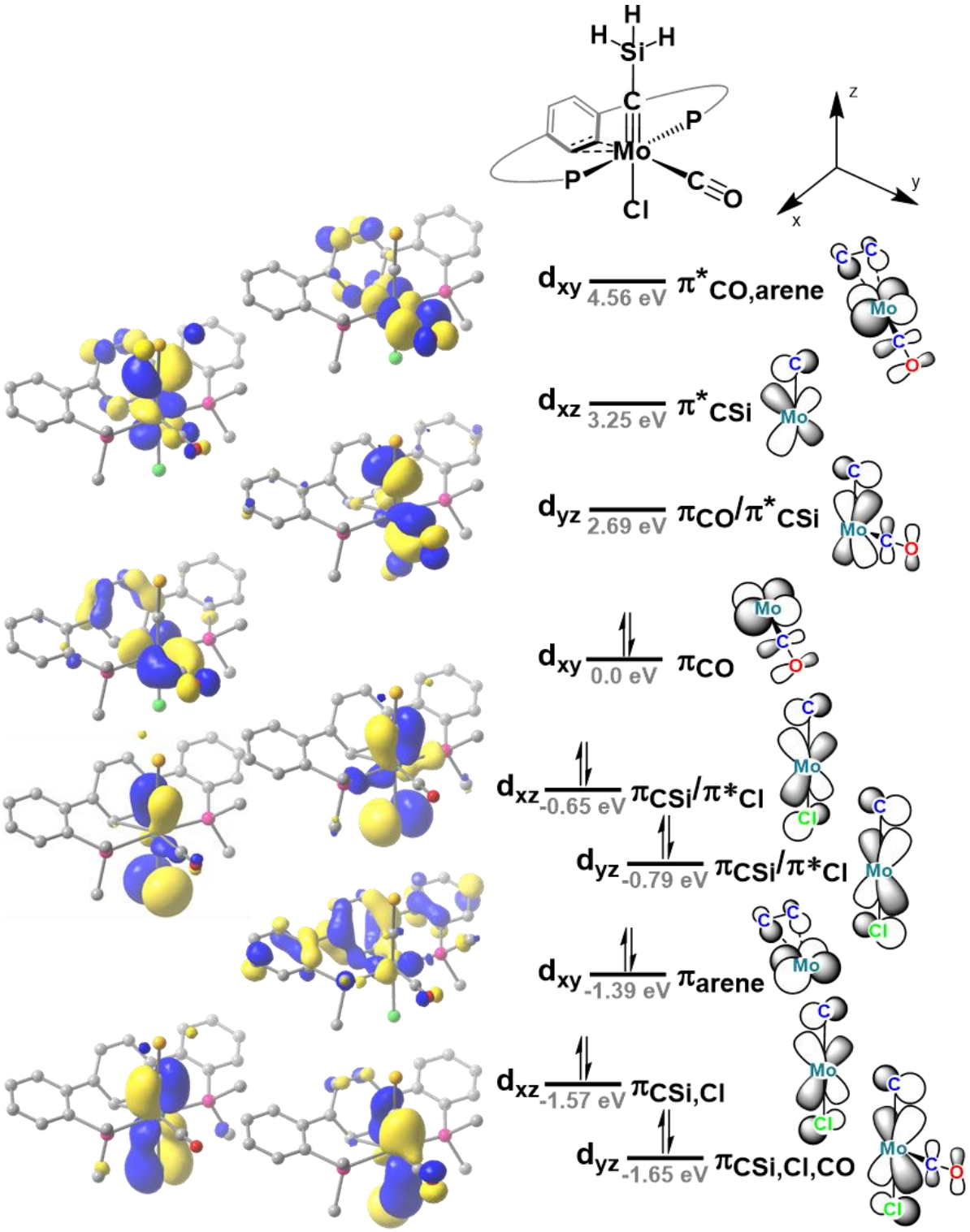

Figure S50—Partial qualitative MO diagram outlining the π-bonding interactions with the carbyne, carbonyl, and chloride ligands in **11**. Orbital energies relative to the HOMO are given in eV and calculated MOs are depicted with a 0.04 e/Å^3 isosurface value. In the depiction of the molecule's orientation, the phosphine ligands and the terphenyl linker have been truncated for clarity.

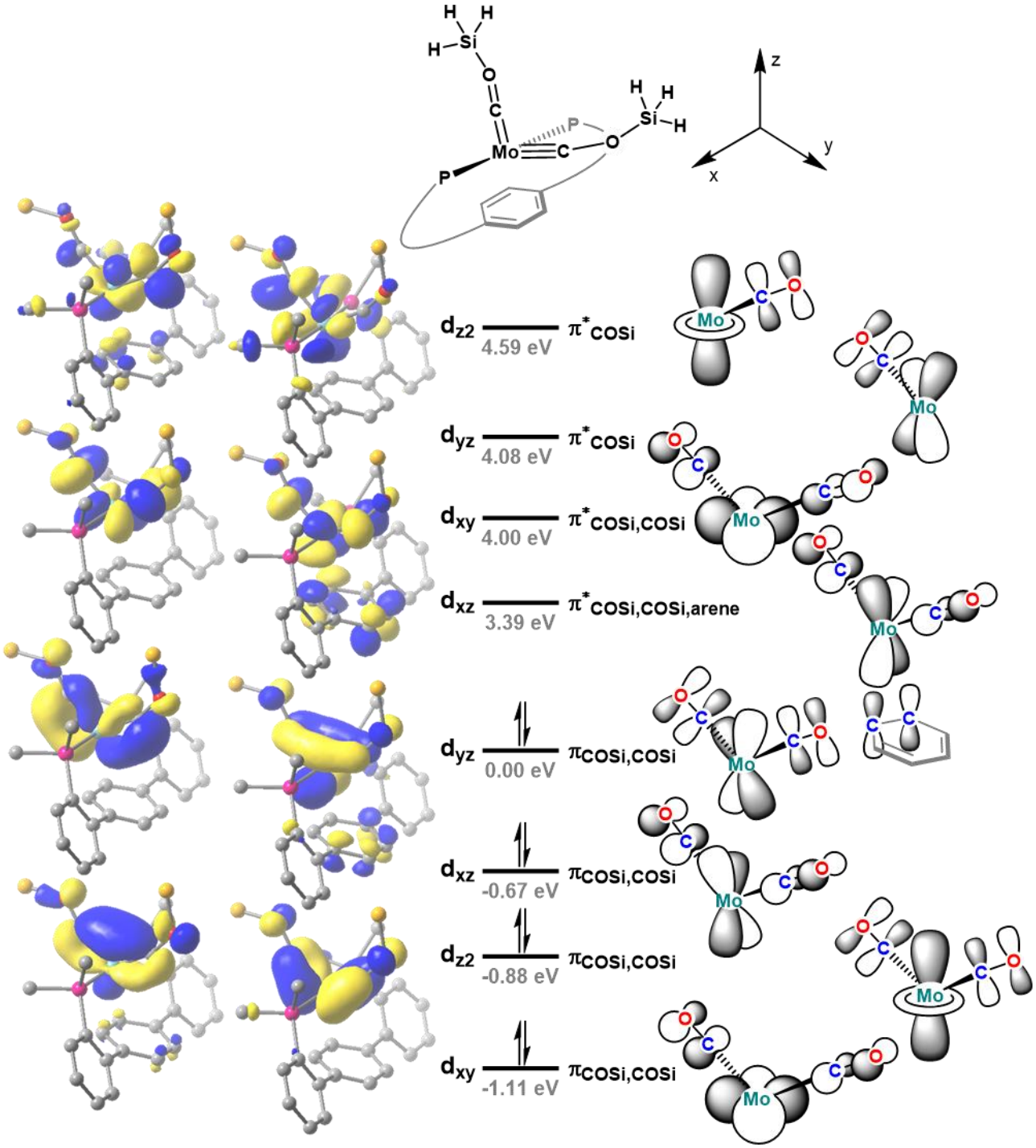

Figure S51—Partial qualitative MO diagram outlining the π-bonding interactions with the carbyne ligands in **9**. Orbital energies relative to the HOMO are given in eV and calculated MOs are depicted with a 0.04 e/Å^3 isosurface value. In the depiction of the molecule's orientation, the phosphine ligands and the terphenyl linker have been truncated for clarity.

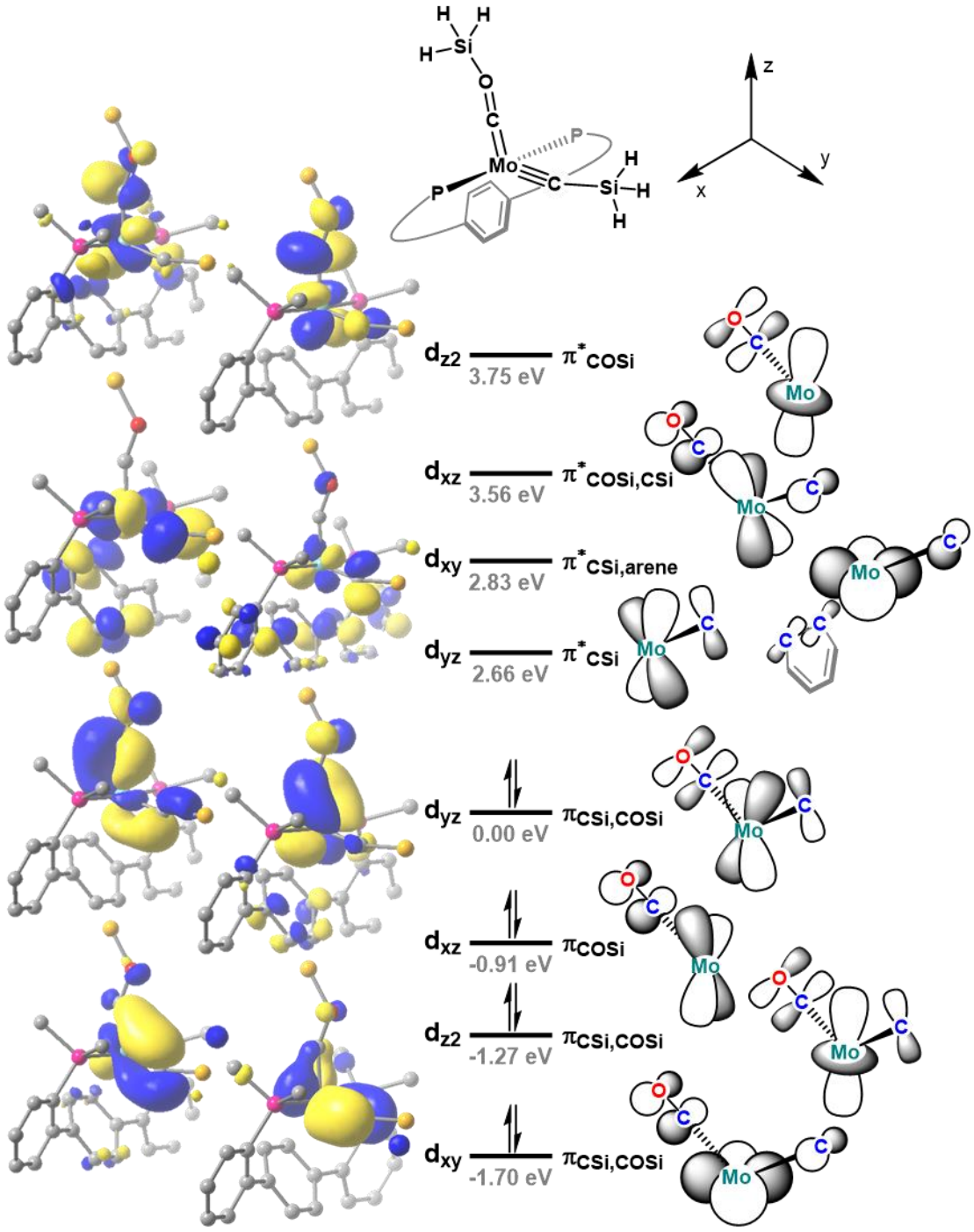

Figure S52—Partial qualitative MO diagram outlining the π-bonding interactions with the carbyne ligands in **15**. Orbital energies relative to the HOMO are given in eV and calculated MOs are depicted with a 0.04 e/Å^3 isosurface value. In the depiction of the molecule's orientation, the phosphine ligands and the terphenyl linker have been truncated for clarity.

Computation was employed to rationalize the thermodynamic preference for five-coordinate **8** over *pseudo*-octahedral **11**. Surprisingly, the absolute energy of silyl carbyne **8** was calculated to be 4.4 kcal/mol *higher* than that of silyl carbyne **11**. Optimizing both structures with a trimethylsilyl substituent on the alkylidyne ligand still predicted **11** to be more stable than **8**, but reduced the energetic difference to 2.9 kcal/mol. Changing the phosphine substituents to isopropyl groups inverted the relative energies, favoring five-coordinate **8** by 2.3 kcal/mol in accord with experimental results (Table S2). The calculated electronic structures of **8** and **11** are quite similar, both exhibiting complimentary π-acidic/π-basic interactions from the mixed ligand set (Figures S49 and S50). These data, in conjunction with the reluctance of bulkier $^{i}Pr_3SiCl$ to silylate **7** at low temperatures support a steric, rather than electronic, preference for the five-coordinate silyl carbyne isomer.

Table S2—Optimized Gas-Phase Single-Point Energies for Variants of **8** and **11**

	SiH_3, $ArPMe_2$	**$SiMe_3$, $ArPMe_2$**	**$SiMe_3$, ArP^iPr_2**
cis arene/carbyne, **11**	-1105.54210326 a.u.	-1223.53528943 a.u.	-1538.01876179 a.u.
trans arene/carbyne, **8**	-1105.53681517 a.u.	-1223.53075602 a.u.	-1538.02236210 a.u.
Δ (**8** – **11**)	3.32 kcal/mol	2.84 kcal/mol	-2.26 kcal/mol
Δ (**8** – **11**)‡	4.44 kcal/mol	2.85 kcal/mol	-2.26 kcal/mol

‡Energies include single-point dispersion correction terms.

Table S3—Comparison of Experimental and Calculated Spectroscopic Data for **2**, **7-11**, and **15**

	2		**7**		**8**		**9**		**10**		**11**		**15**	
	Exp.	Calc.	Exp.	Calc.	Exp.	Calc.	Exp.	Calc.	Exp.	Calc.	Exp.	Calc.	Exp.	Calc.
δ_{C31} (ppm)‡	228.5	235.3	233.2	239.4	247.4	253.2	285.8	313.6	207.9	203.5	241.9	249.9	378.9	359.1
δ_{C32} (ppm)‡	228.5	234.7	546.2	567.7	355.9	323.7	279.8	286.2	207.9	205.7	344.9	297.2	283.7	311.5
ν_{CO} (cm^{-1})	1887	1805	N/A	1780	1873	1787	N/A	N/A	N/A	N/A	N/A	1817	N/A	N/A
ν_{CO} (cm^{-1})	1832	1764	N/A	N/A	N/A	N/A	N/A	N/A	N/A	N/A	N/A	N/A	N/A	N/A

‡Chemical shifts are referenced to the GIAO calculated ^{13}C NMR shift of Me_4Si optimized using the same basis set (LANL2DZ) and functional (RTPSSTPSS) as the metal complexes.

Table S4—Comparison of Experimental and Calculated Structural Metrics for **2**, **8**, **10**, and **11**

	2		**8**			**10**		**11**		
	Exp.	**Calc.**	**Exp.**	**Calc.**	**^{i}Pr$_2$-Me$_3$Si Calc.**	**Exp.**	**Calc.**	**Exp.**	**Calc.**	**^{i}Pr$_2$-Me$_3$Si Calc.**
C1-C2	1.4183(8)	1.445	1.395(3)	1.423	1.423	1.424(2)	1.446	1.424(1)	1.407	1.409
C2-C3	1.4216(8)	1.442	1.392(3)	1.412	1.410	1.427(2)	1.450	1.395(1)	1.422	1.421
C3-C4	1.4210(8)	1.443	1.401(3)	1.423	1.423	1.430(2)	1.465	1.421(1)	1.407	1.406
C4-C5	1.4214(8)	1.444	1.390(3)	1.416	1.416	1.430(2)	1.450	1.382(1)	1.438	1.436
C5-C6	1.4254(8)	1.444	1.393(3)	1.412	1.413	1.426(2)	1.455	1.407(1)	1.422	1.420
C6-C1	1.4272(8)	1.443	1.395(3)	1.416	1.415	1.428(2)	1.451	1.383(1)	1.438	1.439
Mo1-P1	2.4191(2)	2.478	2.5869(6)	2.590	2.671	2.4712(4)	2.522	2.6027(2)	2.586	2.669
Mo1-P2	N/A	N/A	2.5562(6)	2.591	2.670	N/A	N/A	2.5972(2)	2.586	2.657
Mo1-C31	1.9675(7)	1.960	1.974(2)	1.968	1.958	2.054(1)	2.073	1.9758(9)	1.971	1.966
Mo1-C32	1.9710(6)	1.961	1.767(2)	1.793	1.797	2.032(1)	2.048	1.7691(8)	1.811	1.820
Mo–C$_{arene}$ (ave.)	2.3254(6)	2.373	2.82 (C2/C3 contact)	2.84 (C2/C3 contact)	2.85 (C2/C3 contact)	2.280(2)	2.314	2.5220(9)	2.541	2.534
Mo-Cl	N/A	N/A	2.5380(6)	2.570	2.590	N/A	N/A	2.5581(2)	2.620	2.645
C31-O1	1.1632(9)	1.210	1.138(3)	1.211	1.214	1.326(2)	1.384	1.158(1)	1.203	1.208
C32-O2	1.1645(8)	1.209	N/A	N/A	N/A	1.368(2)	1.397	N/A	N/A	N/A
C32-Si1	N/A	N/A	1.877(2)	1.878	1.902	N/A	N/A	1.8815(9)	1.884	1.912
∠P1-Mo1-P2	N/A	N/A	176.12(2)	171.87	172.06	N/A	N/A	171.00(1)	174.00	169.07
∠C31-Mo1-C32	85.01(3)	86.21	87.4(1)	86.15	87.99	38.02(6)	38.46	84.66(4)	89.27	88.11
∠P1-Mo1-C31	94.60(2)	92.03	89.46(7)	92.27	90.32	106.97(6)	113.15	94.48(3)	89.46	94.24
∠P1-Mo1-C32	91.38(2)	92.44	92.50(7)	93.49	93.93	82.70(4)	78.77	93.62(3)	92.93	94.85
∠P2-Mo1-C31	N/A	N/A	88.36(7)	92.28	90.03	N/A	N/A	87.06(3)	89.47	86.73
∠P2-Mo1-C32	N/A	N/A	90.61(7)	93.53	94.01	N/A	N/A	95.35(3)	92.95	96.07
∠C31-Mo1-Cl	N/A	N/A	170.88(7)	167.46	162.76	N/A	N/A	94.17(3)	88.03	91.62
∠C32-Mo1-Cl	N/A	N/A	101.62(7)	106.39	104.25	N/A	N/A	175.82(3)	177.30	176.55

Crystallographic Information

CCDC deposition numbers 1412066 and 1412067 contain the supplementary crystallographic data for this paper. These data can be obtained free of charge from The Cambridge Crystallographic Data Centre via www.ccdc.cam.ac.uk/data_request/cif.

Refinement Details—In each case, crystals were mounted on a glass fiber or MiTeGen loop using Paratone oil, then placed on the diffractometer under a nitrogen stream. Crystals for compounds **3** and **4** were manipulated under an Argon purge due to atmospheric sensitivity. Low temperature (100 K) X-ray data were obtained on a Bruker D8 VENTURE Kappa Duo PHOTON 100 CMOS based diffractometer (Mo $I_{\mu}S$ HB micro-focus sealed X-ray tube, K_{α} = 0.71073 Å OR Cu $I_{\mu}S$ HB micro-focused X-ray tube, K_{α} = 1.54178). All diffractometer manipulations, including data collection, integration, and scaling were carried out using the Bruker APEXII software.[22] Absorption corrections were applied using SADABS.[23] Space groups were determined on the basis of systematic absences and intensity statistics and the structures were solved in the Olex 2 software interface[24] by intrinsic phasing using XT (incorporated into SHELXTL)[25] and refined by full-matrix least squares on F^2. All non-hydrogen atoms were refined using anisotropic displacement parameters. Hydrogen atoms were placed in the idealized positions and refined using a riding model. The structure was refined (weighed least squares refinement on F^2) to convergence. Graphical representation of structures with 50% probability thermal ellipsoids were generated using Diamond 3 visualization software.[26]

Table S5—Crystal and refinement data for complexes **10** and **11**.

	10	**11**
CCDC Number[27]	1412066	1412067
Empirical formula	$C_{42}H_{68}MoO_2P_2Si_2$	$C_{35}H_{49}ClMoOP_2Si$
Formula weight	819.02	707.16
T (K)	100	100
a, Å	12.8387(8)	9.2760(3)
b, Å	13.2552(8)	11.7913(4)
c, Å	14.3715(8)	16.9954(6)
α, °	76.202(2)	108.1820(10)
β, °	75.565(2)	100.2460(10)
γ, °	72.413(2)	98.8360(10)
Volume, Å^3	2222.3(2)	1693.88(10)
Z	2	2
Crystal system	Triclinic	Triclinic
Space group	$P\bar{1}$	$P\bar{1}$
d_{calc}, g/cm^3	1.224	1.386
θ range, °	2.399 to 35.631	2.289 to 36.319
μ, mm^{-1}	0.453	0.623
Abs. Correction	Semi-empirical	Semi-empirical
GOF	1.040	1.039
R_1,[a] wR_2 [b] [I>2 σ(I)]	0.0447, 0.0721	0.0242, 0.0541
Radiation Type	Mo K_α	Mo K_α

[a] $R_1 = \sum||F_o| - |F_c||/\sum|F_o|$. [b] $wR_2 = [\sum[w(F_o^2-F_c^2)^2]/\sum[w(F_o^2)^2]^{1/2}$.

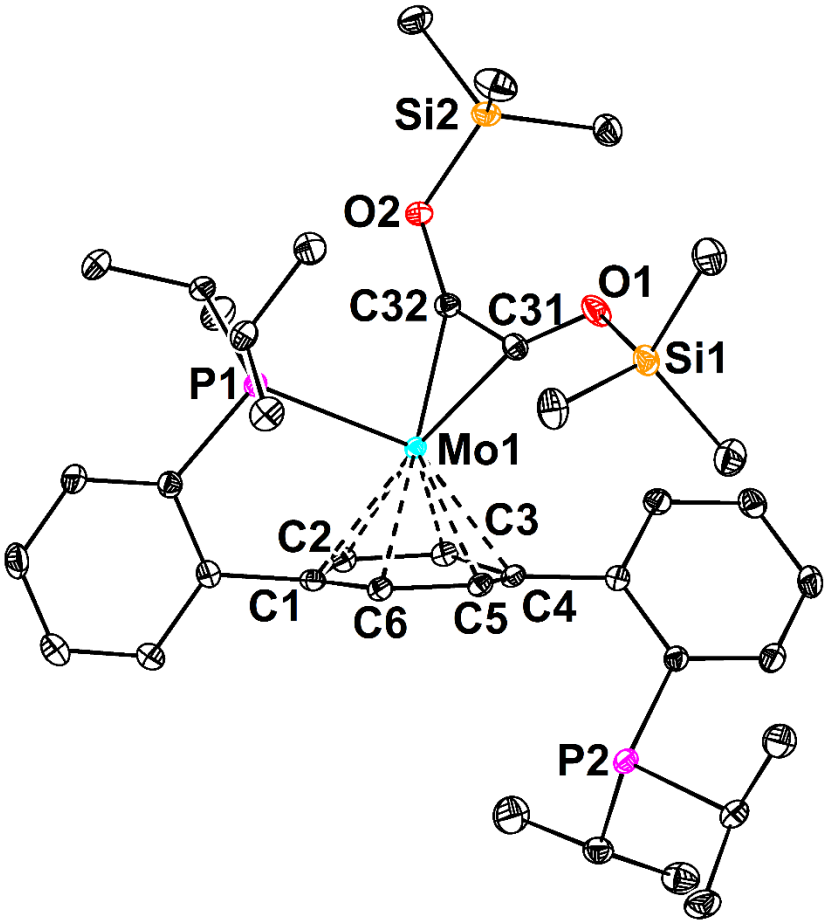

Figure S53—Structural drawing of **10** with 50% probability anisotropic displacement ellipsoids. Co-crystallized butane molecule and hydrogen atoms are omitted for clarity.

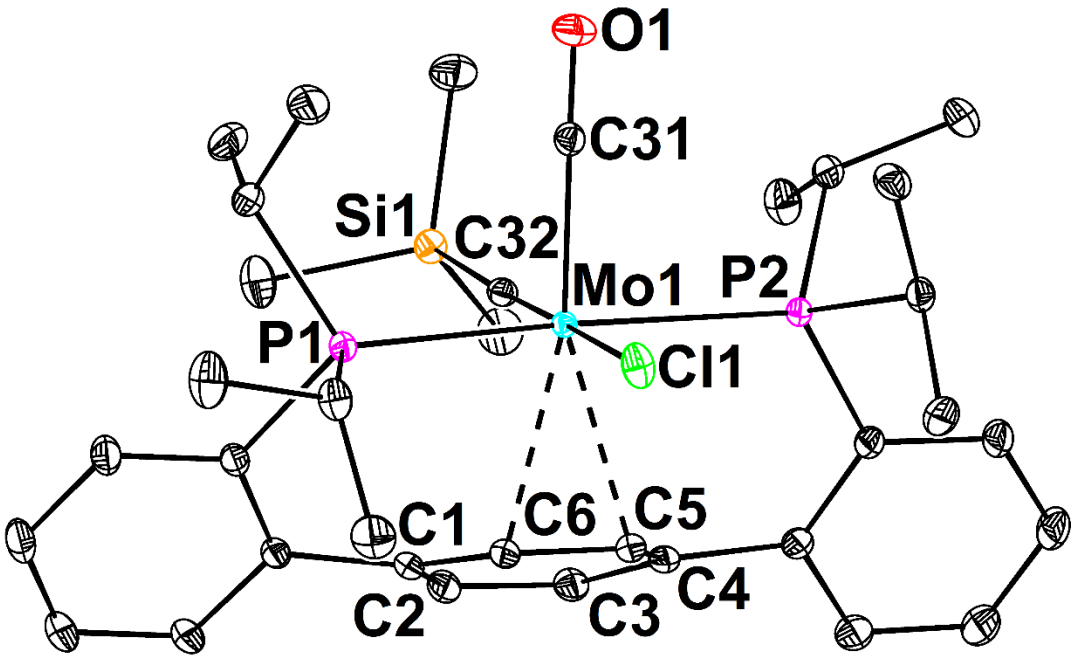

Figure S54—Structural drawing of **11** with 50% probability anisotropic displacement ellipsoids. Hydrogen atoms are omitted for clarity.

References

(1) Pangborn, A. B.; Giardello, M. A.; Grubbs, R. H.; Rosen, R. K.; Timmers, F. J. *Organometallics* **1996**, *15*, 1518.
(2) Buss, J. A.; Edouard, G. A.; Cheng, C.; Shi, J.; Agapie, T. *J. Am. Chem. Soc.* **2014**, *136*, 11272.
(3) Buss, J. A.; Agapie, T. *Nature* **2016**, *529*, 72.
(4) Weitz, I. S.; Rabinovitz, M. *J. Chem. Soc., Perkin Trans. 1* **1993**, 117.
(5) Hyde, J. F.; Johannson, O. K.; Daudt, W. H.; Fleming, R. F.; Laudenslager, H. B.; Roche, M. P. *J. Am. Chem. Soc.* **1953**, *75*, 5615.
(6) Fulmer, G. R.; Miller, A. J. M.; Sherden, N. H.; Gottlieb, H. E.; Nudelman, A.; Stoltz, B. M.; Bercaw, J. E.; Goldberg, K. I. *Organometallics* **2010**, *29*, 2176.
(7) Rohonczy, J. "TEDDY - Dynamic NMR Module (version 1.1.2)" Bruker Biospin, Rheinstetten, Germany.
(8) Ito, M.; Shirakawa, E.; Takaya, H. *Synlett.* **2002**, 1329.
(9) Groh, B. L.; Magrum, G. R.; Barton, T. J. *J. Am. Chem. Soc.* **1987**, *109*, 7568.
(10) Nikolaeva, S. N.; Ponomarev, S. V.; Petrosyan, V. S.; Lorberth, J. *J. Organomet. Chem.* **1997**, *535*, 213.
(11) Gaussian 09, Revision C.01, Frisch, M. J.; Trucks, G. W.; Schlegel, H. B.; Scuseria, G. E.; Robb, M. A.; Cheeseman, J. R.; Scalmani, G.; Barone, V.; Mennucci, B.; Petersson, G. A.; Nakatsuji, H.; Caricato, M.; Li, X.; Hratchian, H. P.; Izmaylov, A. F.; Bloino, J.; Zheng, G.; Sonnenberg, J. L.; Hada, M.; Ehara, M.; Toyota, K.; Fukuda, R.; Hasegawa, J.; Ishida, M.; Nakajima, T.; Honda, Y.; Kitao, O.; Nakai, H.; Vreven, T.; Montgomery, Jr., J. A.; Peralta, J. E.; Ogliaro, F.; Bearpark, M.; Heyd, J. J.; Brothers, E.; Kudin, K. N.; Staroverov, V. N.; Kobayashi, R.; Normand, J.; Raghavachari, K.; Rendell, A.; Burant, J. C.; Iyengar, S. S.; Tomasi, J.; Cossi, M.; Rega, N.; Millam, J. M.; Klene, M.; Knox, J. E.; Cross, J. B.; Bakken, V.; Adamo, C.; Jaramillo, J.; Gomperts, R.; Stratmann, R. E.; Yazyev, O.; Austin, A. J.; Cammi, R.; Pomelli, C.; Ochterski, J. W.; Martin, R. L.; Morokuma, K.; Zakrzewski, V. G.; Voth, G. A.; Salvador, P.; Dannenberg, J. J.; Dapprich, S.; Daniels, A. D.; Farkas, Ö.; Foresman, J. B.; Ortiz, J. V.; Cioslowski, J.; Fox, D. J. Gaussian, Inc., Wallingford CT, 2009.
(12) Perdew, J. P.; Ruzsinszky, A.; Csonka, G. I.; Constantin, L. A.; Sun, J. *Phys. Rev. Lett.* **2009**, *103*, 026403.
(13) Perdew, J. P.; Ruzsinszky, A.; Csonka, G. I.; Constantin, L. A.; Sun, J. *Phys. Rev. Lett.* **2011**, *106*, 179902.
(14) Dunning, T. H.; Hay, P. J. in *Methods of Electronic Structure Theory*; Schaefer, H. F., Ed.; Springer US: Boston, MA, 1977, p 1.
(15) Hay, P. J.; Wadt, W. R. *J. Chem. Phys.* **1985**, *82*, 270.
(16) Wadt, W. R.; Hay, P. J. *J. Chem. Phys.* **1985**, *82*, 284.
(17) Hay, P. J.; Wadt, W. R. *J. Chem. Phys.* **1985**, *82*, 299.
(18) Wolinski, K.; Hinton, J. F.; Pulay, P. *J. Am. Chem. Soc.* **1990**, *112*, 8251.
(19) Cheeseman, J. R.; Trucks, G. W.; Keith, T. A.; Frisch, M. J. *J. Chem. Phys.* **1996**, *104*, 5497.
(20) Grimme, S.; Antony, J.; Ehrlich, S.; Krieg, H. *J. Chem. Phys.* **2010**, *132*, 154104.
(21) Grimme, S.; Ehrlich, S.; Goerigk, L. *J. Comput. Chem.* **2011**, *32*, 1456.
(22) APEX2, Version 2 User Manual, M86-E01078, Bruker Analytical X-ray Systems, Madison, WI, June 2006.
(23) Sheldrick, G.M. "SADABS (version 2008/1): Program for Absorption Correction for Data from Area Detector Frames", University of Göttingen, 2008.
(24) Dolomanov, O. V.; Bourhis, L. J.; Gildea, R. J.; Howard, J. A. K.; Puschmann, H. *J. Appl. Cryst.* **2009**, *42*, 339.
(25) Sheldrick, G.M. (2008). *Acta Cryst.*, A64, 112-122.
(26) Brandenburg, K. (1999). DIAMOND. Crystal Impact GbR, Bonn, Germany.
(27) Crystallographic data have been deposited at the CCDC, 12 Union Road, Cambridge CB2 1EZ, UK and copies can be otained on request, free of charge, by quoting the publication citation and the respective deposition numbers.